PONTIFICIA UNIVERSIDAD CATOLICA DE CHILE
SCHOOL OF ENGINEERING

SHAPE OPTIMIZATION BASED ON EIGENFREQUENCIES

VÍCTOR PRIETO DÍAZ

Thesis submitted to the Office of Research and Graduate Studies
in partial fulfillment of the requirements for the degree of
Master of Science in Engineering

Advisor:
SERGIO GUTIÉRREZ CID

Santiago de Chile, April 2013

PONTIFICIA UNIVERSIDAD CATOLICA DE CHILE
SCHOOL OF ENGINEERING

SHAPE OPTIMIZATION BASED ON EIGENFREQUENCIES

VÍCTOR PRIETO DÍAZ

Members of the Committee:
SERGIO GUTIÉRREZ CID
JOSÉ LUIS ALMAZÁN
JAIME ORTEGA
MARCELO GUARINI

Thesis submitted to the Office of Research and Graduate Studies
in partial fulfillment of the requirements for the degree of
Master of Science in Engineering

Santiago de Chile, April 2013

Gratefully to my family

ACKNOWLEDGEMENTS

It would not have been possible to write this thesis without the help and support of the people around me, to only some of whom it is possible to give particular mention here.

I would like to thank my parents and sister for they unequivocal support and great patience at all time.

This thesis would not have been possible without the help, support, patience and unceasing disposition of my advisor, Professor Sergio Gutiérrez, not to mention his advice and knowledge of Applied Mathematics and Optimization in the field of Civil Engineering. The good advice and support of Professor José Luis Almazán.

I would like to acknowledge the academic and technical support of the Department of Structural and Geotechnical Engineering, Pontificia Universidad Católica de Chile, that provided the facilities, which have been indispensable.

Last, but by no means least, the financial support of the Fondecyt research grant number 1090334.

TABLE OF CONTENTS

LIST OF FIGURES

LIST OF TABLES

ABSTRACT

Many problems in civil engineering consist in finding optimal designs to maximize the rigidity of slender structures such as tall buildings, in order to diminish the relative displacements between floors, or drifts, that the structure may suffer during an earthquake, and also diminish the shear demand capacity (D/C) ratio, because a failure from shear is very fragile, therefore very dangerous. It is known that the rigidity of slender structures is directly related with its eigenfrequencies, specially the first or smallest of them. Another important issue civil engineers have to deal with is finding the optimal shape of structures, such as bridges, to maximize its rigidity using the same amount of material.

In this work we propose two shape optimization methods: geometric optimization and full homogenization; in order to maximize the first eigenfrequency of slender structures such as tall buildings with rectangular plant and uniform in height, and bridges. Computational algorithms are derived for each one of the methods. Furthermore the results for drifts and shear D/C ratios are compared between the two methods, in order to analyze advantages and disadvantages of each of them.

Keywords: eigenfrequencies, optimization, tall buildings, drift, shear demand capacity (D/C) ratio.

RESUMEN

Muchos problemas en ingeniería civil consisten en encontrar diseños óptimos de manera de maximizar la rigidez de estructuras flexibles como edificios altos, ya que así se logran disminuir los desplazamientos relativos de entrepiso, o drifts, que pueda sufrir la estructura durante un sismo, y además disminuir los factores de utilización por corte, ya que las fallas de corte son muy frágiles y, por lo tanto, muy peligrosas. Es sabido que la rigidez de estructuras flexibles, como edificios altos, está directamente relacionada con sus frecuencias propias, especialmente la primera o más pequeña de ellas. Otro problema importante en ingeniería civil es determinar la forma óptima de estructuras como puentes de manera de maximizar su rigidez usando la misma cantidad de material.

En este trabajo se proponen dos métodos de optimización de forma: optimización geométrica y full homogenización; que buscan maximizar la primera frecuencia propia de estructuras flexibles como edificios altos de planta rectangular y uniformes en altura y puentes de acero. Mostraremos la derivación de algoritmos computacionales para cada uno de estos métodos. Además se comparan los resultados de drifts y factores de utilización por corte de los dos métodos en edificios altos para analizar las ventajas y desventajas de cada uno de ellos.

Palabras Claves: frecuencias propias, optimización, edificios altos, drift, factores de utilización.

1. INTRODUCTION

1.1. Motivation

Eigenfrequencies are of a major concern in both Structural and Mechanical Engineering because of their implications in the design of structures and mechanical devices.

In structural engineering, the design of structures are mainly controlled by the effects of earthquakes in structures. And it is well known that earthquakes are excitations that produce displacements in structures with a wide spectrum of frequencies. And if this spectrum covers some of the eigenfrequencies of a structure, specially the smallest of them, the structure will have a considerable increase in its displacements and stresses. For this reason it is important to develop an optimization method dedicated to modify the smallest eigenfrequencies of a structure in order to diminish these increases in displacements and stresses.

In many seismic countries the building codes for design of structures have specific restrictions for the maximum displacements and stresses in a structure produced by earthquakes. For instance, in Chile the building design code NCh433of2010, see INN-Chile (2010), have strict restrictions for relative displacement between two consecutive floors, called drifts. These drifts are directly related to the stiffness of the building, which in turn is related to the first eigenfrequency of the building and its corresponding eigenfunction.

Another important issue engineers have to deal with is the solicitations in the structure induced by an earthquake. These solicitations produce shear stresses, that can produce the collapse of the structure if they overcome the resistance of the materials the building is made of. And as it is shown in this thesis, the shear stresses are related to the rigidity of the building, and the rigidity is directly related to the first eigenfrequency of the building and its corresponding eigenfunction, .

Another problem in structural optimization is to decide where to put reinforcements inside structural components in order to obtain a desired behavior of the structural system.

Walls and beams are usually made of reinforced concrete, that is to say they are a mixture of two different materials, one is rigid and the other is more flexible, say steel and concrete. Also, we would like to know the optimal shape of a structure, such as a bridge, in order to use the same amount of material and for instance maximize the rigidity of the structure. This is done with the full homogenization method simulating the flexible material as a very weak one in a way that in the limit it emulates void.

1.2. Problem Definition/Problem Description

When a structural system, such as a reinforced concrete building or a bridge, suffers and external excitation that is cyclic or harmonic with a singular frequency or a variety of frequencies as in an earthquake or movements produced by winds during a storm, the structural system tends to move in a way that is mainly tuned or syntonized with its natural frequencies or eigenfrequencies. When the frequencies of the external excitation are very similar to the eigenfrequencies of the structural system, specially the first eigenfrequencies, the displacements and stresses in the structural system increase. This phenomenon is called pseudo-resonance.

These eigenfrequencies depend only on the structural system itself and are calculated using the Rayleigh quotient.

Definition: for a given real symmetric matrix A and nonzero vector x, the Rayleigh quotient $R(A, x)$, is defined as:

$$R(A, x) = \frac{x^T A x}{x^T x}\,. \tag{1.1}$$

It can be shown that, $R(A, x)$ reaches its minimal value for a given real-symmetric matrix A. The minimal value of $R(A, x)$ is λ_1, the smallest eigenvalue of A (square of the smallest eigenfrequency in a physical system) and v_1 is its corresponding eigenvector.

In the following chapters we are focus in finding an expression for (1.1) in two different settings. In chapter 2, matrix A is obtained from the weak formulation of equation

(2.1). In chapter 3, matrix A is $M^{-1}K$, where M is obtained from the right- hand side of equation (3.8) and K, from the left-hand side of equation (3.8) in the weak formulation. We use the corresponding expressions for (1.1) as an objective function for optimization algorithms.

1.3. Shape Optimization

Shape Optimization is a very active field of research, located at the crossing of civil, mechanical, aeronautic engineering and applied mathematics and which has seen important progress in the last thirty years or so. One could trace the first attempts to give it a firm mathematical foundation to the work of J. Hadamard at the beginning of the XX century, see Hadamard (1907), with its celebrated theorem that states that the shape derivative will only depend on the deformation of the boundary of the current domain, along its normal direction. Much later, in the 1970's F. Murat and J. Simon significantly expanded the work of Hadamard. See Murat and Simon (1976). There was, however, a fundamental problem with this approach, namely that one could not create holes in the current domain, because this will involve a discontinuous mapping from the current domain to the perturbed one. This has been overcome now days by what is called topology optimization, which has several lines of work, mainly homogenization based techniques, topological derivatives and penalization techniques. See for example Allaire (2002), Novotny and Sokolowski (2010), Bendsøe and Sigmund (2003) and Allaire et al. (2002).

One major difficulty of some of the above mentioned techniques is that they need a fair amount of mathematical training to be safely applied. This has naturally made their popularization among practitioners quite slow. One way around this difficulty is the use of surrogate models, to solve a much simpler optimization problem and then translate its results to the actual problem, hoping that it gives a sufficiently good performance. In this work we concentrate on the problem of maximizing the first eigenfrequency of a

tall slender building, by modifying the depth of its columns, as a function of the vertical direction.

This problem has been studied before by several authors. In Allaire et al. (2001), Gopal (2007), Yoon (2009) and Kim et al. (2003). In this work we first use a surrogate model of the building, based on a membrane of variable thickness, for which we derive a very simple geometric optimization method to maximize its first eigenfrequency by changing its thickness profile. Next, we use the more powerful machinery of homogenization applied to elasticity, that consist on allowing for mixtures of two elastic materials at the micro-scale and obtaining the homogenized characteristics of the material at the macro-scale. This technique is more expensive than geometric optimization used in the previous chapter, but the results obtained are quite similar, validating the use of the surrogate model.

1.4. Summary of Contributions/Original Contributions

Here we present a list of original contributions developed in this thesis.

1. Implementation of a numerical algorithm developed by Arnoldi et al. from the LAPACK group in order to obtain the first eigenvalue of a membrane with variable thickness using FreeFem++. See chapter 2.
2. Find practical applications in structural engineering for the geometric optimization method, such as tall buildings. See chapter 2.
3. Find practical applications in structural engineering for the full homogenization method using FreeFem++, such as walls and bridges. See chapter 3.

1.5. Objectives

In its second chapter this work is concerned with improving the performance of a slender structure as a tall building, by only modifying the depth of the columns of each floor in a way to increase its first natural frequency. This will render the structure more rigid, which is not always what is desired, diminishing its lateral displacements, but what is

more important, diminishing the maximal drift, which is the relative displacement between two consecutive floors, and also diminishing the shear D/C ration, which measures how far from being subject to collapse loads is the building. This optimization problem will be solved by using as a surrogate model of the building a membrane of variable thickness, only subject to transversal displacement, because the optimization technique we will use to make the membrane stiffer, namely geometric optimization, is quite simple and effective. The validity of this surrogate model requires the building to be slender in one horizontal direction and sufficiently tall, so that its first vibration mode, or eigenfunction associated with its first eigenfrequency, will be that of cyclic displacements only in the direction in which the building is slender.

The third chapter is dedicated to a more complex method, full homogenization, which allow us to develop more robust optimization algorithms in order to maximize the first eigenfrequency of structural systems. It is important to notice that with this method we can develop more sophisticated models and obtain better results. A brief description of the mathematical model and the optimization algorithms is presented in chapter 3. Some numerical examples are presented. Although the mathematical description of the method and the numerical examples are in 2D, there is no mathematical obstacle to apply the full homogenization method in the 3D setting. But for reasons of time and computational capacity we were not able to apply it in 3D. However, the mathematical formulation of the full homogenization method in 3D is shown in appendix A.2.3.

1.6. Thesis Outline/Document Organization

The content of the thesis is as follows.

Chapter 2 presents the mathematical formulation and computational algorithm for the maximization of the first eigenfrequency of the surrogate model as a membrane of a slender building, results and comparisons are made for different examples.

Chapter 3 presents a description of the full homogenization method, then the mathematical

formulation and computational algorithm for the maximization of the first eigenfrequency of different structures, such as shear walls and bridges, results and comparisons are made for different examples.

Chapter 4 presents a comparison between geometric optimization from chapter 2 and full homogenization from chapter 3.

Finally chapter 5 presents a series of conclusions for the current thesis.

2. GEOMETRIC OPTIMIZATION USING A MEMBRANE

2.1. Basic Assumptions

If a structural system, such as a tall building, has a regular geometry both in floor and in height, and if in floor one of its dimensions is bigger than the other in a reason of 2:1 or more, it is reasonably to think that its behavior will be similar to that of a 2-D membrane both in displacements and in stresses. Hence we model a tall building, with the mentioned features, as a 2-D membrane. Figure 2.1 shows the geometry of the 2-D membrane. By doing this we can develop an optimization method in a much simpler problem and then translate the results to the actual problem. Now we describe the basic assumptions used for this 2-D membrane model, figure 2.1 shows the geometry of the 2-D membrane.

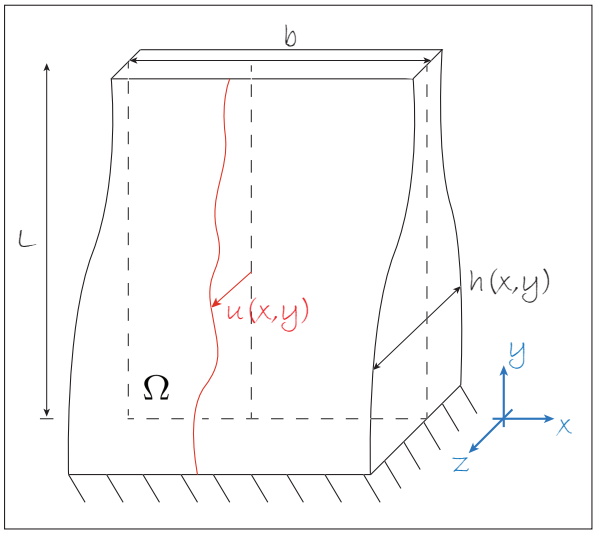

FIGURE 2.1. 2-D Model of a Membrane.

Let Ω be a rectangular domain, representing a membrane of variable thickness $h : \Omega \rightarrow [h_{min}, h_{max}]$, with $0 < h_{min} \leq h_{max}$ being given values. The membrane has only displacements in the perpendicular direction of its plane, z. And its thickness, h is a continuous function in $L^{\infty}(\Omega)$. Ω is a bounded and connected (without holes)

domain with two different boundary conditions. One is a zero displacement Dirichlet condition, in figure 2.1 that condition corresponds with the lower bottom of the membrane. The second boundary condition is a zero-traction Neumann condition, in figure 2.1 this condition corresponds with the upper and lateral boundaries of Ω.

The main assumption we make is that in the case of tall slender buildings, with one dimension in floor bigger than the other in a reason 2:1 or bigger, the first eigenfunction of the building will have only displacements in the direction perpendicular to the plane of the building, similar to the displacements of a 2-D membrane as it is seen in figure 2.1. If this occurs, the error made by modeling the tall building as a 2-D membrane would not be so significant.

In the next sections we develop a method that maximizes the first eigenfrequency of a 2-D membrane by making changes in its thickness h.

2.2. Mathematical Model

The first eigenvalue of a continuous physical system corresponds to the square of the minor natural frequency of the system (eigenfrequency), and to obtain this eigenfrequency we calculate the Rayleigh quotient. For this we need to solve the following problem on the 2-D membrane (see figure 2.1):

$$\left.\begin{aligned} -\text{div}(\, h\, \nabla u) = \omega^2\, u \quad & \text{in } \ \Omega, \\ u = 0 \quad & \text{on } \ \Gamma_D, \\ h\, \nabla u \cdot n = 0 \quad & \text{on } \ \Gamma_N, \end{aligned}\right\} \tag{2.1}$$

where u is the deflection and ω is an eigenfrequency.

To optimize on h we need to look at the variational, or weak, formulation of problem (2.1). Then, as usual, the space where we look for the solution is:

$$V = \{v \in H^1(\Omega);\, v = 0 \ \text{ on } \ \Gamma_D\}.$$

Now we multiply in (2.1) by a test function $v \in V$ and integrate in Ω.

$$\int_\Omega -\text{div}(h\,\nabla u)v\,dx = \omega^2 \int_\Omega u\,v\,dx$$

$$-\int_{\partial\Omega} v\,h\nabla u\cdot n\,ds + \int_\Omega h\,\nabla u\cdot\nabla v\,dx = \omega^2\int_\Omega u\,v\,dx$$

$$-\int_{\Gamma_D} v\,h\nabla u\cdot n\,ds - \int_{\Gamma_N} v\,h\nabla u\cdot n\,ds + \int_\Omega h\,\nabla u\cdot\nabla v\,dx = \omega^2\int_\Omega u\,v\,dx$$

The first and second term on the left-hand side of the last equation are zero because of the boundary conditions stated in (2.1).

Then, the variational formulation of problem (2.1) becomes to look for $u \in V$ such that

$$\int_\Omega h\,\nabla u\cdot\nabla v\,dx = \omega^2\int_\Omega u\,v\,dx \qquad \text{for all } u, v \in V. \tag{2.2}$$

Then if $v = u$ we obtain the Rayleigh quotient

$$\omega^2 = \frac{1}{\|u\|^2_{L^2}}\int_\Omega h|\nabla u|^2\,dx.$$

If $u = u_1$ is the eigenfunction associated with $\omega^2 = \omega_1^2$, the smallest eigenvalue, the objective function we want to maximize becomes:

$$J(u,h) = \frac{1}{\|u\|^2_{L^2}}\int_\Omega h|\nabla u|^2\,dx.$$

The set of admissible thickness functions is given by

$$U_{ad} = \left\{ h : \Omega \to [h_{min}, h_{max}]; h \in L^2(\Omega); \int_\Omega h\,dx = V_0, V_0 \in \mathbb{R}^+ \right\},$$

where V_0 is a given value for the volume constraint on the total volume of the material the membrane is made of. Because if not, the problem has an obvious solution of making $h = h_{max}$.

As we maximize by changing the thickness h, we differentiate the objective function on this variable and evaluate it on a generic admissible perturbation k, then

$$\frac{\partial J}{\partial h}(k) = \frac{1}{\|u\|^2_{L^2}} \int_\Omega k|\nabla u|^2 dx + \frac{2}{\|u\|^2_{L^2}} \int_\Omega h\nabla u \cdot \nabla \frac{\partial u}{\partial h} dx + \frac{\partial}{\partial h}\left(\frac{1}{\|u\|^2_{L^2}}\right) \int_\Omega h|\nabla u|^2 dx, \tag{2.3}$$

we notice that $\frac{\partial u}{\partial h} \in V$ because $u = 0$ on Γ_D for all h, therefore u does not change within a change in h on Γ_D, then $\frac{\partial u}{\partial h} = 0$ on Γ_D. Thus, replacing $\frac{1}{\|u\|^2_{L^2}} \frac{\partial u}{\partial h}$ in (2.2) we get:

$$\frac{1}{\|u\|^2_{L^2}} \int_\Omega h\nabla u \cdot \nabla \frac{\partial u}{\partial h}\, dx = \frac{\omega^2}{\|u\|^2_{L^2}} \int_\Omega u \frac{\partial u}{\partial h}\, dx \tag{2.4}$$

And,

$$\frac{\partial}{\partial h}\left(\frac{1}{\|u\|^2_{L^2}}\right) = -\frac{1}{\|u\|^4_{L^2}} \frac{\partial}{\partial h} \int_\Omega u^2\, dx = -\frac{2}{\|u\|^4_{L^2}} \int_\Omega u \frac{\partial u}{\partial h}\, dx \tag{2.5}$$

Then, replacing (2.4) and (2.5) in (2.3),

$$\begin{aligned} \tfrac{\partial J}{\partial h}(k) &= \tfrac{1}{\|u\|^2_{L^2}} \textstyle\int_\Omega k|\nabla u|^2\, dx + \tfrac{2\omega^2}{\|u\|^2_{L^2}} \int_\Omega u \tfrac{\partial u}{\partial h}\, dx - \tfrac{2}{\|u\|^2_{L^2}} \int_\Omega u \tfrac{\partial u}{\partial h}\, dx \left(\tfrac{1}{\|u\|^2_{L^2}} \int_\Omega h|\nabla u|^2\, dx\right) \\ &= \frac{1}{\|u\|^2_{L^2}} \int_\Omega k|\nabla u|^2\, dx\,. \end{aligned}$$

Clearly if $k = \frac{|\nabla u|^2}{\|u\|^2_{L^2}}$, we obtain a positive value of the derivative and then the objective function will increase if we perturb h in this direction. Therefore, we can now propose a numerical algorithm to maximize ω_1^2, based on the so-called method of perpendicular directions, meaning that we optimize on h and then adjust the eigenfunction u.

2.3. Computational Algorithm

The previous method is encoded in the finite elements software FreeFem++, see Hecht et al. (2007).

The steps of the method described in the previous section are the following:

1. Let h_0 be a given initial thickness.
2. With h_0 we calculate u_0, the first eigenfunction, using the Arnoldi algorithm, see Trefethen and Bau (1997).
3. Evaluate the objective function, $J(u_0, h_0) = \frac{1}{\|u_0\|^2_{L^2}} \int_\Omega h_0 |\nabla u_0|^2 dx$, the initial smallest eigenvalue. Call this J_{old}.
4. Calculate the direction of perturbation of h, $k = \frac{|\nabla u_0|^2}{\|u_0\|^2_{L^2}}$.
5. Calculate the new thickness: $h = h_0 + k \cdot t + l$, where l is the Lagrange multiplier for the volume constraint. Choose l in such a way that $h_{min} \leq h \leq h_{max}$ and $\int_\Omega h \, dx = V_0$.
6. Evaluate $J(h)$. Call this J_{new}. If $J_{new} \geq J_{old}$ we keep maximizing. Make $J_{old} = J_{new}$, recompute u_0 using the new h by the Arnoldi method and go to step (4).
   If $J_{new} < J_{old}$ we diminish the value of t. If t becomes too small, we stop. If not, go to step (5).

2.4. Applications

Now we want to use the numerical algorithm described in section 2.3, to make a tall building stiffer in its most flexible direction. Then, we use a surrogate model of the building as a 2-D membrane, as described in section 2.1. The deflection of the 2-D membrane will now represent the displacement of each point of the building in the most slender direction of the building. Γ_D corresponds to the lower end of the building, the part in contact with the ground that we assume perfectly anchored, while Γ_N is the rest of the boundary, namely, the upper end and the vertical sides of the building.

We model three frame buildings made of reinforced concrete, the difference between them is the number of stories. The first is a 20 story building, the second is 10 stories height and the last one has 9 stories. The buildings have stories of equal height of 250 cm. and have 4 resistent frames. The width of each frame is 3600 cm, see figure 2.2 (right).

Initially all columns in these frames are of 60 cm in width and 60 cm in depth.

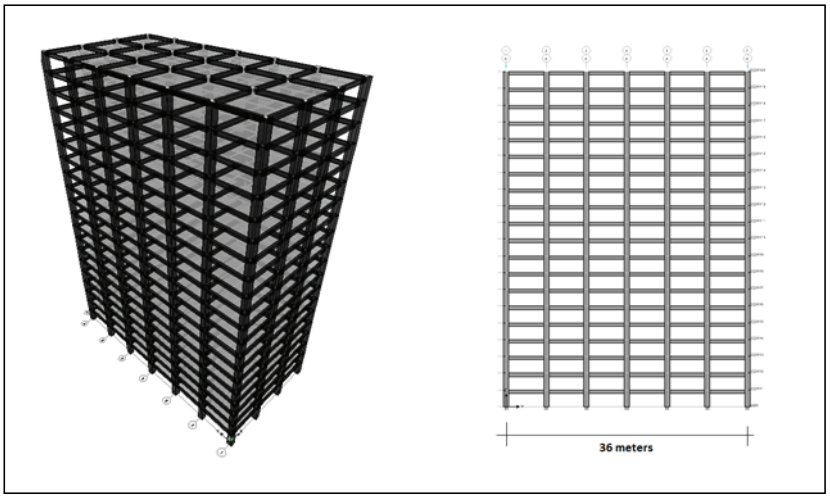

FIGURE 2.2. 3-D Model of the 20 story building (left) and one resistant frame (right).

As seen in the 9 story building, the method is only valid for buildings with more than 9 stories, with the mentioned geometry. Because the first eigenvector of the optimal 9 story building does not correspond with the first eigenvector of the original 9 story building.

The membrane model maintains the aspect ratio of the building, for instance, in the 20 story building (figure 2.2) the total height of the building is 250x20=5000 cm and 3600 cm of width, and the membrane has the same proportions $\frac{Height}{Wide} = \frac{5000}{3600} = 1.3889$. Then, using this simplified model of the building, we optimize on the thickness using the optimization algorithm of section 2.3.

Then, we use the results thus obtained on a 3-D numerical model of the building, changing the depth of the columns. This is done using the commercial software ETABS.

Note: ETABS is a software widely used by civil engineers around the world to analyze and design buildings made of concrete and/or steel. And it can satisfactorily model 3-D buildings and calculate its stresses and deformations when subjected to different kind of

solicitations, including earthquakes and in particular to design spectrums, such as the one used in this thesis, namely NCh433of2010, see INN-Chile (2010).

In ETABS we model the three 3-D buildings and introduce the pseudo-accelerations spectrum, see INN-Chile (2010), and calculate two things, Drifts and Shear Demand Capacity (D/C) Ratios.

Drifts: relative displacement between consecutive floors, see figure 2.3.

$$Drift_i(\%) = \frac{u_i - u_{i-1}}{L_i} 100$$

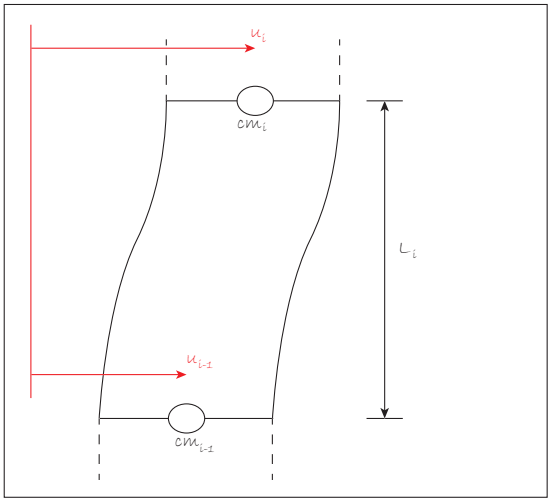

FIGURE 2.3. Drift in floor i.

Shear Demand Capacity (D/C) Ratio: measures how far from being subject to collapse shear loads is the building. Then, the Shear D/C Ratio is calculated as follows,

$$Shear\ D/C\ ratio = \frac{Solicitation}{Resistance}$$

for each floor of the building.

The solicitation in the Shear D/C Ratio comes from the pseudo-acceleration spectrum. We use the Chilean legislation for seismic design of reinforced concrete structures, see

INN-Chile (2010), to calculate the pseudo-acceleration spectrum. We introduce these pseudo-accelerations in ETABS and calculate shear solicitations induced in the building.

To calculate the resistance to shear in the Shear D/C Ratio, we use a constant reinforcement of stirrups made of bars of 8 mm in diameter, with a separation of 20 cm between stirrups. The bars have perfect elasto-plastic behavior with a yield tension of $f_y = 4200\, kg/cm^2$. The other part of the shear resistance comes from the area of concrete. To calculate the resistance of one column we use the following equation, see American-Concrete-Institute (2008).

$$V_n = 0.53\sqrt{f'_c}\, b\, d + A_v\, f_y\, d/s,$$

where b is the width of the column, d is the depth of the column, s is the distance between stirrups and $f'c$ is the cylindric resistance of concrete, in this case we use $250\ kg/cm^2$. Finally A_v is the area of steel crossing a crack. The resistance of one floor is calculated as follows:

$$Resistance = V_n \cdot (\text{number of columns per floor})$$

The three models have the same amount of stirrups, and the only difference in resistance comes from the depth of each column that changes from the initial model to the optimal model.

Remark: It is important to notice that even though we change the first eigenfrequency of the building with our optimization method, we use the same pseudo-acceleration spectrum for both models, the initial one (with all the columns of the same depth) and the optimal model, because the Chilean legislation have a clause that requires a maximum amount of total shear solicitation on the building depending on the weight of the building, and both models have the same weight because that is one of the constraints of our optimization method (constant volume implies constant weight in our case). We use the pseudo-accelerations spectrum to calculate this maximum shear solicitation for the initial

model, and use the same amount of solicitations in the optimal model. For this reason both models, the initial and the optimal, have the same total shear solicitation and a change in the first eigenfrequency does not affect these shear solicitation because we use that Chilean legislation clause.

2.5. Results

As mentioned above, the 3-D model of the building has initially all columns with square section of 60x60 cm^2. We only make changes on the depth of the columns. We use a minimum depth $h_{min} = 30$ cm and a maximum depth $h_{max} = 90$ cm. We analyze the movement in the direction perpendicular to the plane in which the building is slender.

We show first the results of the optimization of the 2-D membrane model in FreeFem++. This optimization gives us the thickness of the membrane and then, as mentioned before, we extrapolate this thickness to the columns of the 3-D model of the building in ETABS.

Let us recall that the smallest eigenvalue is denoted by $\lambda_1 = \omega_1^2$. Then, $T_1 = \frac{2\pi}{\omega_1}$ is the period of the first eigenfunction.

Remark: We notice that the thickness of the optimal membrane is constant in the short direction, and only depends on the long direction of the membrane that corresponds with the vertical direction on the 3-D model of the building. This is because the displacements of the first eigenfunction of the membrane are in the perpendicular direction of the plane of the membrane. Thus, ∇u is zero in the short direction. Therefore the gradient $\frac{\partial J}{\partial h}$ does not variate its value in the short direction.

For this reason we use only the information in the long direction and change the columns depth only in the vertical direction.

2.5.1. Results for the 20 story building

In FreeFem++ we run the optimization described on section 2.3, to maximize the smallest eigenvalue of the membrane model. Figure 2.4 (left) shows the depth configuration of the columns proposed by the optimization in FreeFem++. Figure 2.4 (right) shows the convergence history.

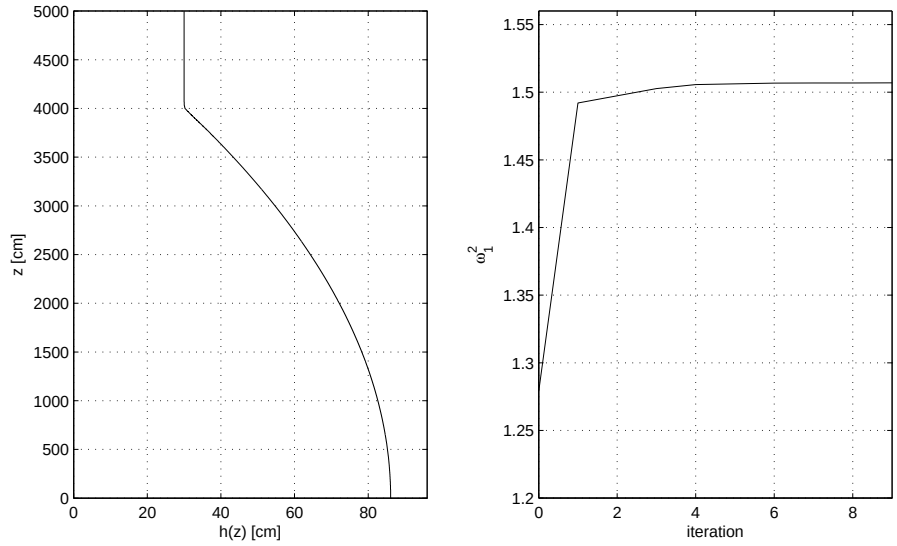

FIGURE 2.4. Proposed Thickness and Convergence History for the 20 story building.

We use the proposed thickness obtained by optimization in FreeFem++ in the columns of the 3-D model in ETABS. Then, we use the pseudo-acceleration spectrum described in the previous section to calculate solicitations and displacements in the 3-D model in ETABS. Remember that we use the pseudo-acceleration spectrum to calculate the maximum shear solicitation and maintain this solicitation in both models, initial and optimal.

Figure 2.5 shows both models, initial uniform (all columns with the same depth) and optimal, in ETABS. Figure 2.5 (up-left) shows a cut of the initial building in its slender

direction. Figure 2.5 (down-left) shows a cut of the optimal building in its slender direction. Figure 2.5 (up-right) shows the first eigenfunction of the initial building. Figure 2.5 (down-right) shows the first eigenfunction of the optimal building.

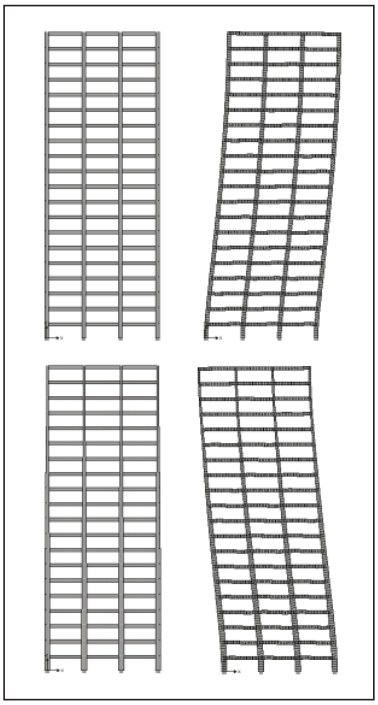

FIGURE 2.5. 20 Story building: initial and optimal in ETABS

We notice that the first eigenfunction of both models, initial and optimal, corresponds with the form of the displacements of the 2-D membrane, indicating that the surrogate model represents in a good way the displacements of the 3-D model in the slender direction.

We can see in figure 2.4 (left) that the optimal depth configuration of the columns tends to achieve the minimal value h_{min} on the upper floors of the building, and tends to h_{max} on the lower floors. For this reason we propose an initial condition different from the initial uniform condition (all columns of the same depth, $h_0 = 60cm$), this initial condition, divides the building into three equal parts, the lower one with thickness $h_{max} =$

$90cm$, a middle part with thickness $h_0 = 60cm$, and an upper part with thickness $h_{min} = 30cm$. Also we notice that the derivative of the proposed depth function, figure 2.4 (left), is not continuous in floor 16, for this reason we propose a smoothed depth configuration, that manually changes the depth of the columns on the sixteenth and seventeenth floors such that the derivative of this new configuration depth function is continuous. Figure 2.6 shows the proposed depth configuration of the columns.

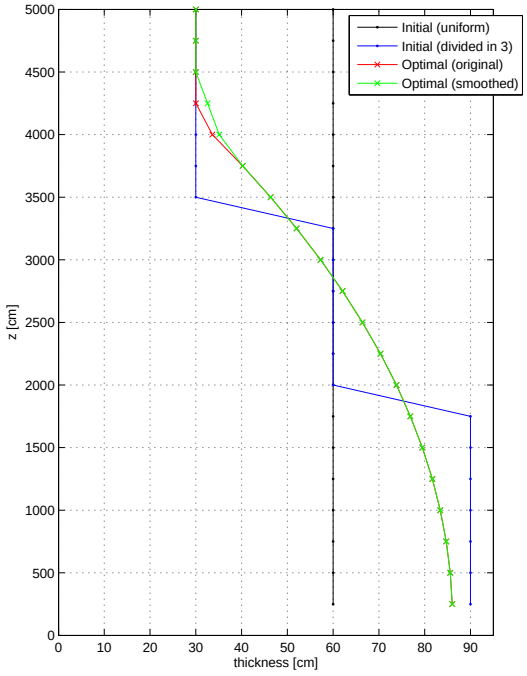

FIGURE 2.6. Depth configuration functions for the 20 story building.

Now we proceed to calculate the Drifts and Shear D/C Ratios.

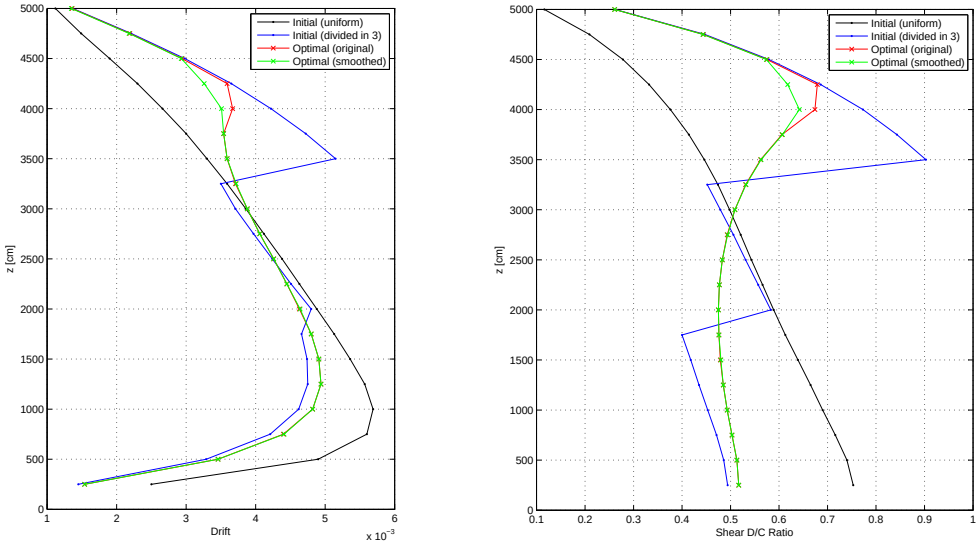

FIGURE 2.7. Drifts (left) and Shear D/C Ratios (right) for the 20 story building.

The initial (divided in 3) model has the worst results in Shear D/C Ratios because of the discontinuity in the thirteenth floor when we pass from depth $h_0 = 60cm$ to $h_{min} = 30cm$, this can cause the failure of the building in this floor. Also this model has the second maximal drift, after the initial (uniform) model.

Table 2.1 sumarizes the results obtained and also shows a comparison with the initial (uniform) model with both optimal models.

TABLE 2.1. Comparison between the optimal model and the initial model for the 20 story building.

	I.U.	O.O.	O.S.	% of Benefit (O.O.)	% of Benefit (O.S.)
$T =$ Period in sec. (from ETABS)	2.9901	2.8062	2.8033	6.15	6.25
Maximal Drift	0.0057	0.0049	0.0049	13.17	13.13
Maximal Shear D/C Ratio	0.75	0.68	0.64	9.83	14.76
Max. displacement on the top (cm)	19.00	18.69	18.56	1.64	2.29

I.U.=Initial uniform. O.O.=Optimal original. O.S.=Optimal smoothed.

The Optimal smoothed model has the lowest Shear D/C Ratios because by smoothing the depth configuration function in the Optimal original we ease the transition to h_{min} in the upper floors, and reducing the peak in the Shear D/C Ratios function in those floors. The reduction in Drifts are not significant because the optimal smoothed function is different from the optimal function.

It is important to notice that the Optimal smoothed model does not fully satisfy the volume constraint.

2.5.2. Results for the 10 story building

In FreeFem++ we run the optimization described on section 2.3, to maximize the smallest eigenvalue of the membrane model. Figure 2.8 (left) shows the depth configuration of the columns proposed by the optimization in FreeFem++. Figure 2.8 (right) shows the convergence history.

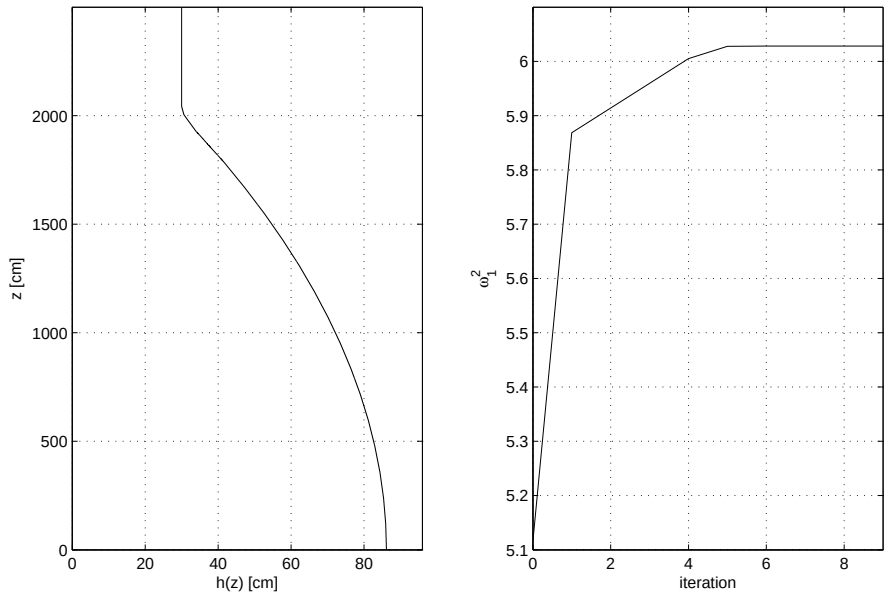

FIGURE 2.8. Proposed Thickness and Convergence History for the 10 story building.

We use the proposed thickness obtained by optimization in FreeFem++ in the columns of the 3-D model in ETABS. Then we use the pseudo-acceleration spectrum described in the previous section to calculate solicitations and displacements in the 3-D model in ETABS. Remember that we use the pseudo-acceleration spectrum to calculate the maximum shear solicitation and maintain this solicitation in both models, initial and optimal.

Figure 2.9 shows both models, initial uniform (all columns with the same depth) and optimal, in ETABS. Figure 2.9 (up-left) shows a cut of the initial building in its slender direction. Figure 2.9 (down-left) shows a cut of the optimal building in its slender direction. Figure 2.9 (up-right) shows the first eigenfunction of the initial building. Figure 2.9 (down-right) shows the first eigenfunction of the optimal building.

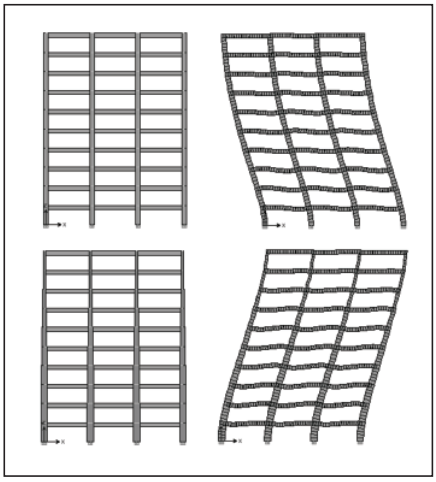

FIGURE 2.9. 10 Story building: initial and optimal in ETABS

We notice that the first eigenfunction of both models, initial and optimal, corresponds with the form of the displacements of the 2-D membrane, indicating that the surrogate model represents in a good way the displacements of the 3-D model in the slender direction.

Repeating the procedure of the previous building (20 story building), we generate an initial condition divided in three equal parts. Figure 2.10 shows the proposed depth configuration of the columns. Also we notice that the derivative of the proposed depth function, figure 2.8 (left), is not continuous in floor 8, for this reason we propose a smoothed depth configuration, that manually changes the depth of the columns on the eighteenth floor such that the derivative of this new configuration depth function is continuous. Figure 2.10 shows the proposed depth configuration of the columns.

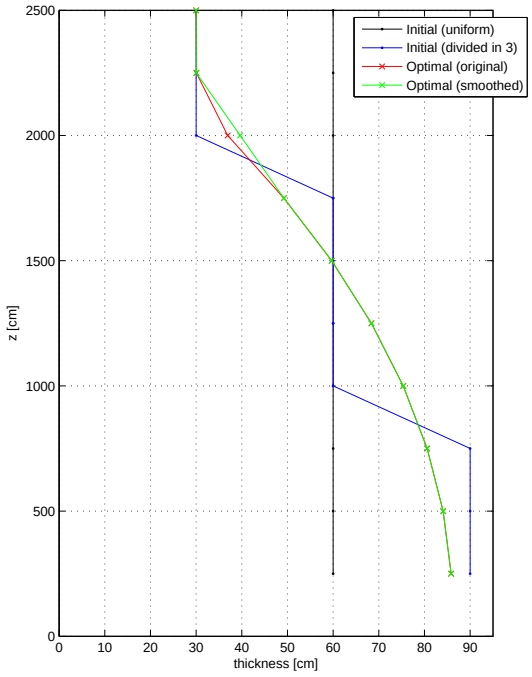

FIGURE 2.10. Depth configuration functions for the 10 story building.

Now we proceed to calculate the Drifts and the Shear D/C Ratios.

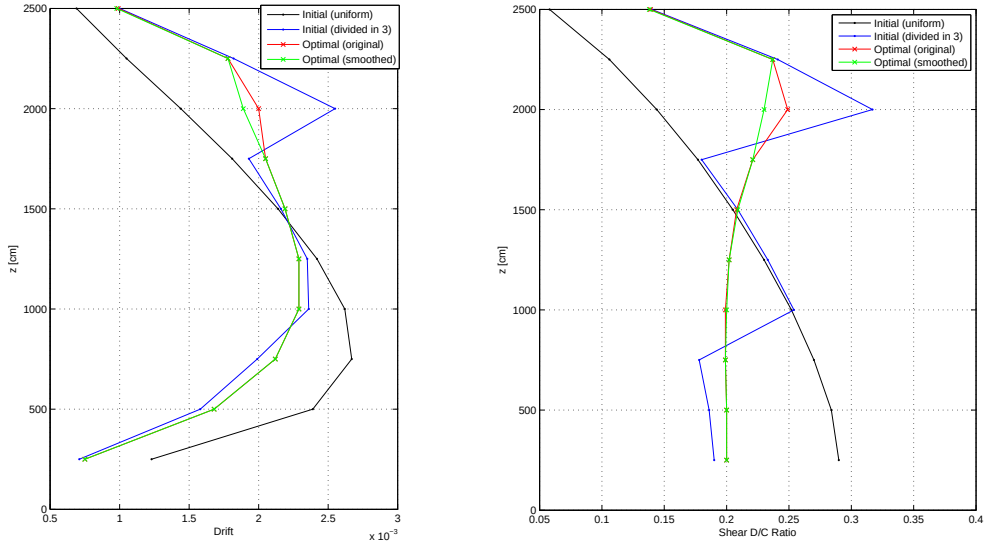

FIGURE 2.11. Drifts (left) and Shear D/C Ratios (right) for the 10 story building.

The initial (divided in 3) model has the worst results in Shear D/C Ratios because of the discontinuity in the seventh floor when we pass from depth $h_0 = 60cm$ to $h_{min} = 30cm$, this can cause the failure of the building in this floor. Also this model has the second biggest maximal drift, after the initial (uniform) model.

Table 2.2 summarizes the results obtained and also shows a comparison between the initial model having columns with equal depth and the optimal model.

TABLE 2.2. Comparison between the optimal model and the initial model for the 10 story building.

	I.U.	O.O.	O.S.	% of Benefit (O.O.)	% of Benefit (O.S.)
T = Period in sec. (from ETABS)	1.4143	1.3100	1.3076	7.37	7.54
Maximal Drift	0.0027	0.0023	0.0023	14.47	14.47
Maximal Shear D/C Ratio	0.29	0.25	0.24	14.22	18.45
Max. displacement on the top (cm)	4.61	4.53	4.50	1.76	2.48

I.U.=Initial uniform. O.O.=Optimal original. O.S.=Optimal smoothed.

The Optimal smoothed model has the lowest Shear D/C Ratios because by smoothing the depth configuration function in the Optimal original we ease the transition to h_{min} in the upper floors, reducing the peak in the Shear D/C Ratios function in those floors. The reductions in Drifts are not significant because the optimal smoothed function is quite similar to the original function.

It is important to notice that the Optimal smoothed model does not fully satisfy the volume constraint.

2.5.3. Results for the 9 story building

When a slender building is shorter than those shown above, the surrogate model of a membrane representing the 3-D model of the building is not accurate, because the first eigenfunction of the optimal building would not correspond with the displacements of the 2-D membrane. In the examples chosen for this thesis this problem occurs in buildings with less than 10 stories.

We model a 9 story building, and run the optimization algorithm described in the previous sections. Figure 2.5.3 (left) shows the first eigenfunction of the initial building in ETABS, and figure 2.5.3 (right) shows the first eigenfunction of the optimal building in ETABS.

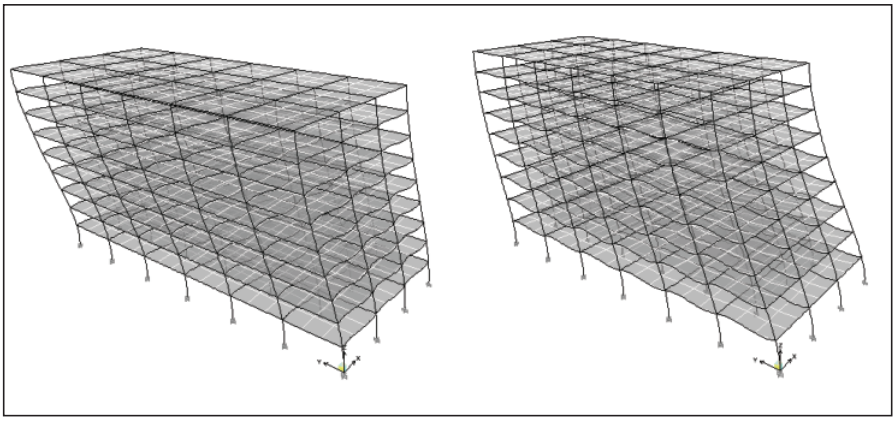

In this case the second eigenfunction of the optimal building corresponds with the displacements of the 2-D model. Hence the surrogate model is not accurate for the optimization in slender buildings with less than 10 stories, with the geometric characteristics described at the beginning of this chapter.

3. FULL HOMOGENIZATION

3.1. Full Homogenization Method

The full homogenization method is a technique developed by F.Murat and L.Tartar in Murat and Tartar (1983). Its main objective is to obtain characteristic of an element or domain composed of a mixture of two different materials. The mixture of this two materials is in a micro-scale with a very small size or diameter, called ε. The full homogenization method gives us sufficient conditions to pass to the limit when ε goes to 0^+. It is important to notice that the micro-scale does not go to the level of the atomic particles of the material, but it is sufficiently small so the heterogeneity in the small scale fades to an homogeneous material at the macro-scale.

The full homogenization theory gives us the tools to safely apply the limit when ε goes to 0 and obtain the characteristics of the homogenized material with proportion θ of the more rigid material B and $1-\theta$ of the less rigid material A.

Note that θ can take values in the interval $[0,1]$, thus by taking the limit $\varepsilon \to 0$ we are allowing designs with fine mixtures of the two materials, and that is impossible in practice. But this relaxation, in general, makes the problem well-posed and makes possible to find an optimal design that afterwards, by means of penalization (see 3.2.4), can be passed to a classical or constructible design.

An advantage of the full homogenization method is that it can be used in the elasticity setting. Hence, with this method, we can model more complex structures such as shear walls and bridges.

Another important feature of the method is that, thanks to the relaxation we make by allowing fine mixtures, we can develop optimization algorithms for different objective functions, in our case to maximize the first eigenvalue (square of the first eigenfrequency) of a domain containing two elastic materials.

There are two optimization methods based on full homogenization, one is the so called optimality criteria method and the second is the gradient method. Sometimes both methods are complementary as seen in example $iii)$ in 3.2.6.1.

In this chapter we briefly describe the mathematical basis of the two methods and show some numerical examples in order to validate the methods. A more complete description of the method can be found in Allaire (2002) and specifically for Eigenfrequency optimization in Allaire et al. (2001).

3.2. Full Homogenization in 2D

3.2.1. Mathematical Model

Let $\Omega \subset \mathbb{R}^2$ be a bounded open set in $\mathbb{R}^2$. In Ω we have two linearly elastic materials with elasticity tensors A and B. Let ϵ be a positive real number, $\epsilon \approx 0$, such that $A = \epsilon B$. This way A is the tensor of a very flexible material, and in the limit when $\epsilon \to 0^+$ imitates void.

Let $\chi(x) \in L^\infty(\Omega; \{0, 1\})$ be a characteristic function of the most rigid material, i.e., $\chi(x) = 1$ if material B is present at x, and $\chi(x) = 0$ otherwise. The heterogeneous Hooke's law in Ω is

$$A_\chi(x) = (1 - \chi(x))\, A + \chi(x) B$$

The heterogeneous density in Ω is

$$\rho_\chi(x) = (1 - \chi(x))\, \rho_A + \chi(x) \rho_B$$

where $\rho_A, \rho_B > 0$ are the mass densities of the materials.

The boundary $\partial\Omega$ is divided in two disjoint parts Γ_D and Γ_N supporting respectively Dirichlet boundary condition (zero displacement) and Neumann boundary condition (zero traction).

The vibration frequencies ω of the heterogeneous domain Ω, filled by A and B, are the square roots of the eigenvalues of the following problem:

$$\left.\begin{array}{rcll} -\text{div}\,(A_\chi\, e(u)) & = & \omega^2 \rho_\chi u & \text{in}\,\Omega \\ A_\chi\, e(u)\cdot \vec{n} & = & 0 & \text{on}\,\Gamma_N \\ u & = & 0 & \text{on}\,\Gamma_D \end{array}\right\} \tag{3.1}$$

where $u \in H^1(\Omega)^2$ is the displacement vector, and $e(u) = \frac{1}{2}\left(\nabla u + \nabla^t u\right)$ is the strain tensor. As is well known, problem (3.1) admits a countable family of positive eigenvalues

$$0 < \omega_1^2 \leq \omega_2^2 \leq ... \leq \omega_k^2 \to +\infty\,,$$

In this work we want to maximize the first eigenvalue, which is given by the following formula

$$\omega_1^2 = \min_{u\in\mathcal{H}} \frac{\displaystyle\int_\Omega A_\chi e(u)\cdot e(u)\,dx}{\displaystyle\int_\Omega \rho_\chi\,|u|^2\;dx}$$

where $\mathcal{H} = \{u \in H^1(\Omega)^2 \,|\, u = 0\,\text{on}\,\Gamma_D\}$.

We want to find the best arrangement of A and B in Ω that would maximize ω_1^2. If we assume that $\rho_A = \rho_B$, the problem has a trivial solution, that is to fill Ω with the most rigid material B only. Therefore, we add a constraint on the volume of B. Introducing a Lagrange multiplier $l \in \mathbb{R}$, our objective functional is

$$\sup_{\chi\in L^\infty(\Omega;\{0,1\})} \left\{\omega_1^2(\chi) - l\int_\Omega \chi(x)\,dx\right\} \tag{3.2}$$

We want to find a sequence of characteristic functions $\chi_n(x)$ that maximize (3.2). But it is known that this problem admits no optimal solution. Hence, one needs to enlarge the class of admissible designs by allowing fine mixtures of the two materials in a scale which is much smaller than the mesh used for the actual computation. Full homogenization gives us the tools to determine the effective properties of these fine mixtures and find the optimal ones. In the case of eigenfrequency optimization, the set of effective elasticity tensors

can be computed among the well-known subset of sequential laminates. This process of enlarging the set of admissible designs in order to get a well-posed problem is called relaxation. The derivation of the relaxed formulation was done by the pioneering work of Murat and Tartar, see Murat and Tartar (1983). Now we briefly sketch it for the reader.

Let $\{\chi_n\} \subseteq L^\infty(\Omega;\{0,1\})$ be a maximizing sequence for (3.2). We want to pass to the limit in (3.2) and compute its maximal value. The sequence $\chi_n(x)$ is bounded in $L^\infty(\Omega)$, therefore one can extract a subsequence, still denoted by $\chi_n(x)$, such that it converges weakly-* in $L^\infty(\Omega)$ to a limit $\theta(x)$. The limit $\theta(x)$ has no reason to be a characteristic function, but is rather a density, i.e., it belongs to $L^\infty(\Omega;[0,1])$. According to the theory of H- or G-convergence (see Murat and Tartar (1983)), a subsequence of $A_{\chi_n} = (1-\chi_n(x))A+\chi_n(x)B$ H- or G-converges to a homogenized tensor A^* as $n \to \infty$. As a consequence the eigenvalue $(\omega_1^n)^2$ and its corresponding normalized eigenvector u_1^n, solutions of

$$\left.\begin{array}{rcll} -\text{div}\,(A_{\chi_n}\, e(u_1^n)) &=& (\omega_1^n)^2 \rho_{\chi_n} u_1^n & \text{in}\,\Omega \\ A_{\chi_n}\, e(u_1^n)\cdot \vec{n} &=& 0 & \text{on}\,\Gamma_N \\ u_1^n &=& 0 & \text{on}\,\Gamma_D \end{array}\right\} \tag{3.3}$$

satisfy $\lim_{n\to+\infty} \omega_1^n = \omega_1$, and the sequence of eigenvectors u_1^n converges weakly in $H^1(\Omega)^2$ and strongly in $L^2(\Omega)^2$ to a limit eigenvector u_1 such that

$$\left.\begin{array}{rcll} -\text{div}\,(A^*\, e(u_1)) &=& (\omega_1)^2 \bar{\rho} u_1 & \text{in}\,\Omega \\ A^*\, e(u_1)\cdot \vec{n} &=& 0 & \text{on}\,\Gamma_N \\ u_1 &=& 0 & \text{on}\,\Gamma_D \end{array}\right\} \tag{3.4}$$

with $\bar{\rho}(x)$, the weak limit of the sequence ρ_{χ_n}, i.e.,

$$\bar{\rho}(x) = (1-\theta(x))\rho_A + \theta(x)\rho_B\,,$$

A^* belongs to $\mathcal{G}_\theta$, defined by

$$\mathcal{G}_\theta = \{\text{H-limits of } A_{\chi_n} = (1-\chi_n)A + \chi_n B \,|\, \chi_n \rightharpoonup \theta\}$$

Thanks to the work of Francfort and Murat (see Francfort and Murat (1986)), following the lead of Tartar (see Tartar (1985)), we can find the optimal elasticity tensor A^* in the subset $L_\theta \subset G_\theta$ of sequential laminates obtained by laminating B around a core of A in proportion θ and $1-\theta$ respectively. Where G_θ is the closure of the set of effective Hooke's laws obtained by periodic homogenization of a mixture of A and B in proportions $1-\theta$ and θ.

Thus, we define a relaxed objective functional by

$$\max_{\theta \in L^\infty(\Omega;[0,1])} \max_{A^* \in L_\theta} \left\{ \omega_1^2(\theta, A^*) - l \int_\Omega \theta(x)\, dx \right\}, \tag{3.5}$$

The new material is built by laminating a proportion θ_1 of B with a proportion $1-\theta_1$ of A in one direction, let us say e^1, and then the resultant tensor A^1 is laminated again, let us say in a direction e^2, and in proportion θ_2 with one of the pure materials, say A, and obtain A^*, a rank 2 laminate. Figure 3.1 illustrate the situation.

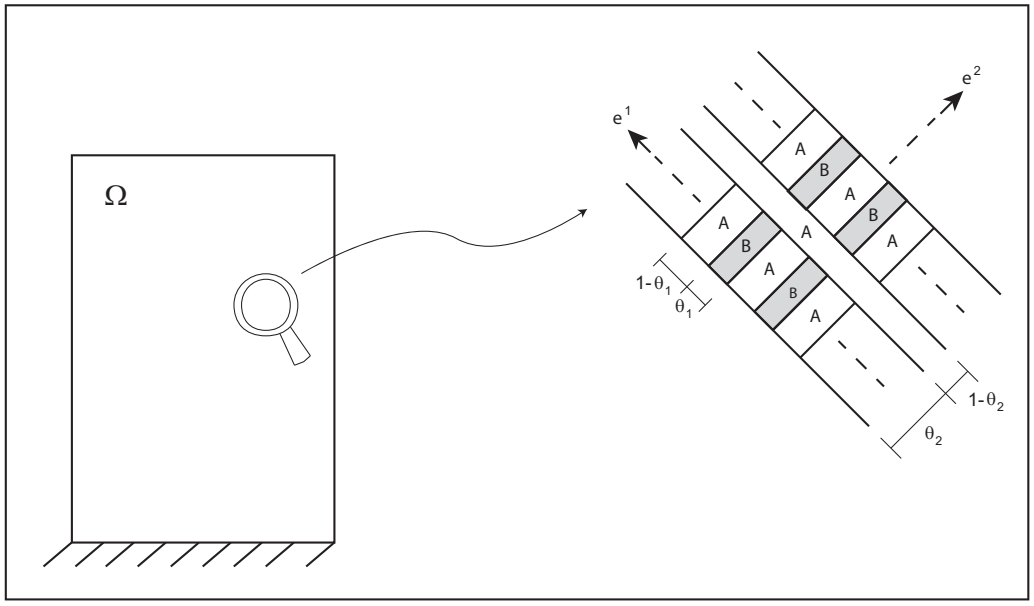

FIGURE 3.1. Homogenized Material

Its effective tensor is obtained from equation (2.68) in Allaire (2002) by interchanging the roles of A and B and calling A_p^* as A^*,

$$A^* = B + (1-\theta)\left((A-B)^{-1} + \theta\left(m_1\, f_B(e^1) + m_2\, f_B(e^2)\right)\right)^{-1} \tag{3.6}$$

Where $\theta = \theta_1\theta_2$ is the total proportion of material B, the unit vectors e^1, e^2 are the lamination directions, and the real numbers $0 \leq m_1, m_2 \leq 1$ such that $\sum_{i=1}^{2} m_i = 1$, are the lamination parameters, and $f_B(e^i)$ is a nonpositive definite fourth-order tensor defined for any symmetric matrix ξ by the following quadratic form

$$f_B(e^i)\xi : \xi = \frac{1}{\mu}\left|\xi\, e^i\right|^2 - K\left(\xi\, e^i \cdot e^i\right)^2 \tag{3.7}$$

where $K = \frac{\mu+\lambda}{\mu(2\mu+\lambda)}$ and μ, λ are the Lamé parameters of material B.

In appendix A.3.4 we verify equation (3.6) obtaining the effective elasticity tensor using successive laminations in perpendicular directions (see Gutiérrez (1998) and Gutiérrez (2004)) and compare the results.

3.2.2. Optimality criteria method

By means of theorem $(2.3.35)$ in Allaire (2002) we can find the optimal lamination parameters and lamination directions in order to maximize our objective function. This is called the optimality criteria method.

If the eigenvalues of the stress tensor $\sigma = A^* e(u_1)$ are σ_1 and σ_2, given by

$$\sigma_1 = \frac{1}{2}\left(\sigma_{11} + \sigma_{22} + \sqrt{(\sigma_{11}-\sigma_{22})^2 + 4\sigma_{12}^2}\right),$$

$$\sigma_2 = \frac{1}{2}\left(\sigma_{11} + \sigma_{22} - \sqrt{(\sigma_{11}-\sigma_{22})^2 + 4\sigma_{12}^2}\right),$$

The lamination parameters are

$$m_1 = \frac{|\sigma_2|}{|\sigma_1| + |\sigma_2|} \qquad \text{and} \qquad m_2 = \frac{|\sigma_1|}{|\sigma_1| + |\sigma_2|},$$

therefore the intermediate proportions are:

$$\theta_1 = \frac{|\sigma_1| + \theta|\sigma_2|}{|\sigma_1| + |\sigma_2|} \qquad \text{and} \qquad \theta_2 = \frac{\theta(|\sigma_1| + |\sigma_2|)}{|\sigma_1| + \theta|\sigma_2|}.$$

The lamination directions are chosen as the eigenvectors of σ. Then

$$e^1 = \begin{pmatrix} \frac{\sigma_{12}}{\sqrt{\sigma_{12}^2+(\sigma_1-\sigma_{11})^2+\delta^2}} \\ \\ \frac{\sigma_1-\sigma_{11}}{\sqrt{\sigma_{12}^2+(\sigma_1-\sigma_{11})^2+\delta^2}} \end{pmatrix} \quad e^2 = \begin{pmatrix} e_y^1 \\ -e_x^1 \end{pmatrix},$$

where $\delta = \epsilon\, 10^{-6}$ is introduced to avoid numerical problems in FreeFem++.

The optimal density of rigid material is chosen by:

$$\theta = \min\left\{1, \sqrt{\frac{g^*(\sigma)}{l \int_\Omega \bar{\rho}\,|u|^2}}\right\},$$

where:

$$\begin{aligned} g^*(\sigma) &= \tfrac{2\mu+\lambda}{4\mu(\mu+\lambda)}\left(|\sigma_1| + |\sigma_2|\right)^2 \\ l &= \text{Lagrange multiplier for the volume constraint of the rigid material} \\ \bar{\rho} &= \theta_p\,\rho_B + (1-\theta_p)\,\rho_A \\ \theta_p &= \text{optimal density of rigid material obtained in the previous iteration} \\ u &= \text{first eigenvector obtained in the previous iteration.} \end{aligned}$$

Appendix A.1.2 shows the implementation of the method in the 2D setting, to be programmed in FreeFem++.

3.2.3. Gradient Method

As in the previous sections, $\Omega \subset \mathbb{R}^2$ is a bounded open set containing two elastic materials with elasticity tensors A and B. Being A the elasticity tensor of a very flexible material.

We want to make a mixture of these two materials in proportions θ of B and $1-\theta$ of A. The new material is built by laminating a proportion θ_1 of B with a proportion $1-\theta_1$ of A in one direction, let us say e^1, and then the resultant tensor A^1 gets laminated again, let us say in direction e^2, and in proportion θ_2 with one of the pure materials, say A, and obtain A^*, a rank 2 laminate. See figure 3.2.

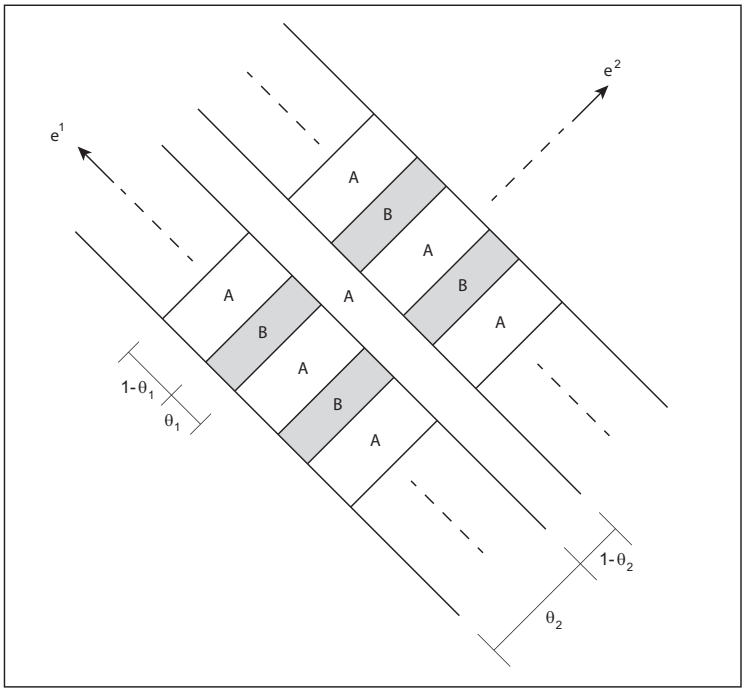

FIGURE 3.2. Laminated Material

The basis of the method is to differentiate the first eigenvalue with respect to the design parameters, we still assume that the first eigenvalue is simple, and thus differentiable. A gradient method for maximizing the first eigenvalue ensures that it will always increase through the iterations (although it can fall into a local maximum).

By theorem $4.1.46$ in Allaire (2002) we can restrict the set G_θ of homogenized Hooke's laws A^* to the subset of rank-2 sequential laminates with orthogonal lamination directions. Such a laminated composite is parameterized by three variables: The density of

rigid material (B) $\theta \in [0,1]$, the lamination parameter $m \in [0,1]$, and an angle of rotation $\phi \in [0,\pi]$. More precisely, by formula (2.69) in Allaire (2002) its homogenized Hooke's law $A^*(\theta,\phi,m)$ is given by

$$(1-\theta)\,(A^*-B)^{-1} = (A-B)^{-1} + \theta R(\phi)^t \left(m\, f_B(e^1) + (1-m)\, f_B(e^2)\right) R(\phi)$$

Solving for $A^*(\theta,\phi,m)$

$$A^* = B + (1-\theta)\left[(A-B)^{-1} + \theta R(\phi)^t \left(m\, f_B(e^1) + (1-m)\, f_B(e^2)\right) R(\phi)\right]^{-1}$$

where (e^1,e^2) is the canonical basis of $\mathbb{R}^2$, $R(\phi)$ is a fourth order tensor corresponding to a rotation $Q(\phi)$ of angle ϕ in the physical space $\mathbb{R}^2$ defined by
$R(\phi)\xi = Q^t(\phi)\xi Q(\phi)$, where $\xi \in Sim_{2\times 2}$

$$Q(\phi) = \begin{bmatrix} cos(\phi) & -sin(\phi) \\ sin(\phi) & cos(\phi) \end{bmatrix} \qquad Q^t(\phi) = Q^{-1}(\phi) = \begin{bmatrix} cos(\phi) & sin(\phi) \\ -sin(\phi) & cos(\phi) \end{bmatrix}$$

$R(\phi)^{-1}\xi = Q(\phi)\xi Q^t(\phi)$

and $f_B(e)$ is defined, for any symmetric matrix ξ, by

$$f_B(e)\xi : \xi = \frac{1}{\mu}\,|\xi\, e|^2 - K\,(\xi\, e\cdot e)^2$$

where $K = \frac{\mu+\lambda}{\mu(2\mu+\lambda)}$ and $\mu\,,\lambda$ are the Lamé parameters of the rigid material B.

As new design parameters, we choose the material density $\theta \in [0,1]$, the angle of rotation $\phi \in [0,\pi]$, and the proportion $m \in [0,1]$. The relaxed optimal design problem is equivalent to

$$\max_{(\theta,\phi,m)\in L^\infty(\Omega;[0,1]\times[0,\pi]\times[0,1])} \left\{ J^*(\theta,\phi,m) = \omega_1^2(\theta,\phi,m) + l\int_\Omega \theta\, dx \right\},$$

where ω_1^2 is the first eigenvalue of

$$\left.\begin{array}{rcll} -\text{div}\,(A^*\,e(u)) & = & \omega^2\bar{\rho}u & \text{in}\,\Omega \\ A^*\,e(u)n & = & 0 & \text{on}\,\Gamma_N \\ u & = & 0 & \text{on}\,\Gamma_D \end{array}\right\} \tag{3.8}$$

and is given by

$$\omega_1^2(\theta, A^*) = \min_{u\in\mathcal{H}} \frac{\displaystyle\int_\Omega A^* e(u) : e(u)\,dx}{\displaystyle\int_\Omega \bar{\rho}\,|u|^2\;dx}\,.$$

with $\bar{\rho} = \theta\rho_B + (1-\theta)\rho_A$, where $\rho_B, \rho_A > 0$ are the densities of materials B and A respectively.

$\mathcal{H}$ is the displacement space, defined by

$$\mathcal{H} = \left\{u \in H^1(\Omega)^2 \text{ such that } u = 0 \text{ on } \Gamma_D\right\}\,,$$

We assume the parameters $(\theta, \phi, m) \in L^\infty(\Omega; [0,1]\times[0,\pi]\times[0,1])$ are such that the first eigenvalue $\omega_1^2(\theta,\phi,m)$ is simple. Then, for a given direction $(\delta\theta, \delta\phi, \delta m) \in L^\infty(\Omega)^3$, we define a function of t in the neighborhood of zero by

$$F(t) = J^*(\theta + t\delta\theta, \phi + t\delta\phi, m + t\delta m)\,.$$

By a classical result of spectral perturbation, for sufficiently small positive values of t the first eigenvalue in $F(t)$ is simple and $F(t)$ is differentiable.

Then J^* is Gateaux differentiable at (θ,ϕ,m),

$$F'(0) = \delta J^*(\theta,\phi,m) = \int_\Omega \nabla_\theta J^*\delta\theta\,dx + \int_\Omega \nabla_\phi J^*\delta\phi\,dx + \int_\Omega \nabla_m J^*\delta m\,dx$$

with partial derivatives given by

$$\begin{aligned}
\nabla_\theta J^* &= \frac{\frac{\partial A^*}{\partial \theta} e(u) : e(u) - \omega_1^2 (\rho_B - \rho_A) |u|^2}{\int_\Omega \bar{\rho} |u|^2 \, dx} + l \\
\nabla_\phi J^* &= \frac{\frac{\partial A^*}{\partial \phi} e(u) : e(u)}{\int_\Omega \bar{\rho} |u|^2 \, dx} \\
\nabla_m J^* &= \frac{\frac{\partial A^*}{\partial m} e(u) : e(u)}{\int_\Omega \bar{\rho} |u|^2 \, dx} \,,
\end{aligned}$$

where u is the first eigenvector of (3.8) associated to the first eigenvalue $\omega_1^2(\theta, \phi, m)$ and

$$\begin{aligned}
\frac{\partial A^*}{\partial \theta} &= -T^{-1} - (1-\theta) T^{-1} M(\phi, m) T^{-1} \\
\frac{\partial A^*}{\partial \phi} &= -\theta(1-\theta) T^{-1} \frac{\partial M}{\partial \phi} \, T^{-1} \\
\frac{\partial A^*}{\partial m} &= -\theta(1-\theta) T^{-1} S \, T^{-1}
\end{aligned}$$

with

$$\begin{aligned}
M(\phi, m) &= R(\phi)^t (m f_B(e^1) + (1-m) f_B(e^2)) R(\phi) \,, \\
T(\theta, \phi, m) &= (A - B)^{-1} + \theta M(\phi, m) \,, \\
S(\phi) &= R(\phi)^t (f_B(e^1) - f_B(e^2)) R(\phi) \,.
\end{aligned}$$

We have to use the standard isometry (see A.1.1) to obtain these relationships in the space of 3×3 matrices in order to implement the method in FreeFem++. The process is very similar to the one described in section 3.2.2 with the complication that the fourth-order tensor f_B has a rotation in between.

Let $\xi \in Sim_{2\times 2}(\mathbb{R})$. Then

$$\begin{aligned} R^T(\phi) f_B(e) R(\phi)\, \xi : \xi &= R^T(\phi) f_B(e) Q^T(\phi) \xi Q(\phi) : \xi \\ &= R^T(\phi) f_B(e) \tilde{\xi} : \xi\,, && \text{where } \tilde{\xi} = Q^T(\phi)\xi Q(\phi) \\ &= R^T(\phi) \tilde{\psi} : \xi\,, && \text{where } \tilde{\psi} = f_B(e)\tilde{\xi} \\ &= Q(\phi)\tilde{\psi} Q^T(\phi) : Q(\phi)\tilde{\xi} Q^T(\phi) \\ &= \tilde{\psi} : \tilde{\xi} \end{aligned}$$

Because the inner product remains unchanged under a rotation . And replacing $\tilde{\psi}$ we get:

$$R^T(\phi) f_B(e) R(\phi)\, \xi : \xi = f_B(e)\, \tilde{\xi} : \tilde{\xi}\,.$$

Therefore we use the rotated base of $Sim_{2\times 2}$.

$$\begin{aligned} \tilde{A}^1 &= Q^T(\phi) A^1 Q(\phi) = \begin{bmatrix} cos^2(\phi) & -cos(\phi)sin(\phi) \\ -cos(\phi)sin(\phi) & sin^2(\phi) \end{bmatrix} \\ \tilde{A}^2 &= Q^T(\phi) A^2 Q(\phi) = \begin{bmatrix} sin^2(\phi) & cos(\phi)sin(\phi) \\ cos(\phi)sin(\phi) & cos^2(\phi) \end{bmatrix} \\ \tilde{A}^3 &= Q^T(\phi) A^3 Q(\phi) = \begin{bmatrix} sin(2\phi) & cos(2\phi) \\ cos(2\phi) & -sin(2\phi) \end{bmatrix} \end{aligned}$$

We use this base to calculate the components of the gradient vector $\nabla_\theta J^*$, $\nabla_\phi J^*$ and $\nabla_m J^*$ through the tensors $M(\phi, m)$, $T(\theta, \phi, m)$ and $S(\phi)$. Then we can develop a gradient algorithm.

3.2.4. Penalization

Penalization is a process used during the iterations of the computational algorithm to obtain classical designs, say for example, if the density of rigid material is close to 1 the penalization process replaces the density by 1. See Allaire (2002) chapter 5.2.4.

3.2.5. Computational Algorithm

We develop computational algorithms based on the optimality criteria method, and if necessary, we pass to a gradient method, namely when the optimality criteria method does not give satisfactory results. These algorithms are written in the free finite element software FreeFem++.

3.2.5.1. Optimality criteria method

Section 3.2.2 shows the formulas necessary to implement an algorithm, sometimes called Alternate Directions algorithm. The algorithm is constructed as follows:

1. Initialization of the design parameters (θ_0, A_0^*) (for example, taking $\theta_0 = 0.35$ and $A_0^* = \theta_0 B + (1 - \theta_0)A$ everywhere in the domain).

2. Iteration until convergence, for $k \geq 0$:

   (a) Computation of the first eigenvector u_k with the previous design parameters θ_k, A_k^*, and calculate σ_k.

   (b) Updating of the design variables $(\theta_{k+1}, A_{k+1}^*)$ by using the stress σ_k in the explicit optimality formulas.

3.2.5.2. Gradient method

Section 3.2.3 shows the formulation to obtain the gradient $\delta J^*(\theta, \phi, m) = (\nabla_\theta J^*(\theta, \phi, m), \nabla_\phi J^*(\theta, \phi, m), \nabla_m J^*(\theta, \phi, m))$ of the objective function J^*. But, since there are constraints on the parameters m and θ (which must stay both in the range $[0, 1]$), the formulas for the gradient are combined with a projection step in order to satisfy the constraints. The projected gradient algorithm is thus:

1. Initialization of the design parameters θ_0, ϕ_0, m_0 (for example, we take them to be constant).

2. Iteration until convergence, for $k \geq 0$:

   (a) Computation of the first eigenvector u_k with the previous design parameters θ_k, ϕ_k, m_k.

   (b) Updating of these parameters by

$$\begin{aligned} \theta_{k+1} &= \max(0, \min(1, \theta_k + t_k \nabla_\theta J_k^*)) \,, \\ m_{k+1} &= \max(0, \min(1, m_k + t_k \nabla_m J_k^*)) \,, \\ \phi_{k+1} &= \phi_k + t_k \nabla_\phi J_k^* \end{aligned}$$

   where $t_k > 0$ is a small step such that

$$J^*(\theta_{k+1}, \phi_{k+1}, m_{k+1}) > J^*(\theta_k, \phi_k, m_k) \,.$$

A good step t_k is computed through a line search that may be expensive, especially if there is also a total volume constraint. (Recall that each evaluation of the objective function requires the solution of an eigenvalue problem.) The gradient method is usually more expensive than the optimality criteria method (section 3.2.2). Therefore, in practice the best strategy is to start with the optimality criteria method and switch to the gradient method only when the computed eigenvalue becomes lower than the previous one.

3.2.6. Applications

3.2.6.1. Shear Wall

Walls designed to support shear forces in a building, due to wind or seismic solicitations, for example, are called Shear Walls. This walls are of major concern in structural

engineering because they are usually in the first floors of the building and if one of these walls collapse, probably the whole building will collapse.

In order to validate the method, we show the examples from Allaire et al. (2001), that are solved. We show that the method described in this chapter delivers optimal designs for the reinforcement of Shear Walls, because by maximizing the first eigenvalue of the wall (square of the first eigenfrequency) we can improve the behavior of this kind of walls against lateral solicitations such as wind and earthquakes.

We run the optimization algorithm for three different domains. They contain two elastic materials, a more rigid one with elasticity modulus $E = 9/7$ (all the parameters are dimensionless to avoid numerical problems in FreeFem++) and density $\rho = 1$, and a weaker one with elasticity modulus $E' = 0,01\,E$ and density $\rho = 0,01$. Also a resource constraint for the most rigid material of $\theta_0 = 0,35$, namely only 35% of the domain, because if not the problem has an obvious solution of filling the domain with the most rigid material.

We choose three different domains to run the optimization described in 3.2.5, $i)$ Ω is a 1×2 rectangle with a small fixed zone of density 10 in the middle of the upper side, $ii)$ Ω is a 1×2 rectangle with two small fixed zones of density 10 in the left and right corners of the upper side, and $iii)$ Ω is a 2×1 rectangle with a small fixed zone of density 10 in the middle of the upper side.

$i)$ First we choose a domain $\Omega \subset \mathbb{R}^2$ as a wall with dimensions 1×2, say 1 in the fixed bottom and 2 of height. Figure 3.3 shows the initial configuration of the problem, notice that we fix a small zone of density 10 in the middle of the upper side because if not, the optimal design will not connect the top of the wall with the fixed bottom of the wall.

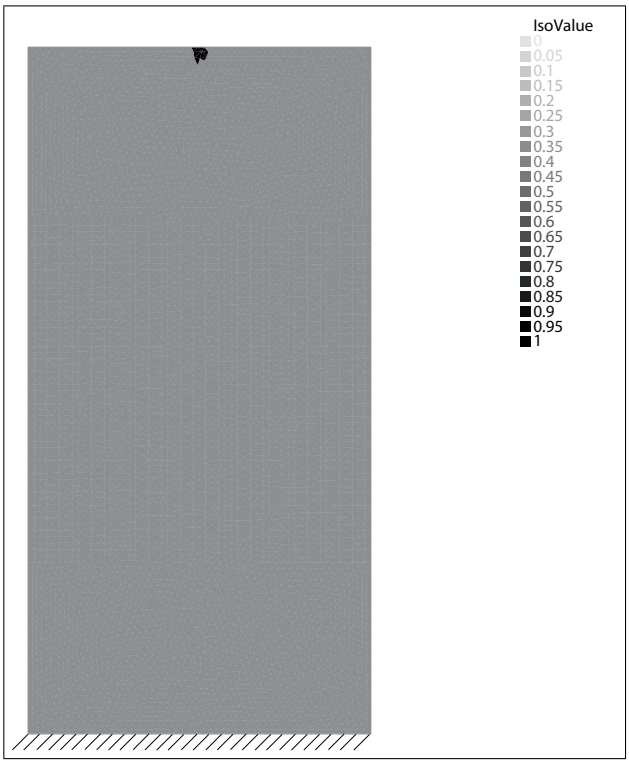

FIGURE 3.3. Initial configuration and boundary conditions for domain i)

In this case it is not necessary to use the gradient method of section 3.2.5.2 because the optimality criteria method of section 3.2.5.1 does not oscillate nor decrease the objective function between two or more consecutive iterations as seen in figure 3.6. After few iterations we obtain a design with many homogenized areas with density $\theta \in]0, 1[$, see figure 3.4.

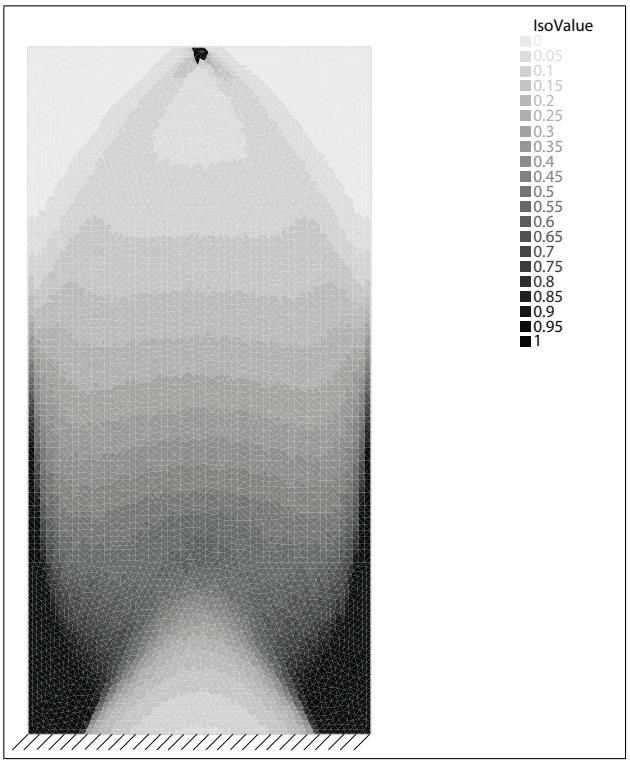

FIGURE 3.4. Optimal design without penalization

Then we run additional iterations of the algorithm but using penalization and obtain a penalized or classical design, see figure 3.5.

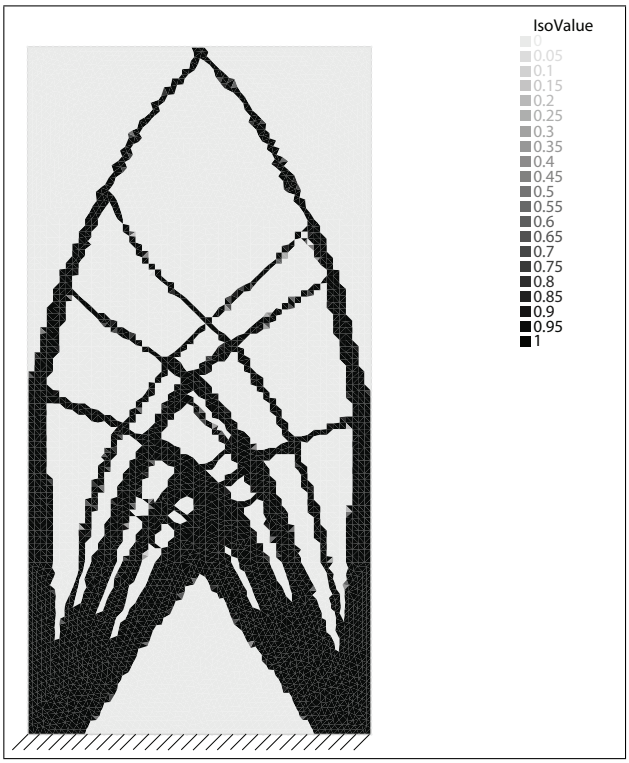

FIGURE 3.5. Optimal design with penalization

The first eigenvalue (square of the first eigenfrequency) of the penalized optimal design is multiplied by 8.29 compared to the first eigenvalue of the initial configuration in figure 3.3.

Now we show the converge history of the method.

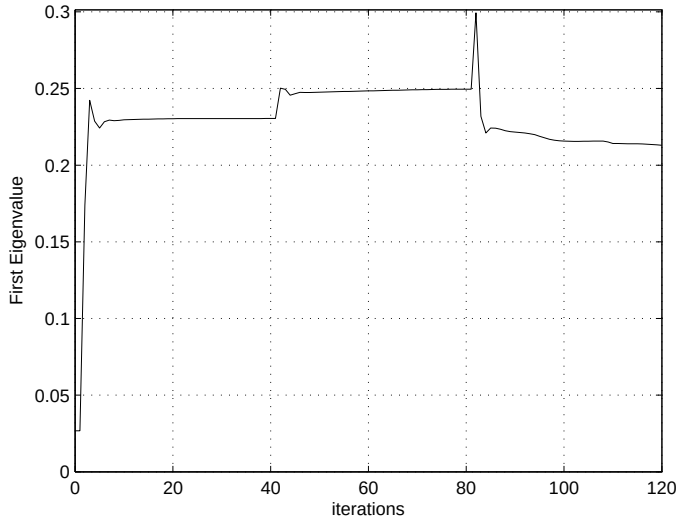

FIGURE 3.6. Convergence history

The peaks at iteration 40 and 80 are due to not fulfilling the volume of rigid material constraint because of the partial penalization at iteration 40 and full penalization at iteration 80.

$ii)$ Second, we choose a domain $\Omega \subset \mathbb{R}^2$ as a wall with dimensions 1×2, say 1 in the fixed bottom and 2 of height. Figure 3.7 shows the initial configuration of the problem, notice that we fix two small zones of density 10 in the left and right corners of the upper side of the domain because if not, the optimal design will not connect the upper corners of the wall with the fixed bottom of the wall. Another reason to do this is that the optimal design would be more constructible, say with reinforcement similar to classical walls with vertical bars on the sides.

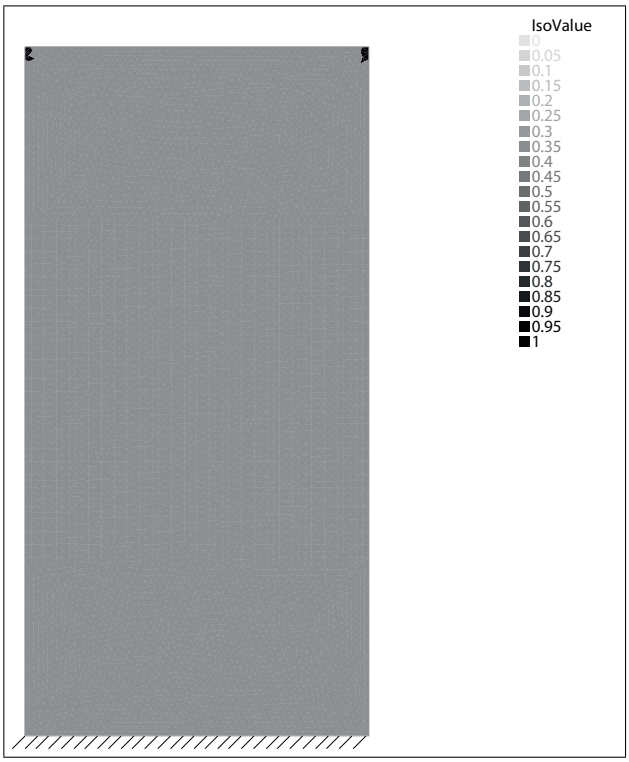

FIGURE 3.7. Initial configuration and boundary conditions for domain ii)

Like the previous case we also does not need to use the Gradient method. After few iterations we obtain a design with many homogenized areas with density $\theta \in]0, 1[$, see figure 3.8.

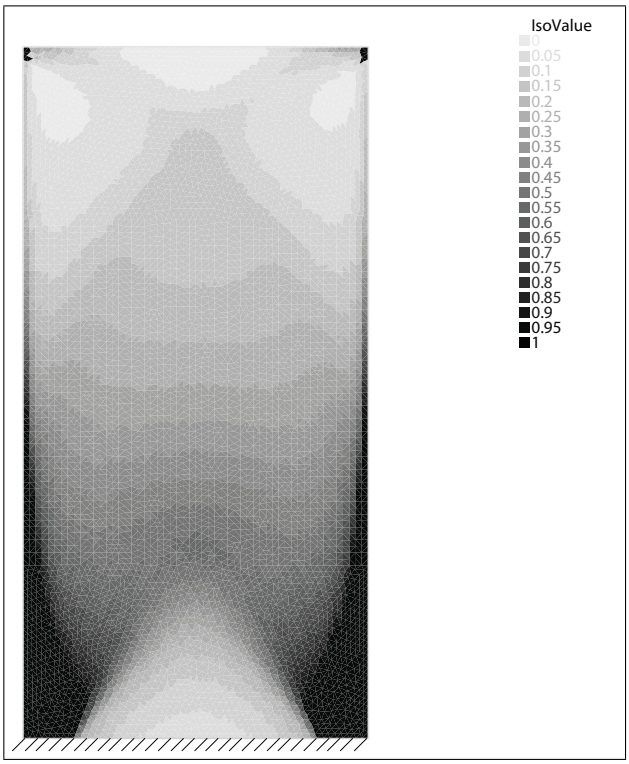

FIGURE 3.8. Optimal design without penalization

Then we run additional iterations of the algorithm but using penalization an obtain a penalized or classical design, see figure 3.9.

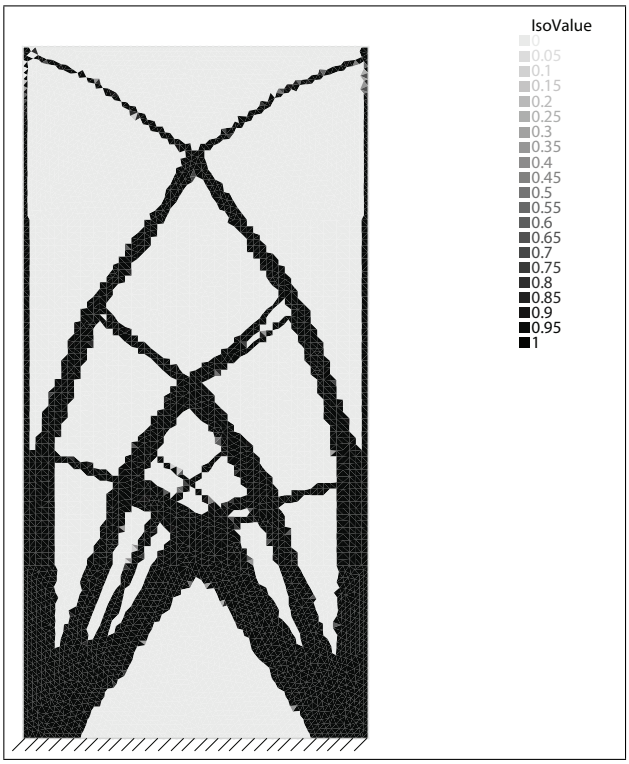

FIGURE 3.9. Optimal design with penalization

The first eigenvalue (square of the first eigenfrequency) of the penalized optimal design is multiplied by 8.12 compared to the first eigenvalue of the initial configuration in figure 3.7.

Now we show the converge history of the method.

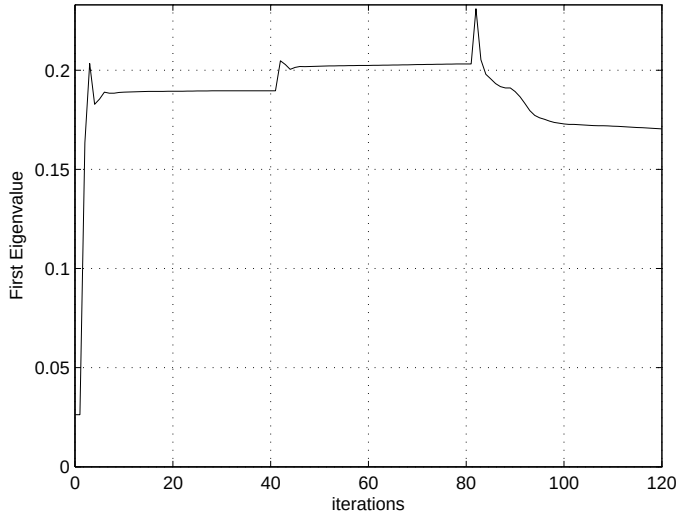

FIGURE 3.10. Convergence history

The peaks at iteration 40 and 80 are again due to not fulfilling the volume of rigid material constraint because of the partial penalization at iteration 40 and full penalization at iteration 80.

$iii)$ Third, we choose a domain $\Omega \subset \mathbb{R}^2$ as a wall with dimensions 2×1, say 2 in the fixed bottom and 1 of height. Figure 3.11 shows the initial configuration of the problem, notice that we fix a zone of density 10 in the middle of the upper side because if not, the optimal design will not connect the top of the wall with the fixed bottom of the wall. Another reason to do this is that the optimal design would be more constructible.

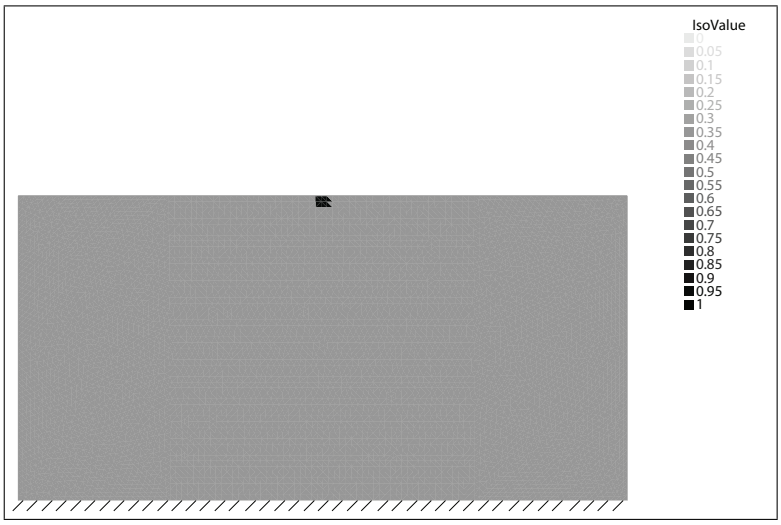

FIGURE 3.11. Initial configuration and boundary conditions for domain iii)

After few iterations of the optimality criteria method, the shape of the function θ of rigid material B breaks its symmetry and the eigenvalue starts to oscillate. For this reason we decided to stop this algorithm at the third iteration and from there use the gradient method of section 3.2.5.2. We obtain a design with many homogenized areas with density $\theta \in]0, 1[$, see figure 3.12.

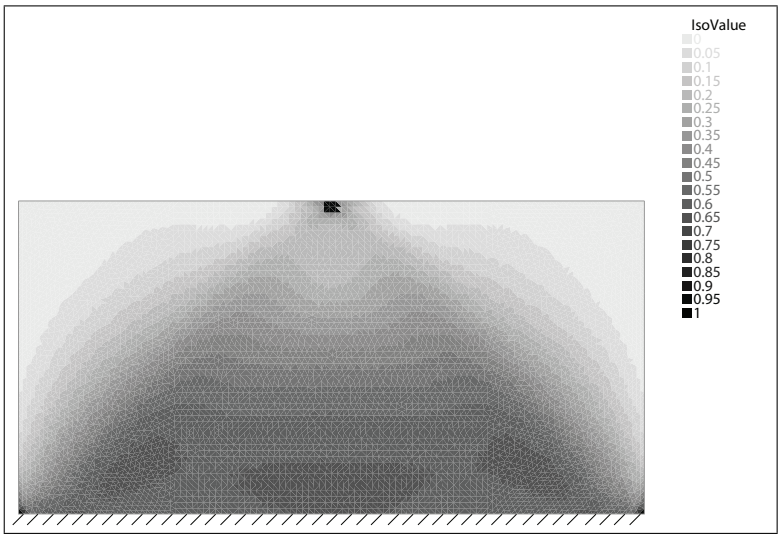

FIGURE 3.12. Optimal design without penalization

Now we show the converge history of the method.

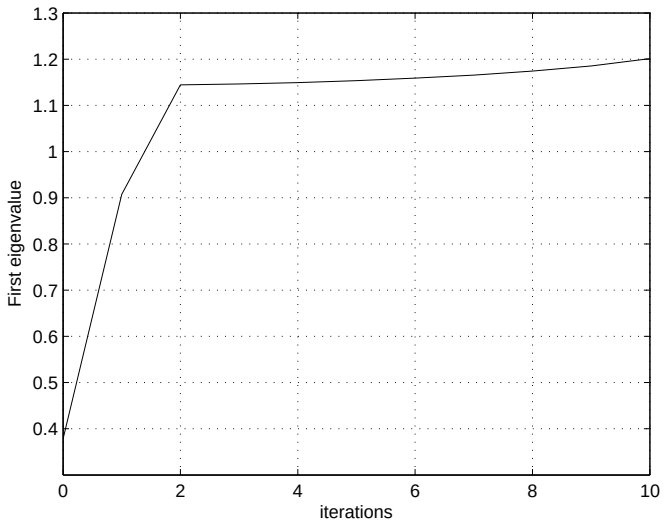

FIGURE 3.13. Convergence history

The first eigenvalue does not grow much after the gradient algorithm is used. The first eigenvalue is multiplied by 1.32 compared to the first eigenvalue of the initial configuration in figure 3.11.

3.2.6.2. Steel Bridge

Steel bridges are structures used to connect two places, often separated by a river or strait. One major problem steel-bridge-designers have to deal with is the high-price of steel. Therefore it is a good idea to increase the rigidity of steel bridges, by means of its first eigenfrequency, with a volume constraint in the amount of steel. In most bridges the value of the first eigenfrequency is low, making the bridge very flexible against excitations with a range of frequencies containing the first eigenfrequency of the bridge, such as wind and earthquakes. The purpose of this section is to maximize the first eigenfrequency of a bridge in order to increase its rigidity with a constraint in the amount of rigid material (steel).

We use the computational algorithm described in this chapter, say optimality criteria method and gradient method if necessary, to maximize the first eigenfrequency of a steel bridge with volume constraint for the rigid material. We use a rigid material B (for example steel), with Lamé parameters μ and λ, and a flexible material degenerating to void, that is to say material A with Lamé parameters $\mu = \varepsilon\mu$ and $\lambda = \varepsilon\lambda$ with $\varepsilon \to 0^+$.

We model a bridge as a domain $\Omega \subset \mathbb{R}^2$, see figure 3.14. The value of the parameters are the same as those from the shear walls shown in the previous section. We fix a zone with density 10 in the place where the highway its supposed to be. This part is not subject to optimization and its Lamé coefficients are the same as those from material B.

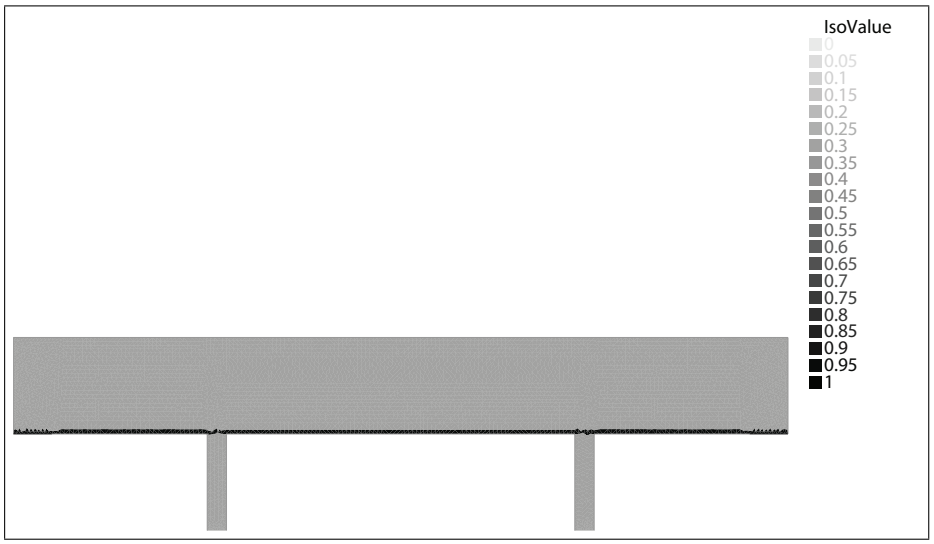

FIGURE 3.14. Initial configuration and boundary conditions

After few iterations we obtain a design with many homogenized areas with density $\theta \in]0,1[$, see figure 3.15.

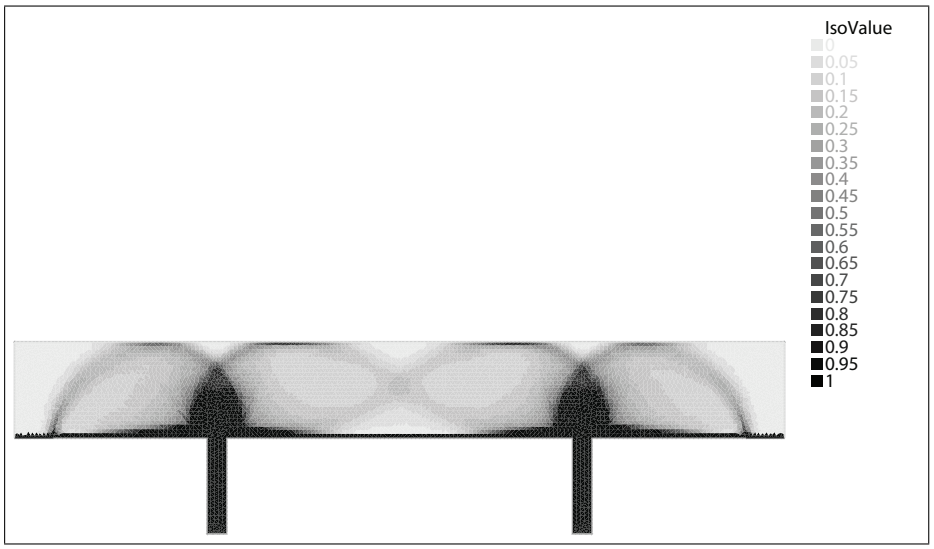

FIGURE 3.15. Optimal design without penalization

Then we run additional iterations of the algorithm but using penalization and obtain a penalized or classical design, see figure 3.16.

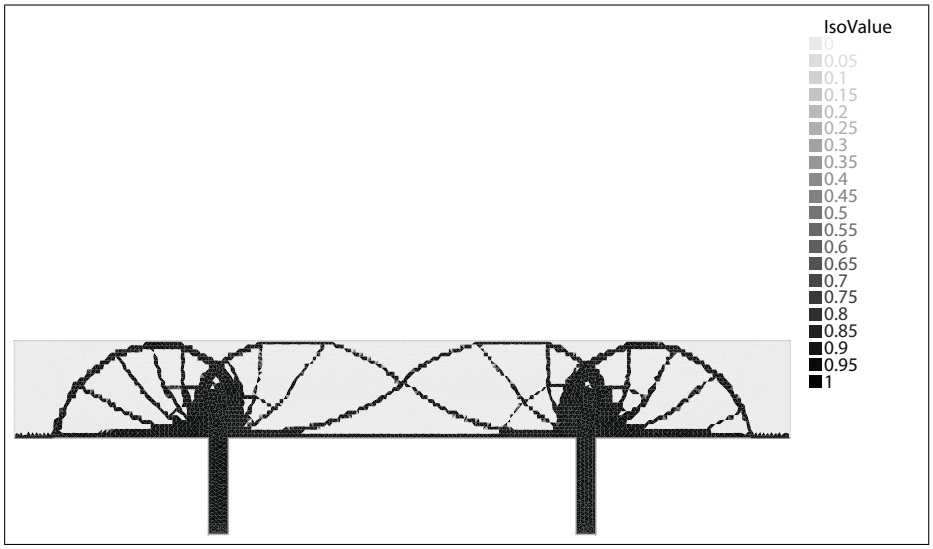

FIGURE 3.16. Optimal design with penalization

The first eigenvalue (square of the first eigenfrequency) of the penalized optimal design is multiplied by 8.05 compared to the first eigenvalue of the initial configuration in figure 3.14.

The first eigenvector is the same for the initial configuration, figure 3.14, and the optimal design with penalization, figure 3.16, with displacements only in the horizontal direction of the plane. Now we show the converge history of the method.

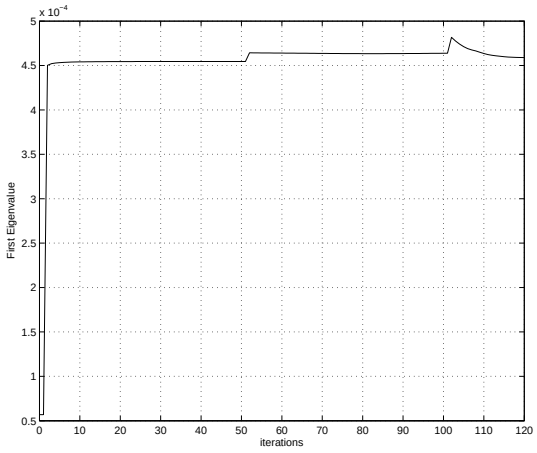

FIGURE 3.17. Convergence history

The peaks at iteration 60 and 120 are due to not fulfilling the volume of rigid material constraint because of the partial penalization at iteration 60 and full penalization at iteration 120.

4. COMPARISON BETWEEN GEOMETRIC OPTIMIZATION AND FULL HOMOGENIZATION

As seen in chapters 2 and 3, geometric optimization (chapter 2) and full homogenization (chapter 3) are able to satisfactorily increase the first eigenvalue (square of the first vibration eigenfrequency) of slender structures. In chapter 2 we use geometric optimization to obtain optimal configurations for column-thickness of slender buildings. In this chapter we show that the full homogenization method can be easily adapted to optimization in slender buildings. By doing this we can compare the results thus obtained between the two methods.

We use both methods, full homogenization and geometric optimization, to maximize the first eigenvalue of the same slender structures and compare the results. We compare the results for 3 different buildings, 13 story, 20 story and 30 story building.

It is important to notice that the full homogenization method is computationally more expensive than the geometric optimization method. Also the mathematical model and the differential equations used by the full homogenization method are more accurate for the examples we want to analyze.

4.1. Procedure

The procedure to pass the results of geometric optimization to optimal designs in ETABS is the same as the one shown in chapter 2.

In the case of full homogenization, the procedure to obtain optimal designs in ETABS variates mainly because, unlike geometric optimization, full homogenization gives us a detailed arrangement of material and void, instead of geometric optimization that only gives us the contour of the material, namely the thickness. Therefore the procedure to obtain optimal designs in ETABS from full homogenization is a little more complicated. The procedure is as follows.

We want to pass the optimal design obtained by full homogenization to thickness configuration for the columns of a building. Then the optimal design, obtained by full homogenization, is divided in equal horizontal laminates among the number of floors the building is compound, and in each floor we calculate the area of rigid material, divide it by the area of the laminate and obtain a coefficient $c_i \in [0, 1]$. Where $i \in \{1, 2, ..., n\}$, $n =$ number of stories the building is made of. Then the thickness of the columns in the floor i is $h_i = h_{min} + c_i(h_{max} - h_{min})$. Where h_{min}, h_{max} are defined in section 2.5.

Another difference between geometric optimization and full homogenization is that the latter model the 3D building as a 2D rectangular domain simulating the transversal area of the building. This way the displacements of the 2D domain in its plane represent the displacements of the building in its slender direction. And geometric optimization model the 3D building as a membrane with displacements perpendicular to its plane, simulating the displacements of the building in its slender direction.

For each example, we run first the full homogenization method to obtain an optimal design. Then we pass the optimal design to the column-thickness configuration for the 3D model of the building. Now the column-thickness configuration is compared with the configurations shown in chapter 2, say initial (uniform), initial (divided by 3), optimal (geometric optimization) called optimal (original) in chapter 2, and optimal (smoothed) which is the optimal (geometric optimization) with a few manually-changed floor's column thickness. See the examples in chapter 2.

4.1.1. Results for the 13 story building

Figure 4.1 shows the model in ETABS of a 13 story building made of reinforced concrete. To use the full homogenization method we model the building as a rectangular 2D domain simulating the transversal area of the building by looking at the building from the y direction, see figure 4.1(right).

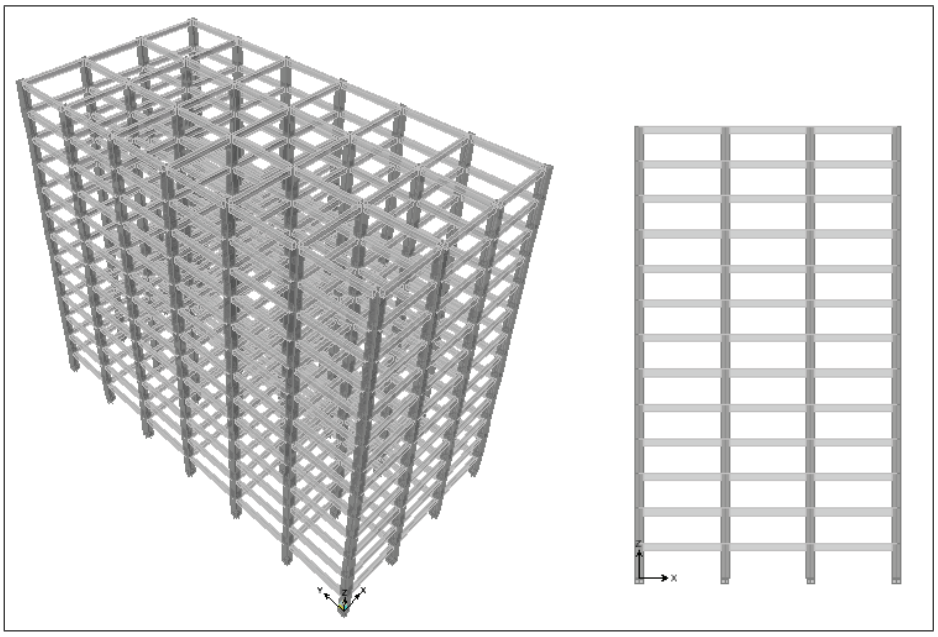

FIGURE 4.1. Model of the 13 story building in ETABS.

Figure 4.2(left) shows the model in FreeFem++ of the building (figure 4.1 right), the total height of the building is $13 \cdot 250 = 3250cm$ and width $3 \cdot 600 = 1800cm$. Then the reason between height and width is $Height/Width = 3250/1800 = 1.8056/1$.

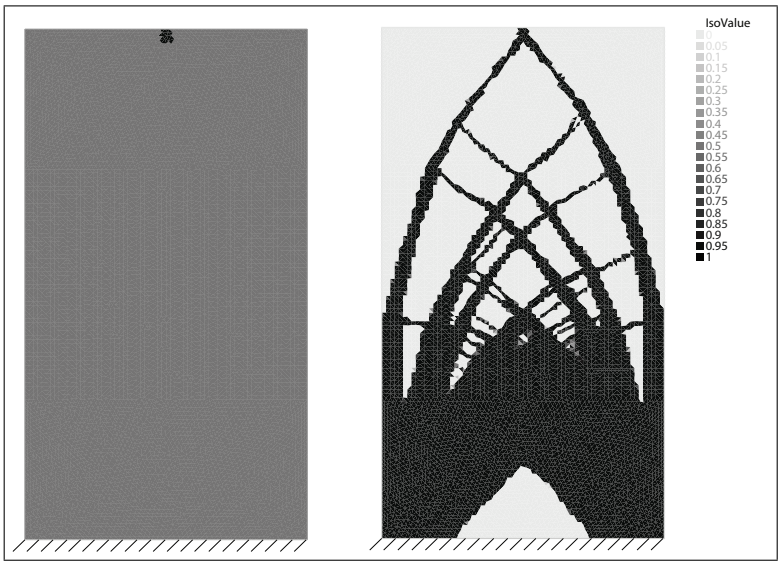

FIGURE 4.2. 2D model in FreeFem++. Initial (left) and Optimal with penalization (right)

Figure 4.2 (right) shows the penalized optimal design obtained by the full homogenization method using the algorithm of section 3.2.5.1, the convergence is smooth so the gradient method of section 3.2.5.2 is not needed. The first eigenvalue (square of the first eigenfrequency) of the penalized optimal design is multiplied by 6.83 compared to the first eigenvalue of the initial configuration in figure 4.2 (left).

Now using the procedure described in 4.1 we obtain the thickness of the columns for each floor of the 13 story building. Table 4.1 shows the proposed thickness for the columns of the building.

TABLE 4.1. Column-thickness of the 13 story building proposed by the full homogenization method

Floor	thickness (cm)
13	33.61
12	34.74
11	37.12
10	40.13
9	44.83
8	48.66
7	55.58
6	68.94
5	81.13
4	88.62
3	90.00
2	83.38
1	67.75

Figure 4.3 shows the thickness configuration of the columns proposed by the full homogenization method, and the four other cases mentioned at the end of section 4.1.

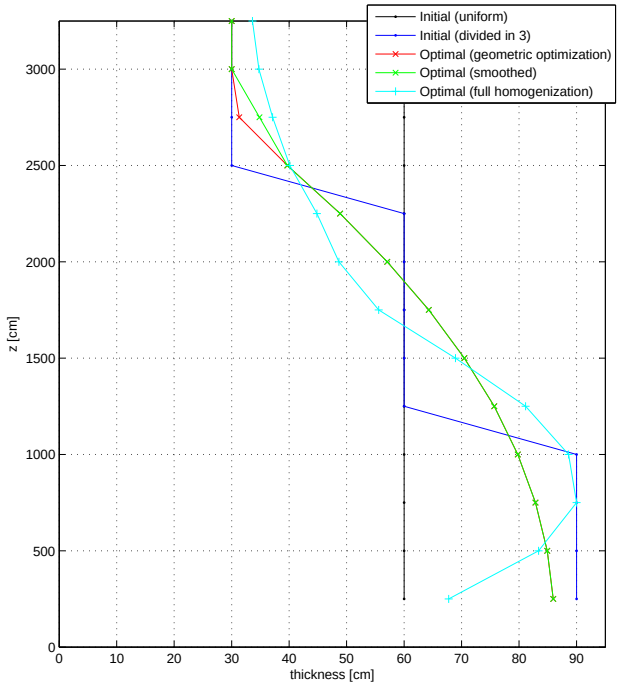

FIGURE 4.3. Proposed thickness functions

Initial (uniform) is the model with all the columns of the same thickness $h_0 = 60cm$. Initial (divided in 3) is the model with three different thickness, $h_{max} = 90cm$ for the lower floors, $h_0 = 60cm$ for the middle ones, and $h_{min} = 30cm$ for the upper floors. Optimal (geometric optimization) is the optimized model directly obtained from geometric optimization (chapter 2). Optimal (smoothed) is the same as Optimal (geometric optimization), but with a softer thickness function for the columns (described in chapter 2). Optimal (full homogenization) is the model obtained by the full homogenization method.

The Optimal (full homogenization) column-thickness function does not reach the $h_{max} = 90cm$ value, because as seen in figure 4.2 (right) the rigid material does not fill the lower part of the domain. This makes the building model more flexible in the lower floors, increasing the Shear D/C Ratio in these floors.

Now we compare the results of Drifts and Shear D/C Ratios for the two optimization methods. Figure 4.4 show the results.

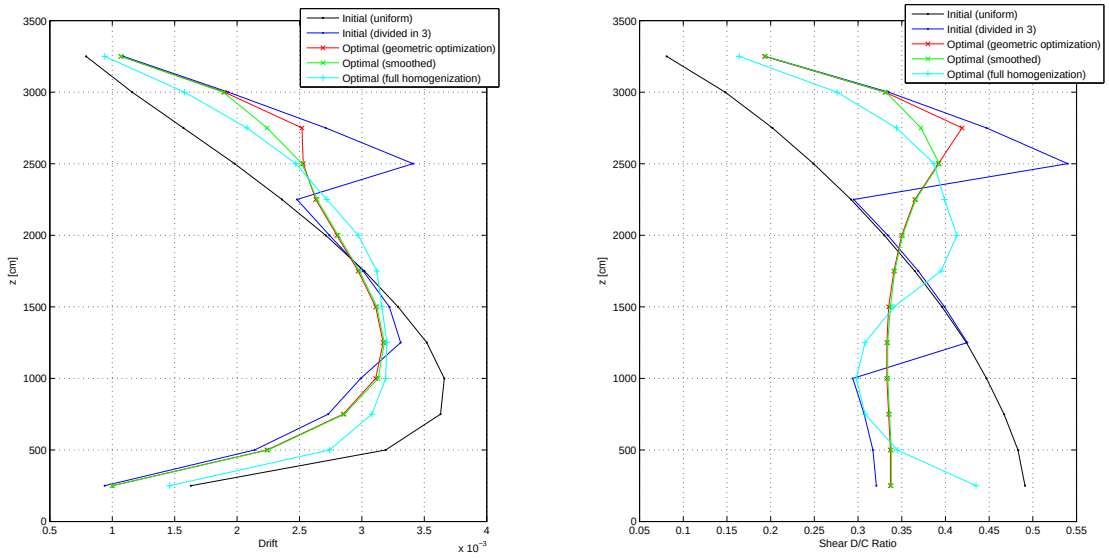

FIGURE 4.4. Drifts (left) and Shear D/C Ratios (right)

It is important to notice that in terms of Drifts, both models, Optimal (smoothed) and Optimal (full homogenization) are very similar, considerably reducing the Drifts in the lower floors, but increasing them in the upper floors. Although both reduce the maximal Drift.

Initial (uniform) and initial (divided in 3) have the worst results, showing that it is not a good idea to have all the columns of the same thickness or doing a very rough distribution of thickness.

In terms of Shear D/C Ratios, the worst results come from the Initial (divided in 3) model, because it has a huge discontinuity when we pass from $h_0 = 60cm$ to $h_{min} = 30cm$ in the upper floors, producing an increase in the Shear D/C Ratios.

Maximal Shear D/C Ratios are very close in value in models Optimal (geometric optimization), Optimal (smoothed) and Optimal (full homogenization), but Optimal (full homogenization) has larger Shear D/C Ratios in the lower floors because of a reduction in the thickness of the columns in those floors.

Table 4.2 resumes the results.

TABLE 4.2. Comparison between the optimal model and the initial model for the 13 story building.

	I.U.	O.P.O.S.	O.F.H.	% of Benefit(O.P.O.S.)	% of Benefit(O.F.H.)
$T =$ Period in secs.(from ETABS)	1.8808	1.7530	1.8070	6.79	3.92
Maximal Drift	0.0037	0.0032	0.0032	13.32	12.99
Maximal Shear D/C Ratio	0.49	0.42	0.39	14.58	19.81
Max. Displacement on the top(cm)	8.13	7.98	8.18	1.86	-0.59

I.U.=Initial uniform. O.P.O.S.=Optimal with geometric optimization smoothed. O.F.H=Optimal with full homogenization.

The Optimal model obtained by the method of full homogenization has very similar results in Drift and Shear D/C Ratio to the results of geometric optimization, and by doing simple changes to the later one, we can obtain even better results.

4.1.2. Results for the 20 story building

Figure 4.5 shows the model in ETABS of a 20 story building made of reinforced concrete (the same of section 2.5.1). As in the 13 story building, in order to use the full homogenization method we model the building as a rectangular 2D domain simulating the transversal area of the building by looking at the building from the y direction, see figure 4.5(right).

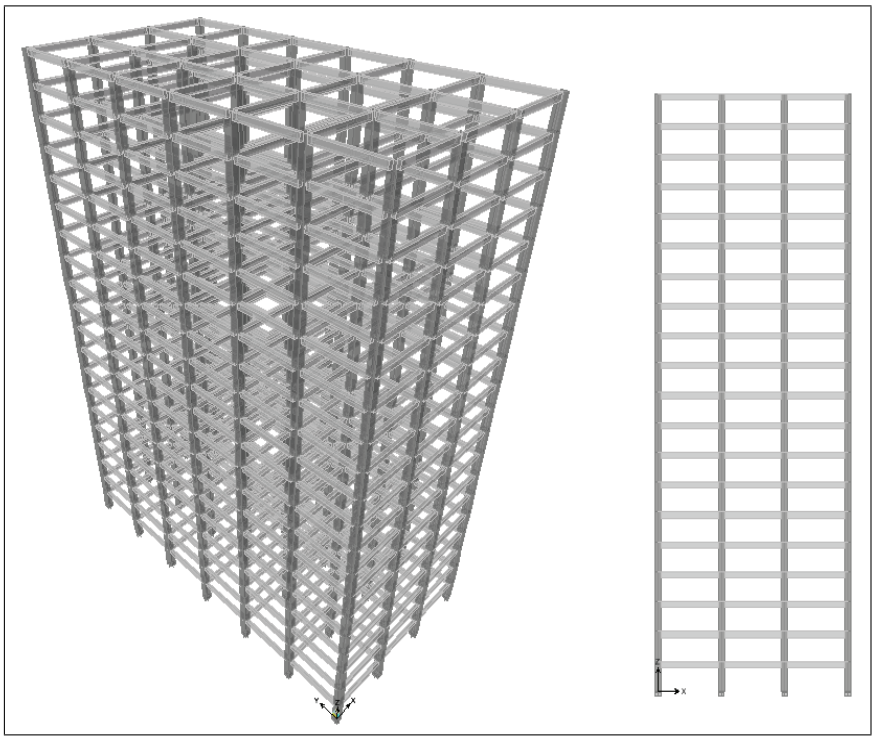

FIGURE 4.5. Model of the 20 story building in ETABS.

Figure 4.6(left) shows the model in FreeFem++ of the building (figure 4.5 right), the total height of the building is $20 \cdot 250 = 5000cm$ and width $3 \cdot 600 = 1800cm$. Then the reason between height and width is $Height/Width = 5000/1800 = 2.7778/1$.

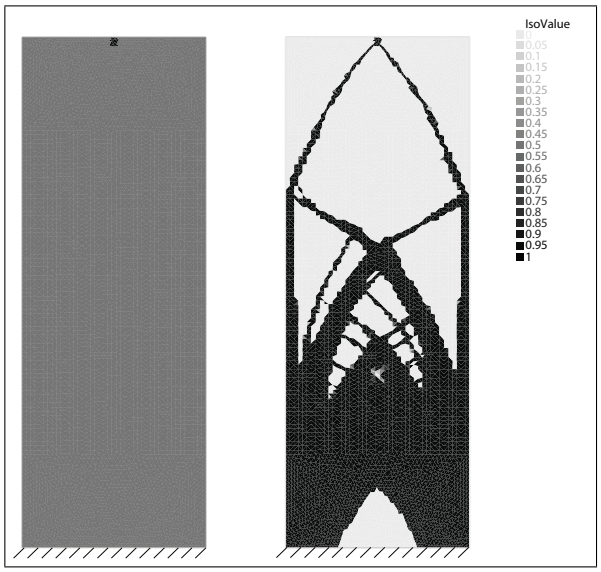

FIGURE 4.6. 2D model in FreeFem++. Initial (left) and Optimized (right)

Figure 4.6 (right) shows the penalized optimal design obtained by the full homogenization method using the algorithm of section 3.2.5.1, the convergence is smooth so the gradient method of section 3.2.5.2 is not needed. The first eigenvalue (square of the first eigenfrequency) of the penalized optimal design is multiplied by 9.17 compared to the first eigenvalue of the initial configuration in figure 4.6 (left).

Now using the procedure described in 4.1 we obtain the thickness of the columns for each floor of the 20 story building. Table 4.3 shows the proposed thickness for the columns of the building.

TABLE 4.3. Proposed thickness for columns of the 20 story building

Floor	thickness (cm)	Floor	thickness (cm)
20	32.51	10	55.87
19	32.58	9	66.05
18	33.64	8	72.80
17	34.11	7	84.24
16	34.85	6	89.91
15	35.52	5	90.00
14	43.55	4	90.00
13	48.15	3	89.49
12	48.00	2	78.29
11	53.52	1	67.75

Figure 4.7 shows the thickness configuration of the columns proposed by the full homogenization method, and the four other cases mentioned at the end of section 4.1.

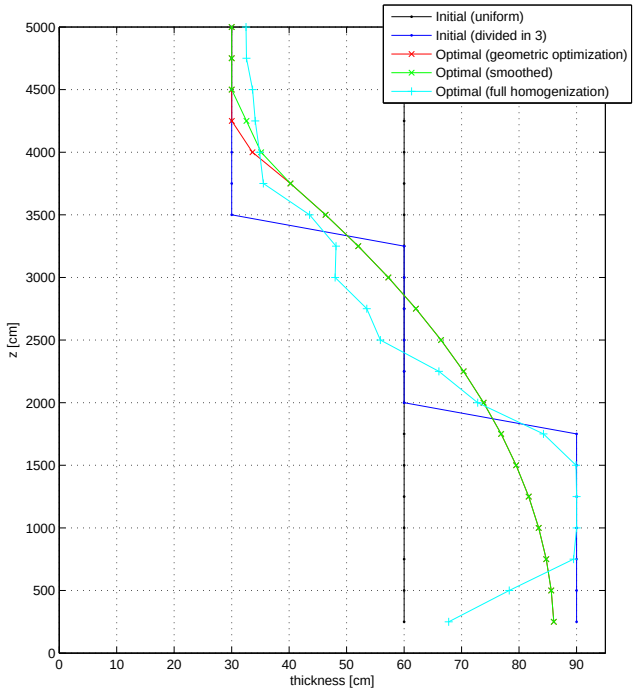

FIGURE 4.7. Proposed thickness functions

As in the 13 story building, the Optimal (full homogenization) column-thickness function does not reach the $h_{max} = 90cm$ value, because as seen in figure 4.6 (right) the rigid material does not fill the lower part of the domain. This make the building model more flexible in the lower floors, increasing the Shear D/C Ratio in these floors.

Now we compare the results of Drifts and Shear D/C Ratios for the two optimization methods. Figure 4.8 show the results.

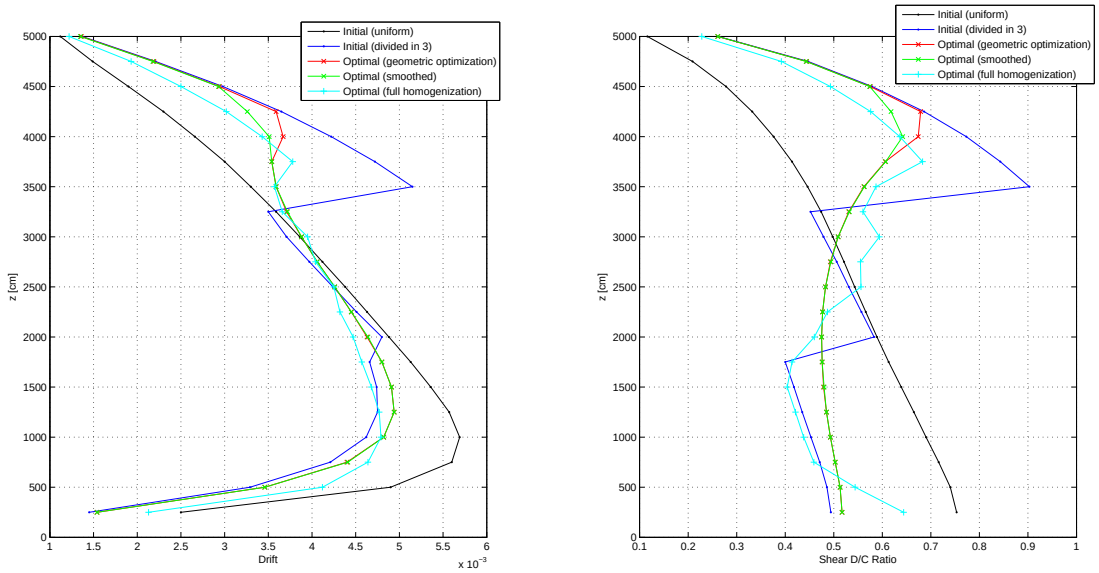

FIGURE 4.8. Drifts (left) and Shear D/C Ratios (right)

In general, the results are similar to the ones shown in the previous example (13 story building). That is to say, both models, Optimal(smoothed) and Optimal(full homogenization), reduce the Drifts in the lower floors, but increasing them in the upper floors, although reducing the maximal Drift. Also, initial models (Initial(uniform) and initial(divided in 3)) have the worst results in Drifts and in Shear D/C Ratios.

Table 4.4 resumes the results.

TABLE 4.4. Comparison between the optimal model and the initial model for the 20 story building.

	I.U.	O.P.O.S.	O.F.H.	% of Benefit(O.P.O.S.)	% of Benefit(O.F.H.)
T = Period in secs.(from ETABS)	2.9901	2.8062	2.8735	6.15	3.90
Maximal Drift	0.0057	0.0049	0.0048	13.17	15.90
Maximal Shear D/C Ratio	0.75	0.68	0.68	9.83	9.36
Max. Displacement on the top(cm)	19.00	18.69	18.46	1.64	2.82

4.1.3. Results for the 30 story building

Figure 4.9 shows the model in ETABS of a 30 story building made of reinforced concrete. As in the previous buildings, in order to use the full homogenization method we model the building as a rectangular 2D domain simulating the transversal area of the building by looking at the building from the y direction, see figure 4.9(right).

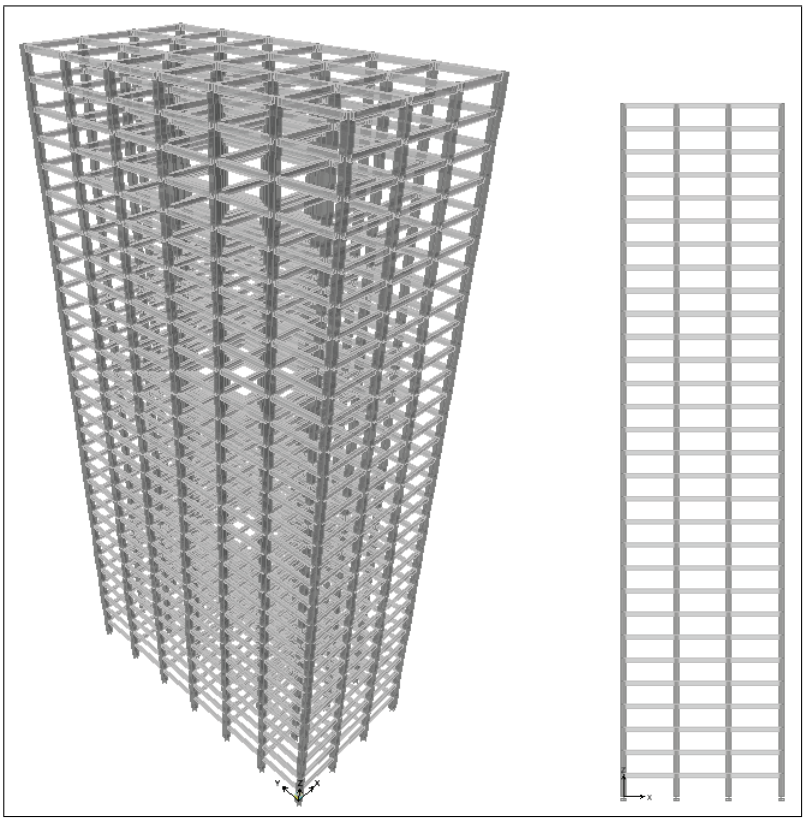

FIGURE 4.9. Model of the 30 story building in ETABS.

Figure 4.10(left) shows the model in FreeFem++ of the building (figure 4.9 right), the total height of the building is $30 \cdot 250 = 7500cm$ and width $3 \cdot 600 = 1800cm$. Then the reason between height and width is $Height/Width = 7500/1800 = 4.1667/1$.

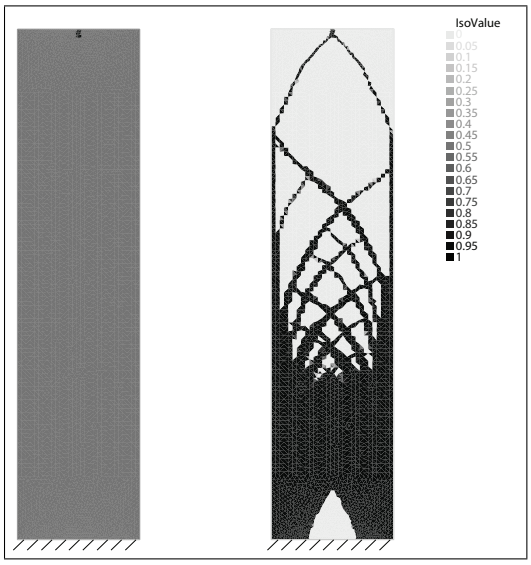

FIGURE 4.10. 2D model in FreeFem++. Initial (left) and Optimized (right)

Figure 4.10 (right) shows the penalized optimal design obtained by the full homogenization method using the algorithm of section 3.2.5.1, the convergence is smooth so the gradient method of section 3.2.5.2 is not needed. The first eigenvalue (square of the first eigenfrequency) of the penalized optimal design is multiplied by 10.48 compared to the first eigenvalue of the initial configuration in figure 4.10 (left).

Now using the procedure described in 4.1 we obtain the thickness of the columns for each floor of the 30 story building. Table 4.5 shows the proposed thickness for the columns of the building.

TABLE 4.5. Proposed thickness for columns of the 30 story building

Floor	thickness (cm)	Floor	thickness (cm)	Floor	thickness (cm)
30	32.57	20	42.58	10	87.19
29	32.64	19	43.37	9	89.91
28	32.34	18	47.03	8	89.97
27	32.58	17	49.81	7	89.97
26	32.90	16	53.25	6	89.99
25	32.82	15	59.82	5	90.00
24	35.48	14	60.63	4	90.00
23	37.04	13	69.64	3	85.49
22	39.75	12	73.25	2	76.15
21	42.47	11	78.33	1	68.80

Figure 4.11 shows the thickness configuration of the columns proposed by the full homogenization method, and the four other cases mentioned at the end of section 4.1.

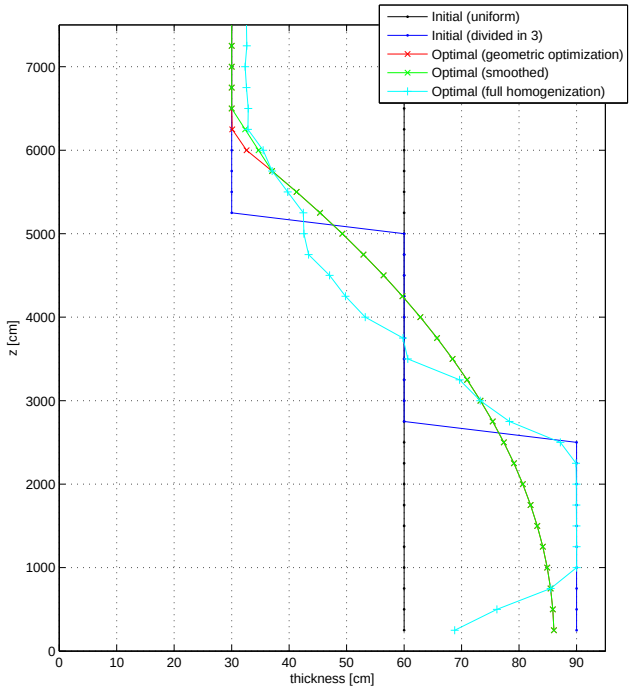

FIGURE 4.11. Proposed thickness functions

As in the previous buildings, the Optimal (full homogenization) column-thickness function does not reach the $h_{max} = 90cm$ value, because as seen in figure 4.10 (right) the rigid material does not fill the lower part of the domain. This make the building model more flexible in the lower floors, increasing the Shear D/C Ratio in these floors.

Now we compare the results of Drifts and Shear D/C Ratios for the two optimization methods. Figure 4.12 show the results.

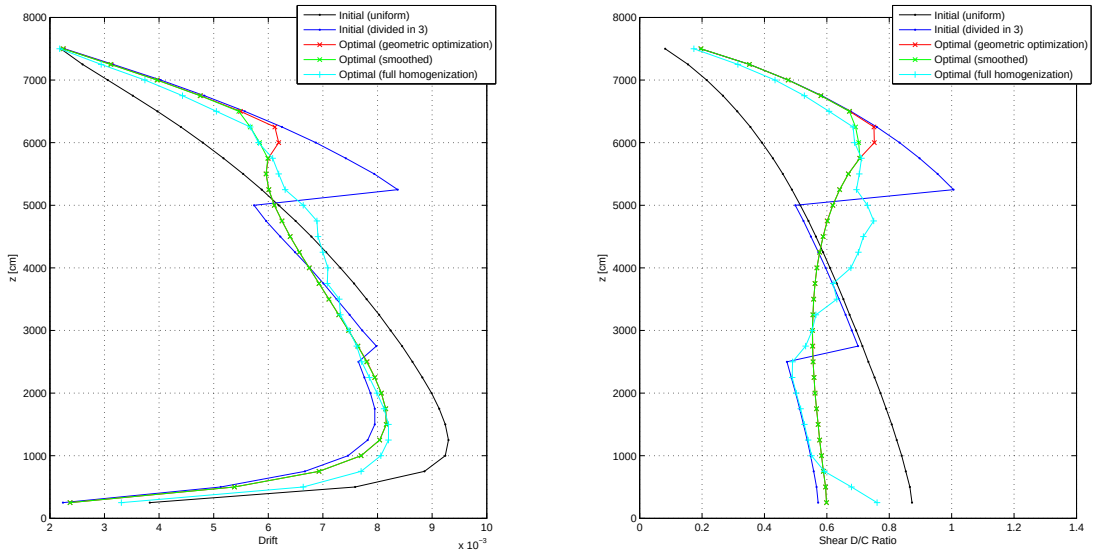

FIGURE 4.12. Drifts (left) and Shear D/C Ratios (right)

In general, the results are similar to the ones shown in the previous examples (13 story and 20 story buildings). That is to say, both models, Optimal(smoothed) and Optimal(full homogenization), reduce the Drifts in the lower floors, but increasing them in the upper floors, although reducing the maximal Drift. Also, initial models (Initial(uniform) and initial(divided in 3)) have the worst results in Drifts and in Shear D/C Ratios.

Table 4.6 resumes the results.

TABLE 4.6. Comparison between the optimal model and the initial model for the 30 story building.

	I.U.	O.P.O.S.	O.F.H.	% of Benefit(O.P.O.S.)	% of Benefit(O.F.H.)
T = Period in secs.(from ETABS)	4.6900	4.4028	4.4727	6.09	4.59
Maximal Drift	0.0093	0.0082	0.0082	12.26	11.88
Maximal Shear D/C Ratio	0.87	0.71	0.76	19.14	12.82
Max. Displacement on the top(cm)	49.68	47.02	48.38	5.36	2.62

5. CONCLUSION AND FUTURE RESEARCH

5.1. Review of the Results and General Remarks

From the results presented in this thesis we can conclude that both methods, geometric optimization (chapter 2) and full homogenization (chapter 3), are able to maximize the first eigenfrequency of elastic structures such as tall buildings, in order to make them stiffer and as a consequence we get to reduce its drifts and shear D/C ratio.

Although for slender structures the convergence of both methods is smooth, the computer capacity needed is greater in the case of full homogenization. Because the differential equation used by full homogenization (elasticity) is more complex than the membrane equation of geometric optimization. Also, full homogenization requires more iterations to converge than geometric optimization. Hence, full homogenization is more demanding for computer capacity than geometric optimization.

In the case of tall slender buildings we show in chapter 2 that by using a surrogate model of the building as a membrane we can derive a gradient algorithm that in few iterations we can increase its first eigenfrequency reducing its drifts and shear D/C ratio. But the method is only valid for tall buildings, because in the case of shorter buildings, as the one showed in example 2.5.3, the method is invalid, because the first eigenfunction in the 3D model of the optimal building is not compatible with the displacements of the membrane.

By using a continuous model in elasticity we develop a more complex optimization method based in full homogenization, as seen in chapter 3. This method can effectively increase the value of the first eigenfrequency of several structures as walls and bridges. The convergence of the method is very smooth for slender structures such as tall walls (with a reason $height/width > 1.5$). But for shorter and stiffer structures we need to use a gradient method due to a crossing of the first eigenfunction, similar to the problem with short buildings in chapter 2. We can only guess that this problem occurs because

the original building is rigid, therefore by making its first eigenfrequency stiffer we are making that eigenfrequency to cease to be the first eigenfrequency. Therefore in the case of shorter and stiffer buildings the approach we follow is not entirely correct.

Although for slender structures the convergence of the full homogenization method is smooth, it takes more iterations to converge than the optimization algorithm using geometric optimization of chapter 2.

Chapter 4 shows that both optimization methods, geometric optimization and optimization based in full homogenization, can effectively reduce Drifts and Shear D/C Ratios in tall, slender buildings. And the benefit we earn by using a more sophisticated method, such as full homogenization, is not significant in the final 3D design of the building, because the processing to pass the optimal design in the 2D model to the 3D model is very rough, loosing the fine geometry given by the full homogenization. Therefore a less expensive optimization method using a simpler model of the building can deliver almost as good results, and by means of a post-processing technique (smoothing the thickness function) we can obtain even better results, as we can see in model 3 in chapter 4.1 where the benefit in maximal Drift and maximal Shear D/C Ratio are 0.38% and 6.32% bigger in the smoothed optimal (geometric optimization) than the optimal (full homogenization).

The effectiveness of both methods gets dimmish when applying to taller buildings, as can be seen in the last two columns of table 4.6 in the T (period) line in the models shown in chapter 4.1, where the percentage of benefit for both methods diminishes for taller buildings (30 stories or more). This phenomenon could be explained because in taller buildings the difference between the optimal design and the original (uniform) design is not as big as the case of shorter buildings. This tendency is not seen in the results of Drift and Shear D/C Ratio because the latter two were not our objective functions, that is to say, the optimization was focused in maximizing the first eigenfrequency of the building, and diminishing Drifts and Shear D/C Ratios is a positive side-effect.

It is important to notice that diminishing the maximal Shear D/C Ratio in tall buildings produces a considerable decrease in the total cost of the building, because designers will not need big amounts of steel for shear solicitations. Also, the maximal Shear D/C Ratio in the original designs was always in the lower floors and in the optimal design the maximal Shear D/C Ratio is in the upper floors, and it is known that the latter situation is preferable for designers, because a failure of some parts of the upper floors is more manageable than a failure in the lower floors.

The main conclusion of this work is that through a very simple mathematical model of a tall, slender building, by means of geometric optimization with a post-processing technique, we can obtain significant improvements in the behavior of the building facing a cyclic excitation like an earthquake, as a side-effect of maximizing the first eigenfrequency of the building. More complex and expensive method, such as full homogenization, is not needed because it gives us sufficiently similar results.

5.2. Future Research Topics and Applications

There is no mathematical difficulty to implement an optimization method based in full homogenization in 3D, the formulation is described in appendix A.2.3, but because of computational capacity, we were not able to run a numerical algorithm in order to maximize the first eigenvalue of different domains in 3D settings.

In a future work, the maximization of the first eigenfrequency can be mixed with a compliance minimization or a stress reduction. Also, a selective optimization algorithm can be developed, that is to say, a part of the domain subjected to compliance optimization while the rest of the domain is subjected to a maximization of the first eigenfrequency, similar to the algorithm developed for steel bridges in chapter 3, where a small zone of the domain were out of the optimization.

From the application point of view, the developing of a friendly-user software for eigenfrequency optimization is to be explored, in order that practitioners without further knowledge in the mathematics behind optimization, can safely apply the optimization methods presented in this thesis in the design of tall, slender buildings.

REFERENCES

G. Allaire. *Shape Optimization by the Homogenization Method*. Springer, 2002.

G. Allaire, S. Aubry, and F. Jouve. Eigenfrequency optimization in optimal design. *Comp. Meth. Appl. Mech. Eng.*, v. 19:3365–3579, 2001.

G. Allaire, F. Jouve, and A. Toader. A level-set method for shape optimization. *C. R. Acad. Sci.*, 1(1), 2002.

American-Concrete-Institute. Concrete Building Code. American Concrete Institute, 2008.

M.P. Bendsøe and O. Sigmund. *Topology Optimization. Theory, Methods and Applications*. Springer, 2003.

Ph.G. Ciarlet. *Mathematical Elasticity*. North-Holland, 1988.

G. Francfort and F. Murat. Homogenization and optimal bounds in linear elasticity. *Arch. Rat. Mech. Anal., 94, pp.307-334*, 1(1), 1986.

K. Gopal. Eigenvalue optimization and its applications in buckling and vibration. *Dissertation in the Department of Mechanical Engineering, Louisiana State University*, 1(1), 2007.

S. Gutiérrez. Laminations in linearized elasticity: The isotropic non-very strongly elliptic case. *Journal of elasticity*, 53(3), 1998.

S. Gutiérrez. Laminations in planar anisotropic linear elasticity. *The quarterly journal of mechanics and applied mathematics*, 1(1), 2004.

J. Hadamard. *Mémoire sur le problème d'analyse relatif a l'équilibre des plaques élastiques encastrées*. lala, 1907.

F. Hecht, O. Pironneau, A. Le Hyaric, and K. Ohtsuka. *FreeFem++, code and user manual freely available at www.freefem.org*. Laboratoire Jacques-Louis Lions, 2007.

INN-Chile. *Chilean Seismic Building Code NCh433*. INN-Chile, 2010.

T. Kim, J. Kim, and Y. Kim. Parallelized structural topology optimization for eigenvalue problems. *International Journal of Solids and Structures*, 1(1), 2003.

F. Murat and J. Simon. Sur le contrôle par un domaine géométrique. *Laboratoire d'Analyse Numérique de l'Université Paris VI*, 1(Internal report N. 76 015), 1976.

F. Murat and L. Tartar. Calculus of variations and homogenization. *Collection d'Etudes de Electricité de France*, 1, 1983.

A. Novotny and J. Sokolowski. *Topological Derivatives in Shape Optimization, Lecture Notes*. lala, 2010.

L. Tartar. Estimations fines descoefficients homogénéisés. *Ennio de Giorgi Colloquium, P. Krée ed., Pitman Research Notes in Math., 125, pp.168-187*, 1(1), 1985.

L. Tartar. H-measures, a new approach for studying homogenization, oscillations and concentration effects in partial differential equations. *Proc. of the Royal Soc. Edinburgh*, 115A, 1990.

L. Tartar. *The General Theory of Homogenization*. Springer, 2009.

L.N. Trefethen and D. III Bau. *Numerical Linear Algebra*. SIAM, 1997.

G. Yoon. Maximizing the fundamental eigenfrequency of geometrically nonlineal structures by topology optimization based on element connectivity parameterization. *Computers and Structures*, 1(1), 2009.

APPENDIX A. ADDITIONAL RESOURCES

A.1. Implementation of the Optimality criteria method in 2D

A.1.1. Standard Isometry

Since during the calculations we need to invert several fourth-order tensors which could be a little difficult, we prefer to write these tensors as 2x2 matrices, because their inverses are standard. We identify the space of symmetric 2x2 matrices with $\mathbb{R}^3$ using the following isometry:

$$\Phi\left(\begin{bmatrix} x & z \\ z & y \end{bmatrix}\right) = \begin{pmatrix} x \\ y \\ \sqrt{2}\,z \end{pmatrix}.$$

Now we can write the constitutive relation as

$$\hat{\sigma} = \Phi(\sigma) = \hat{c}\;\Phi(\epsilon) = \hat{c}\;\hat{\epsilon},$$

where $\hat{c}$ is defined as the following 3×3 matrix:

$$\hat{c}_{11} = C_{1111}, \qquad \hat{c}_{12} = C_{1122}, \qquad \hat{c}_{13} = \sqrt{2}\,C_{1112},$$

$$\hat{c}_{21} = C_{2211}, \qquad \hat{c}_{22} = C_{2222}, \qquad \hat{c}_{23} = \sqrt{2}\,C_{2212},$$

$$\hat{c}_{31} = \sqrt{2}\,C_{1211}, \quad \hat{c}_{32} = \sqrt{2}\,C_{1222}, \quad \hat{c}_{33} = 2\,C_{1212}.$$

And C_{ijkl}, for $i, j, k, l = 1, 2$ is the fourth-order elasticity tensor of an elastic material, and μ, λ are its Lamé parameters.

In the isotropic case $\hat{c}_{11} = \hat{c}_{22} = 2\mu + \lambda$, $\hat{c}_{33} = 2\,\mu$, $\hat{c}_{12} = \hat{c}_{21} = \lambda$ and $\hat{c}_{13} = \hat{c}_{31} = \hat{c}_{23} =$

$\hat{c}_{32} = 0$. Also:

$$C \begin{bmatrix} x & z \\ z & y \end{bmatrix} : \begin{bmatrix} x & z \\ z & y \end{bmatrix} = \begin{pmatrix} x \\ y \\ \sqrt{2}\, z \end{pmatrix} \cdot \hat{c} \begin{pmatrix} x \\ y \\ \sqrt{2}\, z \end{pmatrix}.$$

Let $\hat{c} = \Psi(C)$, we have that $\hat{\epsilon} = \Psi(C^{-1})\hat{\sigma} = \Psi(C^{-1})\hat{c}\hat{\epsilon}$, therefore $\hat{c}^{-1} = \Psi(C^{-1})$, then $C^{-1} = \Psi^{-1}(\hat{c}^{-1})$.

A.1.2. Implementation

We need to apply f_B of equation 3.7 to the elements of a base of the space of symmetric 2×2 matrices. We use the following base:

$$A^1 = e_1 \otimes e_1 = \begin{bmatrix} 1 & 0 \\ 0 & 0 \end{bmatrix} \qquad A^2 = e_2 \otimes e_2 = \begin{bmatrix} 0 & 0 \\ 0 & 1 \end{bmatrix}$$

$$A^3 = e_1 \otimes e_2 + e_2 \otimes e_1 = \begin{bmatrix} 0 & 1 \\ 1 & 0 \end{bmatrix}.$$

Then

$$\begin{aligned}
f_B(e)A^1 : A^1 &= \tfrac{1}{\mu}\left(e_x^2\right) - K\left(e_x^2\right)^2, \\
f_B(e)A^2 : A^2 &= \tfrac{1}{\mu}\left(e_y^2\right) - K\left(e_y^2\right)^2, \\
f_B(e)A^3 : A^3 &= \tfrac{1}{\mu}\left(e_x^2 + e_y^2\right) - K\left(2e_x e_y\right)^2, \\
f_B(e)(A^1 + A^2) : (A^1 + A^2) &= \tfrac{1}{\mu}\left(e_x^2 + e_y^2\right) - K\left(e_x^2 + e_y^2\right)^2, \\
f_B(e)(A^1 + A^3) : (A^1 + A^3) &= \tfrac{1}{\mu}\left((e_x + e_y)^2 + e_x^2\right) - K\left(e_x(e_x + 2e_y)\right)^2, \\
f_B(e)(A^2 + A^3) : (A^2 + A^3) &= \tfrac{1}{\mu}\left((e_x + e_y)^2 + e_y^2\right) - K\left(e_y(2e_x + e_y)\right)^2,
\end{aligned}$$

$$
\begin{aligned}
f_B(e)A^1 : A^2 &= \tfrac{1}{2}\left(f_B(e)(A^1+A^2) : (A^1+A^2) - f_B(e)A^1 : A^1 - f_B(e)A^2 : A^2\right) \\
&= -K\, e_x^2 e_y^2, \\
f_B(e)A^1 : A^3 &= \tfrac{1}{2}\left(f_B(e)(A^1+A^3) : (A^1+A^3) - f_B(e)A^1 : A^1 - f_B(e)A^3 : A^3\right) \\
&= \tfrac{1}{\mu}\left(e_x\, e_y\right) - K\left(2e_x^3 e_y\right), \\
f_B(e)A^2 : A^3 &= \tfrac{1}{2}\left(f_B(e)(A^2+A^3) : (A^2+A^3) - f_B(e)A^2 : A^2 - f_B(e)A^3 : A^3\right) \\
&= \tfrac{1}{\mu}\left(e_x\, e_y\right) - K\left(2e_x e_y^3\right).
\end{aligned}
$$

Then, given that

$$
(A-B)^{-1} = \left((\epsilon-1)\ B\right)^{-1} = \frac{1}{\epsilon-1}B^{-1},
$$

if $\hat{b} = \Psi(B)$, we have that

$$
\hat{b} = \begin{bmatrix} 2\mu+\lambda & \lambda & 0 \\ \lambda & 2\mu+\lambda & 0 \\ 0 & 0 & 2\mu \end{bmatrix} \qquad \hat{b}^{-1} = \begin{bmatrix} \frac{2\mu+\lambda}{4\mu(\mu+\lambda)} & \frac{-\lambda}{4\mu(\mu+\lambda)} & 0 \\ \frac{-\lambda}{4\mu(\mu+\lambda)} & \frac{2\mu+\lambda}{4\mu(\mu+\lambda)} & 0 \\ 0 & 0 & \frac{1}{2\mu} \end{bmatrix}.
$$

Calling

$$
\hat{d^i} = \begin{bmatrix} A_i & D_i & F_i \\ D_i & B_i & E_i \\ F_i & E_i & C_i \end{bmatrix},
$$

for $i = 0$

$$
\begin{aligned}
A_0 &= m_1 f_B(e^1)A^1 : A^1 + m_2 f_B(e^2)A^1 : A^1 \\
B_0 &= m_1 f_B(e^1)A^2 : A^2 + m_2 f_B(e^2)A^2 : A^2 \\
C_0 &= \tfrac{1}{2}\left(m_1 f_B(e^1)A^3 : A^3 + m_2 f_B(e^2)A^3 : A^3\right) \\
D_0 &= m_1 f_B(e^1)A^1 : A^2 + m_2 f_B(e^2)A^1 : A^2 \\
E_0 &= \tfrac{1}{\sqrt{2}}\left(m_1 f_B(e^1)A^2 : A^3 + m_2 f_B(e^2)A^2 : A^3\right) \\
F_0 &= \tfrac{1}{\sqrt{2}}\left(m_1 f_B(e^1)A^1 : A^3 + m_2 f_B(e^2)A^1 : A^3\right).
\end{aligned}
$$

Therefore

$$\hat{d}^1 = \frac{1}{\epsilon - 1}\hat{b}^{-1} + \theta\,\hat{d}^0$$

and, finally

$$\hat{b^*} = \hat{b} + (1-\theta)(\hat{d}^1)^{-1}.$$

By means of theorem $(2.3.35)$ in Allaire (2002) we can find the optimal lamination parameters and lamination directions in order to maximize our objective function. This is call the optimality criteria method.

If the eigenvalues of the stress tensor σ are σ_1 and σ_2, given by

$$\sigma_1 = \frac{1}{2}\left(\sigma_{11} + \sigma_{22} + \sqrt{(\sigma_{11} - \sigma_{22})^2 + 4\sigma_{12}^2}\right),$$

$$\sigma_2 = \frac{1}{2}\left(\sigma_{11} + \sigma_{22} - \sqrt{(\sigma_{11} - \sigma_{22})^2 + 4\sigma_{12}^2}\right),$$

With lamination parameters

$$m_1 = \frac{|\sigma_2|}{|\sigma_1| + |\sigma_2|} \qquad \text{and} \qquad m_2 = \frac{|\sigma_1|}{|\sigma_1| + |\sigma_2|},$$

therefore the intermediate proportions are:

$$\theta_1 = \frac{|\sigma_1| + \theta|\sigma_2|}{|\sigma_1| + |\sigma_2|} \;\; \theta_2 = \frac{\theta(|\sigma_1| + |\sigma_2|)}{|\sigma_1| + \theta|\sigma_2|}.$$

The lamination directions are chosen as the eigenvectors of σ. Then

$$e^1 = \begin{pmatrix} \frac{\sigma_{12}}{\sqrt{\sigma_{12}^2 + (\sigma_1 - \sigma_{11})^2 + \delta^2}} \\ \\ \frac{\sigma_1 - \sigma_{11}}{\sqrt{\sigma_{12}^2 + (\sigma_1 - \sigma_{11})^2 + \delta^2}} \end{pmatrix} \quad e^2 = \begin{pmatrix} e_y^1 \\ -e_x^1 \end{pmatrix},$$

where $\delta = \varepsilon\, 10^{-6}$.

The optimal density of rigid material is chosen by:

$$\theta = \min\left\{1, \sqrt{\frac{g^*(\sigma)}{l\int_\Omega \bar{\rho}\,|u|^2}}\right\},$$

where:

$$\begin{aligned} g^*(\sigma) &= \tfrac{2\mu+\lambda}{4\mu(\mu+\lambda)}\left(|\sigma_1| + |\sigma_2|\right)^2 \\ l &= \text{lagrange multiplier for the volume constraint of the rigid material} \\ \bar{\rho} &= \theta_p\, B + (1-\theta_p)\, A \\ \theta_p &= \text{optimal density of rigid material obtained in the previous iteration} \\ u &= \text{first eigenvector obtained in the previous iteration.} \end{aligned}$$

A.2. Homogenization in 3D

A.2.1. Mathematical Model

Let $\Omega \subset \mathbb{R}^3$ be a bounded open set in $\mathbb{R}^3$. In Ω we have two linearly elastic materials with elasticity tensors A and B. Let ϵ be a positive real number, $\epsilon \approx 0$, such that $A = \epsilon B$. This way A is the tensor of a very flexible material, and in the limit when $\epsilon \to 0$ imitates void.

We want to make a mixture of these two materials in proportions θ of B and $1-\theta$ of A. The new material is built by laminating a proportion θ_1 of B with a proportion $1-\theta_1$ of A in one direction, let us say e^1, and then the resultant tensor A^1 is laminated again, let us say in a direction e^2, and in proportion θ_2 with one of the pure materials, say A, and we obtain A^2, a rank 2 laminate. This new material is laminated again in direction e^3 in proportion θ_3 with A, and obtain A^3, a rank 3 laminate. Its effective tensor is defined by

$$A^3 = B + (1-\theta)\left((A-B)^{-1} + \theta\left(m_1\, f_B(e^1) + m_2\, f_B(e^2) + m_3\, f_B(e^3)\right)\right)^{-1}$$

Where f_B is a known fourth-order tensor and m_i are the lamination parameters, which depends on the intermediate proportions.

$$m_1 = \frac{1-\theta_1}{1-\theta} \qquad m_i = \frac{1-\theta_i}{1-\theta}\prod_{j=1}^{i-1}\theta_j \quad i = 2, ..., n.$$

A.2.2. Standard Isometry

Since during the calculations we need to invert several fourth-order tensors which could be a little difficult, we prefer to write these tensors as 6x6 matrices, because their inverses are standard. We identify the space of symmetric 3x3 matrices with $\mathbb{R}^6$ using the following isometry:

$$\Phi\left(\begin{bmatrix} a & d & e \\ d & b & f \\ e & f & c \end{bmatrix}\right) = \begin{pmatrix} a \\ b \\ c \\ \sqrt{2}\,d \\ \sqrt{2}\,e \\ \sqrt{2}\,f \end{pmatrix}.$$

Now we can write the constitutive relation as

$$\hat{\sigma} = \Phi(\sigma) = \hat{c}\,\Phi(\epsilon) = \hat{c}\,\hat{\epsilon},$$

In the isotropic case, with Lamé parameters λ, μ, the non-zero entries of the 6×6 matrix $\hat{c}$ are:

$\hat{c}_{11} = \hat{c}_{22} = \hat{c}_{33} = 2\mu + \lambda,$

$\hat{c}_{44} = \hat{c}_{55} = \hat{c}_{66} = 2\,\mu,$

$\hat{c}_{12} = \hat{c}_{21} = \hat{c}_{13} = \hat{c}_{31} = \hat{c}_{23} = \hat{c}_{32} = \lambda$

$$\mathbb{C}\begin{bmatrix} a & d & e \\ d & b & f \\ e & f & c \end{bmatrix} : \begin{bmatrix} a & d & e \\ d & b & f \\ e & f & c \end{bmatrix} = \begin{pmatrix} a \\ b \\ c \\ \sqrt{2}\,d \\ \sqrt{2}\,e \\ \sqrt{2}\,f \end{pmatrix} \cdot \hat{c} \begin{pmatrix} a \\ b \\ c \\ \sqrt{2}\,d \\ \sqrt{2}\,e \\ \sqrt{2}\,f \end{pmatrix}.$$

Let $\hat{c} = \Psi(\mathbb{C})$, we have that $\hat{\epsilon} = \Psi(\mathbb{C}^{-1})\hat{\sigma} = \Psi(\mathbb{C}^{-1})\hat{c}\hat{\epsilon}$, therefore $\hat{c}^{-1} = \Psi(\mathbb{C}^{-1})$, then $\mathbb{C}^{-1} = \Psi^{-1}(\hat{c}^{-1})$.

A.2.3. Sequential Iterative Laminations

Then, we can explicitly find the composite material that maximizes the first eigenvalue by means of a rank-3 sequential laminate in perpendicular directions e^1, e^2 and e^3 and with lamination parameters m_1, m_2 and m_3, using the formula (5.32) to (5.42) in Allaire (2002), this is

$$\mathbb{B}^* = B + (1-\theta)\left((A-B)^{-1} + \theta\left(m_1\, f_B(e^1) + m_2\, f_B(e^2) + m_3\, f_B(e^3)\right)\right)^{-1},$$

where the tensor f_B is defined by the quadratic form induced over the space of symmetric 3×3 matrices. In the case where $\mathbb{B}$ is an isotropic tensor with Lamé parameters μ and λ, that is to say

$$\mathbb{B} = \lambda\, I_2 \otimes I_2 + 2\,\mu\, I_4,$$

we have that:

$$f_B(e)\xi : \xi = \frac{1}{\mu}|\xi\, e|^2 - K\,(\xi\, e \cdot e)^2\,,$$

where $K = \frac{\mu+\lambda}{\mu(2\mu+\lambda)}$.

We need to apply f_B to the elements of a base of the space of symmetric 3×3 matrices. We use the following base:

$$
\begin{aligned}
A^1 &= e_1 \otimes e_1 = \begin{bmatrix} 1 & 0 & 0 \\ 0 & 0 & 0 \\ 0 & 0 & 0 \end{bmatrix} \\
A^2 &= e_2 \otimes e_2 = \begin{bmatrix} 0 & 0 & 0 \\ 0 & 1 & 0 \\ 0 & 0 & 0 \end{bmatrix} \\
A^3 &= e_3 \otimes e_3 = \begin{bmatrix} 0 & 0 & 0 \\ 0 & 0 & 0 \\ 0 & 0 & 1 \end{bmatrix} \\
A^4 &= e_1 \otimes e_2 + e_2 \otimes e_1 = \begin{bmatrix} 0 & 1 & 0 \\ 1 & 0 & 0 \\ 0 & 0 & 0 \end{bmatrix} \\
A^5 &= e_1 \otimes e_3 + e_3 \otimes e_1 = \begin{bmatrix} 0 & 0 & 1 \\ 0 & 0 & 0 \\ 1 & 0 & 0 \end{bmatrix} \\
A^6 &= e_2 \otimes e_3 + e_3 \otimes e_2 = \begin{bmatrix} 0 & 0 & 0 \\ 0 & 0 & 1 \\ 0 & 1 & 0 \end{bmatrix}
\end{aligned}
$$

Then

$$
\begin{aligned}
f_B^c(e)A^1 : A^1 &= \tfrac{1}{\mu}\left(e_x^2\right) - K\left(e_x^2\right)^2, \\
f_B^c(e)A^2 : A^2 &= \tfrac{1}{\mu}\left(e_y^2\right) - K\left(e_y^2\right)^2, \\
f_B^c(e)A^3 : A^3 &= \tfrac{1}{\mu}\left(e_z^2\right) - K\left(e_z^2\right)^2, \\
f_B^c(e)A^4 : A^4 &= \tfrac{1}{\mu}\left(e_x^2 + e_y^2\right) - K\left(2e_xe_y\right)^2, \\
f_B^c(e)A^5 : A^5 &= \tfrac{1}{\mu}\left(e_x^2 + e_z^2\right) - K\left(2e_xe_z\right)^2, \\
f_B^c(e)A^6 : A^6 &= \tfrac{1}{\mu}\left(e_y^2 + e_z^2\right) - K\left(2e_ye_z\right)^2, \\
f_B^c(e)(A^1 + A^2) : (A^1 + A^2) &= \tfrac{1}{\mu}\left(e_x^2 + e_y^2\right) - K\left(e_x^2 + e_y^2\right)^2, \\
f_B^c(e)(A^1 + A^3) : (A^1 + A^3) &= \tfrac{1}{\mu}\left(e_x^2 + e_z^2\right) - K\left(e_x^2 + e_z^2\right)^2, \\
f_B^c(e)(A^1 + A^4) : (A^1 + A^4) &= \tfrac{1}{\mu}\left((e_x + e_y)^2 + e_x^2\right) - K\left(e_x(e_x + 2e_y)\right)^2, \\
f_B^c(e)(A^1 + A^5) : (A^1 + A^5) &= \tfrac{1}{\mu}\left((e_x + e_z)^2 + e_x^2\right) - K\left(e_x(e_x + 2e_z)\right)^2, \\
f_B^c(e)(A^1 + A^6) : (A^1 + A^6) &= \tfrac{1}{\mu}\left(e_x^2 + e_y^2 + e_z^2\right) - K\left(e_x^2 + 2e_ye_z\right)^2, \\
f_B^c(e)(A^2 + A^3) : (A^2 + A^3) &= \tfrac{1}{\mu}\left(e_y^2 + e_z^2\right) - K\left(e_y^2 + e_z^2\right)^2, \\
f_B^c(e)(A^2 + A^4) : (A^2 + A^4) &= \tfrac{1}{\mu}\left((e_x + e_y)^2 + e_y^2\right) - K\left(e_y(2e_x + e_y)\right)^2, \\
f_B^c(e)(A^2 + A^5) : (A^2 + A^5) &= \tfrac{1}{\mu}\left(e_x^2 + e_y^2 + e_z^2\right) - K\left(e_y^2 + 2e_xe_z\right)^2, \\
f_B^c(e)(A^2 + A^6) : (A^2 + A^6) &= \tfrac{1}{\mu}\left((e_y + e_z)^2 + e_y^2\right) - K\left(e_y(e_y + 2e_z)\right)^2, \\
f_B^c(e)(A^3 + A^4) : (A^3 + A^4) &= \tfrac{1}{\mu}\left(e_x^2 + e_y^2 + e_z^2\right) - K\left(e_z^2 + 2e_xe_y\right)^2, \\
f_B^c(e)(A^3 + A^5) : (A^3 + A^5) &= \tfrac{1}{\mu}\left((e_x + e_z)^2 + e_z^2\right) - K\left(e_z(2e_x + e_z)\right)^2, \\
f_B^c(e)(A^3 + A^6) : (A^3 + A^6) &= \tfrac{1}{\mu}\left((e_y + e_z)^2 + e_z^2\right) - K\left(e_z(2e_y + e_z)\right)^2, \\
f_B^c(e)(A^4 + A^5) : (A^4 + A^5) &= \tfrac{1}{\mu}\left((e_y + e_z)^2 + 2e_x^2\right) - K\left(2e_x(e_y + e_z)\right)^2, \\
f_B^c(e)(A^4 + A^6) : (A^4 + A^6) &= \tfrac{1}{\mu}\left((e_x + e_z)^2 + 2e_y^2\right) - K\left(2e_y(e_x + e_z)\right)^2, \\
f_B^c(e)(A^5 + A^6) : (A^5 + A^6) &= \tfrac{1}{\mu}\left((e_x + e_y)^2 + 2e_z^2\right) - K\left(2e_z(e_x + e_y)\right)^2,
\end{aligned}
$$

And,

$$
\begin{aligned}
f_B^c(e)A^1 : A^2 &= \tfrac{1}{2}\left(f_B^c(e)(A^1+A^2) : (A^1+A^2) - f_B^c(e)A^1 : A^1 - f_B^c(e)A^2 : A^2\right) \\
&= -K\,(e_x)^2\,(e_y)^2\,, \\
f_B^c(e)A^1 : A^3 &= \tfrac{1}{2}\left(f_B^c(e)(A^1+A^3) : (A^1+A^3) - f_B^c(e)A^1 : A^1 - f_B^c(e)A^3 : A^3\right) \\
&= -K\,(e_x)^2\,(e_z)^2\,, \\
f_B^c(e)A^1 : A^4 &= \tfrac{1}{2}\left(f_B^c(e)(A^1+A^4) : (A^1+A^4) - f_B^c(e)A^1 : A^1 - f_B^c(e)A^4 : A^4\right) \\
&= \tfrac{e_x\,e_y}{\mu} - 2K\,(e_x)^3\,e_y\,, \\
f_B^c(e)A^1 : A^5 &= \tfrac{1}{2}\left(f_B^c(e)(A^1+A^5) : (A^1+A^5) - f_B^c(e)A^1 : A^1 - f_B^c(e)A^5 : A^5\right) \\
&= \tfrac{e_x\,e_z}{\mu} - 2K\,(e_x)^3\,e_z\,, \\
f_B^c(e)A^1 : A^6 &= \tfrac{1}{2}\left(f_B^c(e)(A^1+A^6) : (A^1+A^6) - f_B^c(e)A^1 : A^1 - f_B^c(e)A^6 : A^6\right) \\
&= -2K\,(e_x)^2\,e_y\,e_z\,, \\
f_B^c(e)A^2 : A^3 &= \tfrac{1}{2}\left(f_B^c(e)(A^2+A^3) : (A^2+A^3) - f_B^c(e)A^2 : A^2 - f_B^c(e)A^3 : A^3\right) \\
&= -K\,(e_y)^2\,(e_z)^2\,, \\
f_B^c(e)A^2 : A^4 &= \tfrac{1}{2}\left(f_B^c(e)(A^2+A^4) : (A^2+A^4) - f_B^c(e)A^2 : A^2 - f_B^c(e)A^4 : A^4\right) \\
&= \tfrac{e_x\,e_y}{\mu} - 2K\,(e_y)^3\,e_x\,, \\
f_B^c(e)A^2 : A^5 &= \tfrac{1}{2}\left(f_B^c(e)(A^2+A^5) : (A^2+A^5) - f_B^c(e)A^2 : A^2 - f_B^c(e)A^5 : A^5\right) \\
&= -2K\,e_x\,(e_y)^2\,e_z\,, \\
f_B^c(e)A^2 : A^6 &= \tfrac{1}{2}\left(f_B^c(e)(A^2+A^6) : (A^2+A^6) - f_B^c(e)A^2 : A^2 - f_B^c(e)A^6 : A^6\right) \\
&= \tfrac{e_y\,e_z}{\mu} - 2K\,(e_y)^3\,e_z\,, \\
f_B^c(e)A^3 : A^4 &= \tfrac{1}{2}\left(f_B^c(e)(A^3+A^4) : (A^3+A^4) - f_B^c(e)A^3 : A^3 - f_B^c(e)A^4 : A^4\right) \\
&= -2K\,e_x\,e_y\,(e_z)^2\,,
\end{aligned}
$$

$$
\begin{aligned}
f_B^c(e)A^3 : A^5 &= \tfrac{1}{2}\left(f_B^c(e)(A^3+A^5) : (A^3+A^5) - f_B^c(e)A^3 : A^3 - f_B^c(e)A^5 : A^5\right) \\
&= \tfrac{e_x\, e_z}{\mu} - 2K\,(e_z)^3\, e_x\,, \\
f_B^c(e)A^3 : A^6 &= \tfrac{1}{2}\left(f_B^c(e)(A^3+A^6) : (A^3+A^6) - f_B^c(e)A^3 : A^3 - f_B^c(e)A^6 : A^6\right) \\
&= \tfrac{e_y\, e_z}{\mu} - 2K\,(e_z)^3\, e_y\,, \\
f_B^c(e)A^4 : A^5 &= \tfrac{1}{2}\left(f_B^c(e)(A^4+A^5) : (A^4+A^5) - f_B^c(e)A^4 : A^4 - f_B^c(e)A^5 : A^5\right) \\
&= \tfrac{e_y\, e_z}{\mu} - 4K\, e_x^2\, e_y\, e_z\,, \\
f_B^c(e)A^4 : A^6 &= \tfrac{1}{2}\left(f_B^c(e)(A^4+A^6) : (A^4+A^6) - f_B^c(e)A^4 : A^4 - f_B^c(e)A^6 : A^6\right) \\
&= \tfrac{e_x\, e_z}{\mu} - 4K\, e_x\, e_y^2\, e_z\,, \\
f_B^c(e)A^5 : A^6 &= \tfrac{1}{2}\left(f_B^c(e)(A^5+A^6) : (A^5+A^6) - f_B^c(e)A^5 : A^5 - f_B^c(e)A^6 : A^6\right) \\
&= \tfrac{e_x\, e_y}{\mu} - 4K\, e_x\, e_y\, e_z^2\,.
\end{aligned}
$$

Then, given that

$$
(\mathbb{A}-\mathbb{B})^{-1} = \left((\varepsilon-1)\ \mathbb{B}\right)^{-1} = \frac{1}{\varepsilon-1}\mathbb{B}^{-1},
$$

if $\hat{b} = \Psi(\mathbb{B})$, we have that

$$
\hat{b} = \begin{bmatrix}
2\mu+\lambda & \lambda & \lambda & 0 & 0 & 0 \\
\lambda & 2\mu+\lambda & \lambda & 0 & 0 & 0 \\
\lambda & \lambda & 2\mu+\lambda & 0 & 0 & 0 \\
0 & 0 & 0 & 2\mu & 0 & 0 \\
0 & 0 & 0 & 0 & 2\mu & 0 \\
0 & 0 & 0 & 0 & 0 & 2\mu
\end{bmatrix}.
$$

The non-zero entries of $\hat{b}^{-1}$ are:

$$
\hat{b}_{11}^{-1} = \frac{1}{9\lambda+6\mu} + \frac{1}{3\mu} = \hat{b}_{22}^{-1} = \hat{b}_{33}^{-1}
$$

$$\hat{b}_{12}^{-1} = \frac{-\lambda}{2\mu(3\lambda+2\mu)} = \hat{b}_{21}^{-1} = \hat{b}_{13}^{-1} = \hat{b}_{31}^{-1} = \hat{b}_{23}^{-1} = \hat{b}_{32}^{-1}$$
$$\hat{b}_{44}^{-1} = \frac{1}{2\mu} = \hat{b}_{55}^{-1} = \hat{b}_{66}^{-1} \, .$$

Calling

$$\hat{d}^i = \begin{bmatrix} A_{11}^i & A_{12}^i & A_{13}^i & A_{14}^i & A_{15}^i & A_{16}^i \\ A_{12}^i & A_{22}^i & A_{23}^i & A_{24}^i & A_{25}^i & A_{26}^i \\ A_{13}^i & A_{23}^i & A_{33}^i & A_{34}^i & A_{35}^i & A_{36}^i \\ A_{14}^i & A_{24}^i & A_{34}^i & A_{44}^i & A_{45}^i & A_{46}^i \\ A_{15}^i & A_{25}^i & A_{35}^i & A_{45}^i & A_{55}^i & A_{56}^i \\ A_{16}^i & A_{26}^i & A_{36}^i & A_{46}^i & A_{56}^i & A_{66}^i \end{bmatrix} ,$$

for $i = 0$

$$
\begin{aligned}
A^0_{11} &= m_1 f^c_B(e^1)A^1 : A^1 + m_2 f^c_B(e^2)A^1 : A^1 + m_3 f^c_B(e^3)A^1 : A^1 \\
A^0_{22} &= m_1 f^c_B(e^1)A^2 : A^2 + m_2 f^c_B(e^2)A^2 : A^2 + m_3 f^c_B(e^3)A^2 : A^2 \\
A^0_{33} &= m_1 f^c_B(e^1)A^3 : A^3 + m_2 f^c_B(e^2)A^3 : A^3 + m_3 f^c_B(e^3)A^3 : A^3 \\
A^0_{44} &= \tfrac{1}{2}\left(m_1 f^c_B(e^1)A^4 : A^4 + m_2 f^c_B(e^2)A^4 : A^4 + m_3 f^c_B(e^3)A^4 : A^4\right) \\
A^0_{55} &= \tfrac{1}{2}\left(m_1 f^c_B(e^1)A^5 : A^5 + m_2 f^c_B(e^2)A^5 : A^5 + m_3 f^c_B(e^3)A^5 : A^5\right) \\
A^0_{66} &= \tfrac{1}{2}\left(m_1 f^c_B(e^1)A^6 : A^6 + m_2 f^c_B(e^2)A^6 : A^6 + m_3 f^c_B(e^3)A^6 : A^6\right) \\
A^0_{12} &= m_1 f^c_B(e^1)A^1 : A^2 + m_2 f^c_B(e^2)A^1 : A^2 + m_3 f^c_B(e^3)A^1 : A^2 \\
A^0_{13} &= m_1 f^c_B(e^1)A^1 : A^3 + m_2 f^c_B(e^2)A^1 : A^3 + m_3 f^c_B(e^3)A^1 : A^3 \\
A^0_{23} &= m_1 f^c_B(e^1)A^2 : A^3 + m_2 f^c_B(e^2)A^2 : A^3 + m_3 f^c_B(e^3)A^2 : A^3 \\
A^0_{14} &= \tfrac{1}{\sqrt{2}}\left(m_1 f^c_B(e^1)A^1 : A^4 + m_2 f^c_B(e^2)A^1 : A^4 + m_3 f^c_B(e^3)A^1 : A^4\right) \\
A^0_{15} &= \tfrac{1}{\sqrt{2}}\left(m_1 f^c_B(e^1)A^1 : A^5 + m_2 f^c_B(e^2)A^1 : A^5 + m_3 f^c_B(e^3)A^1 : A^5\right) \\
A^0_{16} &= \tfrac{1}{\sqrt{2}}\left(m_1 f^c_B(e^1)A^1 : A^6 + m_2 f^c_B(e^2)A^1 : A^6 + m_3 f^c_B(e^3)A^1 : A^6\right) \\
A^0_{24} &= \tfrac{1}{\sqrt{2}}\left(m_1 f^c_B(e^1)A^2 : A^4 + m_2 f^c_B(e^2)A^2 : A^4 + m_3 f^c_B(e^3)A^2 : A^4\right) \\
A^0_{25} &= \tfrac{1}{\sqrt{2}}\left(m_1 f^c_B(e^1)A^2 : A^5 + m_2 f^c_B(e^2)A^2 : A^5 + m_3 f^c_B(e^3)A^2 : A^5\right) \\
A^0_{26} &= \tfrac{1}{\sqrt{2}}\left(m_1 f^c_B(e^1)A^2 : A^6 + m_2 f^c_B(e^2)A^2 : A^6 + m_3 f^c_B(e^3)A^2 : A^6\right)
\end{aligned}
$$

$$
\begin{aligned}
A^0_{34} &= \tfrac{1}{\sqrt{2}}\left(m_1 f^c_B(e^1)A^3 : A^4 + m_2 f^c_B(e^2)A^3 : A^4 + m_3 f^c_B(e^3)A^3 : A^4\right) \\
A^0_{35} &= \tfrac{1}{\sqrt{2}}\left(m_1 f^c_B(e^1)A^3 : A^5 + m_2 f^c_B(e^2)A^3 : A^5 + m_3 f^c_B(e^3)A^3 : A^5\right) \\
A^0_{36} &= \tfrac{1}{\sqrt{2}}\left(m_1 f^c_B(e^1)A^3 : A^6 + m_2 f^c_B(e^2)A^3 : A^6 + m_3 f^c_B(e^3)A^3 : A^6\right) \\
A^0_{45} &= \tfrac{1}{2}\left(m_1 f^c_B(e^1)A^4 : A^5 + m_2 f^c_B(e^2)A^4 : A^5 + m_3 f^c_B(e^3)A^4 : A^5\right) \\
A^0_{46} &= \tfrac{1}{2}\left(m_1 f^c_B(e^1)A^4 : A^6 + m_2 f^c_B(e^2)A^4 : A^6 + m_3 f^c_B(e^3)A^4 : A^6\right) \\
A^0_{56} &= \tfrac{1}{2}\left(m_1 f^c_B(e^1)A^5 : A^6 + m_2 f^c_B(e^2)A^5 : A^6 + m_3 f^c_B(e^3)A^5 : A^6\right)
\end{aligned}
$$

Therefore

$$\hat{d}^1 = \frac{1}{\varepsilon - 1}\hat{b}^{-1} + \theta\,\hat{d}^0$$

and,

$$\hat{b^*} = \hat{b} + (1-\theta)(\hat{d}^1)^{-1}.$$

Theorem 2.3.36 in Allaire (2002) yields, under the assumption that $\lambda \geq 0$, the following result. If $\sigma_1 \leq \sigma_2 \leq \sigma_3$ are the eigenvalues of σ, then

$$g(\sigma, \theta) = B^{-1}\sigma : \sigma + \frac{\theta}{1-\theta} g^*(\sigma)$$

Note: $g(\sigma, \theta)$ depends on the objective function one wants to minimize or maximize which is our case.

with $g^*(\sigma)$ as given in the following cases:

(1) In the case when $0 \leq \sigma_1 \leq \sigma_2 \leq \sigma_3$

$$\text{if} \quad \sigma_3 \leq \sigma_1 + \sigma_2$$

$$g^*(\sigma) = \frac{2\mu + \lambda}{4\mu(2\mu + 3\lambda)} \left(\sigma_1 + \sigma_2 + \sigma_3\right)^2$$

$$m_1 = \frac{\sigma_3 + \sigma_2 - \sigma_1}{\sigma_1 + \sigma_2 + \sigma_3}\,,\ m_2 = \frac{\sigma_1 - \sigma_2 + \sigma_3}{\sigma_1 + \sigma_2 + \sigma_3}\,,\ m_3 = \frac{\sigma_1 + \sigma_2 - \sigma_3}{\sigma_1 + \sigma_2 + \sigma_3}$$

$$\text{if} \quad \sigma_3 \geq \sigma_1 + \sigma_2$$

$$g^*(\sigma) = \frac{1}{2\mu}\left((\sigma_1 + \sigma_2)^2 + \sigma_3^2\right) - \frac{\lambda(\sigma_1 + \sigma_2 + \sigma_3)^2}{2\mu(2\mu + 3\lambda)}$$

$$m_1 = \frac{\sigma_2}{\sigma_1 + \sigma_2}\,,\ m_2 = \frac{\sigma_1}{\sigma_1 + \sigma_2}\,,\ m_3 = 0$$

(2) In the case when $\sigma_1 \le 0 \le \sigma_2 \le \sigma_3$

$$\text{if} \quad \sigma_3 + \sigma_2 \ge -\frac{\mu}{\mu+\lambda}\,\sigma_1\,, \text{ and } \sigma_3 - \sigma_2 \le -\frac{\mu}{\mu+\lambda}\,\sigma_1$$

$$g^*(\sigma) = \frac{2\mu+\lambda}{4\mu(2\mu+3\lambda)}\left(\sigma_3+\sigma_2-\frac{\mu+2\lambda}{\mu+\lambda}\,\sigma_1\right)^2$$

$$m_1 = \frac{\sigma_3+\sigma_2+\frac{\mu}{\mu+\lambda}\,\sigma_1}{\sigma_3+\sigma_2-\frac{\mu+2\lambda}{\mu+\lambda}\,\sigma_1}\,,\ m_2 = \frac{\mu+\lambda}{\mu}\,\frac{\sigma_3-\sigma_2-\frac{\mu}{\mu+\lambda}\,\sigma_1}{\sigma_3+\sigma_2-\frac{\mu+2\lambda}{\mu+\lambda}\,\sigma_1}$$

$$m_3 = -\frac{\mu+\lambda}{\mu}\,\frac{\sigma_3-\sigma_2+\frac{\mu}{\mu+\lambda}\,\sigma_1}{\sigma_3+\sigma_2-\frac{\mu+2\lambda}{\mu+\lambda}\,\sigma_1}$$

$$\text{if} \quad \sigma_3 + \sigma_2 \le -\frac{\mu}{\mu+\lambda}\,\sigma_1$$

$$g^*(\sigma) = \frac{1}{2\mu}\left((\sigma_3+\sigma_2)^2+\sigma_1^2\right) - \frac{\lambda(\sigma_1+\sigma_2+\sigma_3)^2}{2\mu(2\mu+3\lambda)}$$

$$m_1 = 0\,,\ m_2 = \frac{\sigma_3}{\sigma_2+\sigma_3}\,,\ m_3 = \frac{\sigma_2}{\sigma_2+\sigma_3}$$

$$\text{if} \quad \sigma_3 - \sigma_2 \ge -\frac{\mu}{\mu+\lambda}\,\sigma_1$$

$$g^*(\sigma) = \frac{1}{2\mu}\left(\sigma_1^2+\sigma_2^2+\sigma_3^2\right) - \frac{2\mu\sigma_1\sigma_2}{2\mu(\mu+\lambda)} - \frac{\lambda(\sigma_1+\sigma_2+\sigma_3)^2}{2\mu(2\mu+3\lambda)}$$

$$m_1 = \frac{\sigma_2}{\sigma_2-\sigma_1}\,,\ m_2 = \frac{-\sigma_1}{\sigma_2-\sigma_1}\,,\ m_3 = 0$$

(3) In the case when $\sigma_1 \le \sigma_2 \le 0 \le \sigma_3$

$$\text{if} \quad \sigma_1 + \sigma_2 \le -\frac{\mu}{\mu+\lambda}\,\sigma_3\,, \text{ and } \sigma_1 - \sigma_2 \ge -\frac{\mu}{\mu+\lambda}\,\sigma_3$$

$$g^*(\sigma) = \frac{2\mu+\lambda}{4\mu(2\mu+3\lambda)}\left(\sigma_1+\sigma_2-\frac{\mu+2\lambda}{\mu+\lambda}\,\sigma_3\right)^2$$

$$m_1 = \frac{\sigma_1+\sigma_2+\frac{\mu}{\mu+\lambda}\,\sigma_3}{\sigma_1+\sigma_2-\frac{\mu+2\lambda}{\mu+\lambda}\,\sigma_3}\,,\ m_2 = \frac{\mu+\lambda}{\mu}\,\frac{\sigma_1-\sigma_2-\frac{\mu}{\mu+\lambda}\,\sigma_3}{\sigma_1+\sigma_2-\frac{\mu+2\lambda}{\mu+\lambda}\,\sigma_3}$$

$$m_3 = -\frac{\mu+\lambda}{\mu}\,\frac{\sigma_1-\sigma_2+\frac{\mu}{\mu+\lambda}\,\sigma_3}{\sigma_1+\sigma_2-\frac{\mu+2\lambda}{\mu+\lambda}\,\sigma_3}$$

$$\text{if} \quad \sigma_1 + \sigma_2 \ge -\frac{\mu}{\mu+\lambda}\,\sigma_3$$

$$g^*(\sigma) = \frac{1}{2\mu}\left((\sigma_1+\sigma_2)^2+\sigma_3^2\right) - \frac{\lambda\,(\sigma_1+\sigma_2+\sigma_3)^2}{2\mu(2\mu+3\lambda)}$$

$$m_1 = 0\,,\ m_2 = \frac{\sigma_1}{\sigma_2+\sigma_1}\,,\ m_3 = \frac{\sigma_2}{\sigma_2+\sigma_1}$$

$$\text{if} \quad \sigma_1 - \sigma_2 \le -\frac{\mu}{\mu+\lambda}\,\sigma_3$$

$$g^*(\sigma) = \frac{1}{2\mu}(\sigma_1^2+\sigma_2^2+\sigma_3^2) - \frac{2\mu\sigma_3\sigma_2}{2\mu(\mu+\lambda)} - \frac{\lambda\,(\sigma_1+\sigma_2+\sigma_3)^2}{2\mu(2\mu+3\lambda)}$$

$$m_1 = \frac{\sigma_2}{\sigma_2-\sigma_3}\,,\ m_2 = -\frac{\sigma_3}{\sigma_2-\sigma_3}\,,\ m_3 = 0$$

(4) In the case when $\sigma_1 \leq \sigma_2 \leq \sigma_3 \leq 0$

$$\text{if} \quad \sigma_1 \geq \sigma_3 + \sigma_2$$

$$g^*(\sigma) = \frac{2\mu + \lambda}{4\mu(2\mu + 3\lambda)} \left(\sigma_1 + \sigma_2 + \sigma_3\right)^2$$

$$m_1 = \frac{\sigma_1 + \sigma_2 - \sigma_3}{\sigma_1 + \sigma_2 + \sigma_3}\,,\ m_2 = \frac{\sigma_3 - \sigma_2 + \sigma_1}{\sigma_1 + \sigma_2 + \sigma_3}\,,\ m_3 = \frac{\sigma_3 + \sigma_2 - \sigma_1}{\sigma_1 + \sigma_2 + \sigma_3}$$

$$\text{if} \quad \sigma_1 \leq \sigma_3 + \sigma_2$$

$$g^*(\sigma) = \frac{1}{2\mu}\left((\sigma_3 + \sigma_2)^2 + \sigma_1^2\right) - \frac{\lambda\left(\sigma_3 + \sigma_2 + \sigma_1\right)^2}{2\mu(2\mu + 3\lambda)}$$

$$m_1 = \frac{\sigma_2}{\sigma_3 + \sigma_2}\,,\ m_2 = \frac{\sigma_3}{\sigma_3 + \sigma_2}\,,\ m_3 = 0$$

Finally, the lamination directions are chosen as the eigenvectors of σ.

And the optimal density of rigid material is chosen by:

$$\theta = \min\left\{1, \sqrt{\frac{g^*(\sigma)}{l\int_\Omega \bar{\rho}\,|u|^2}}\right\}\,,$$

where:

$$\begin{aligned} \bar{\rho} &= \theta_p\, B + (1 - \theta_p)\, A \\ \theta_p &= \text{optimal density of rigid material obtained in the previous iteration.} \\ u &= \text{first eigenvector obtained in the previous iteration.} \end{aligned}$$

A.3. Effective elasticity tensor for a rank-2 laminate composite

A.3.1. Introduction

Let $\Omega \subset \mathbb{R}^2$ be a bounded open set in $\mathbb{R}^2$. In Ω we have two linearly elastic materials with elasticity tensors A and B. We want to make a mixture of these two materials in proportions θ of A and $1-\theta$ of B. The new material is built by laminating a proportion θ_1 of A with a proportion $1-\theta_1$ of B in one direction, let us say e^1, and then the resultant tensor A_1^* is laminated again in a perpendicular direction e^2, and in proportion $1-\theta_2$ with one of the pure materials, say A, in proportion θ_2 and obtain A_2^*, a rank 2 laminate. See figure A.1.

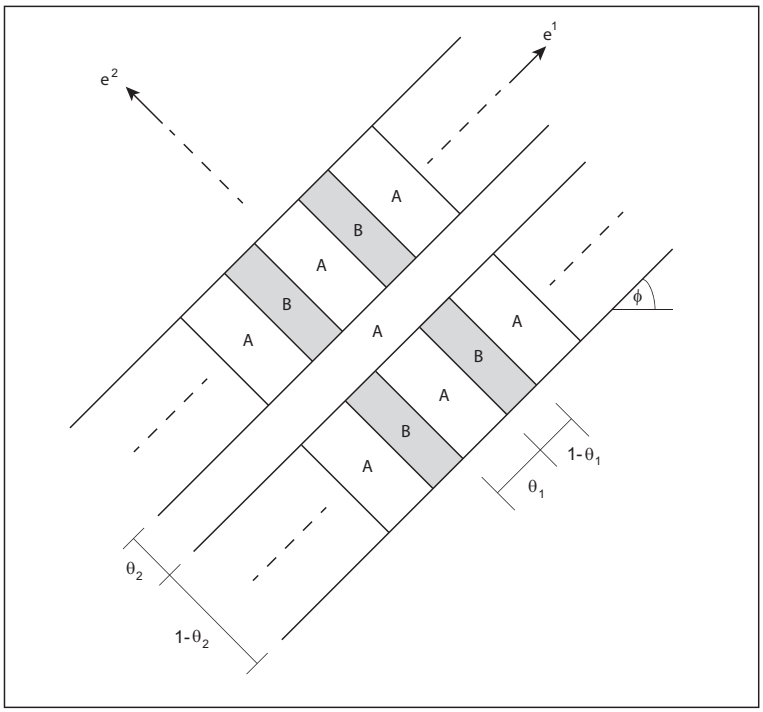

FIGURE A.1. Laminated Material

Notice that e^1, e^2 is the base of $\mathbb{R}^2$ resulting of applying a rotation in angle ϕ to the canonic base of $\mathbb{R}^2$.

According to equation (2.68) in Allaire (2002) the effective tensor of the laminated material is defined by

$$A_2^* = A + (1-\theta)\left((B-A)^{-1} + \theta\left(m_1\, f_A(e^1) + m_2\, f_A(e^2)\right)\right)^{-1}$$

Where, $\theta = \theta_2 + \theta_1(1-\theta_2)$ is the total proportion of material A, $1-\theta = (1-\theta_1)(1-\theta_2)$ is the total proportion of material B, and f_A is a known fourth-order tensor and m_i are the lamination parameters, which depend on the intermediate proportions.

$$m_1 = \frac{\theta_1}{\theta} = \frac{\theta_1}{\theta_1 + \theta_2(1-\theta_1)} \qquad m_2 = \frac{\theta_2(1-\theta_1)}{\theta_1 + \theta_2(1-\theta_1)}.$$

A.3.2. Standard Isometry

Since during the calculations we need to invert several fourth-order tensors which could be a little difficult, we prefer to write this tensors as 3x3 matrices, because their inverses are standard. We identify the space of symmetric 2x2 matrices with $\mathbb{R}^3$ using the following isometry:

$$\Phi\left(\begin{bmatrix} x & z \\ z & y \end{bmatrix}\right) = \begin{pmatrix} x \\ y \\ \sqrt{2}\, z \end{pmatrix}.$$

Now we can write the constitutive relation as

$$\hat{\sigma} = \Phi(\sigma) = \hat{c}\ \Phi(\epsilon) = \hat{c}\ \hat{\epsilon},$$

where $\hat{c}$ is defined as the following 3×3 matrix:

$$\hat{c}_{11} = C_{1111}, \qquad \hat{c}_{12} = C_{1122}, \qquad \hat{c}_{13} = \sqrt{2}\, C_{1112},$$

$$\hat{c}_{21} = C_{2211}, \qquad \hat{c}_{22} = C_{2222}, \qquad \hat{c}_{23} = \sqrt{2}\, C_{2212},$$

$$\hat{c}_{31} = \sqrt{2}\, C_{1211}, \quad \hat{c}_{32} = \sqrt{2}\, C_{1222}, \quad \hat{c}_{33} = 2\, C_{1212}.$$

In the isotropic case $\hat{c}_{11} = \hat{c}_{22} = 2\mu + \lambda$, $\hat{c}_{33} = 2\,\mu$, $\hat{c}_{12} = \hat{c}_{21} = \lambda$ and $\hat{c}_{13} = \hat{c}_{31} = \hat{c}_{23} = \hat{c}_{32} = 0$. Where $\lambda\,,\ \mu$ are the Lamé parameters of an elastic material. Also:

$$C \begin{bmatrix} x & z \\ z & y \end{bmatrix} : \begin{bmatrix} x & z \\ z & y \end{bmatrix} = \begin{pmatrix} x \\ y \\ \sqrt{2}\,z \end{pmatrix} \cdot \hat{c} \begin{pmatrix} x \\ y \\ \sqrt{2}\,z \end{pmatrix}.$$

Let $\hat{c} = \Psi(C)$, we have that $\hat{\epsilon} = \Psi(C^{-1})\hat{\sigma} = \Psi(C^{-1})\hat{c}\hat{\epsilon}$, therefore $\hat{c}^{-1} = \Psi(C^{-1})$, then $C^{-1} = \Psi^{-1}(\hat{c}^{-1})$.

A.3.3. Sequential Iterative Laminations

Then, we can explicitly find the composite material that maximize the first eigenvalue by means of a rank-2 sequential laminate in perpendicular directions e^1 and e^2 and with lamination parameters m_1 and m_2, using the formula (2.68) in Allaire (2002), this is

$$A^* = A + (1-\theta)\left((B-A)^{-1} + \theta\left(m_1\, f_A(e^1) + m_2\, f_A(e^2)\right)\right)^{-1},$$

where the tensor f_A its defined by the quadratic form induced over the space of symmetric 2×2 matrices. In the case where A and B are isotropic tensors with Lamé parameters $\mu_A\,,\ \mu_B$ and $\lambda_A\,,\ \lambda_B$, that is to say

$$A = \lambda_A\, I_2 \otimes I_2 + 2\,\mu_A\, I_4\,, \qquad B = \lambda_B\, I_2 \otimes I_2 + 2\,\mu_B\, I_4,$$

we have that:

$$f_A(e)\xi : \xi = \frac{1}{\mu_A}|\xi\, e|^2 - K\,(\xi\, e \cdot e)^2\,,$$

where $K = \frac{\mu_A + \lambda_A}{\mu_A(2\mu_A + \lambda_A)}$.

We need to apply f_A to the elements of a base of the space of symmetric 2×2 matrices. We use the following base:

$$A^1 = e_1 \otimes e_1 = \begin{bmatrix} 1 & 0 \\ 0 & 0 \end{bmatrix} \qquad A^2 = e_2 \otimes e_2 = \begin{bmatrix} 0 & 0 \\ 0 & 1 \end{bmatrix}$$

$$A^3 = e_1 \otimes e_2 + e_2 \otimes e_1 = \begin{bmatrix} 0 & 1 \\ 1 & 0 \end{bmatrix}.$$

And $e^1 = \begin{pmatrix} cos(\phi) \\ sin(\phi) \end{pmatrix}$, $e^2 = \begin{pmatrix} -sin(\phi) \\ cos(\phi) \end{pmatrix}$,
with $|e^i| = \sqrt{(e^i_x)^2 + (e^i_y)^2} = 1 \quad i = 1, 2$

Then

$$\begin{aligned}
f_A(e^1)A^1 : A^1 &= \tfrac{1}{\mu}\, cos^2(\phi) - K cos^4(\phi), \\
f_A(e^1)A^2 : A^2 &= \tfrac{1}{\mu}\, sin^2(\phi) - K sin^4(\phi), \\
f_A(e^1)A^3 : A^3 &= \tfrac{1}{\mu} - K sin^2(2\phi), \\
f_A(e^1)(A^1 + A^2) : (A^1 + A^2) &= \tfrac{1}{\mu} - K, \\
f_A(e^1)A^1 : A^2 &= \tfrac{1}{2}(f_A(e^1)(A^1 + A^2) : (A^1 + A^2) \\
&\quad -f_A(e^1)A^1 : A^1 - f_A(e^1)A^2 : A^2) \\
&= -K cos^2(\phi) sin^2(\phi), \\
f_A(e^1)(A^2 + A^3) : (A^2 + A^3) &= \tfrac{1}{\mu}\left((cos(\phi) + sin(\phi))^2 + sin^2(\phi)\right) \\
&\quad -K\left(sin(\phi)(2cos(\phi) + sin(\phi))\right)^2, \\
f_A(e^1)A^2 : A^3 &= \tfrac{1}{2}(f_A(e^1)(A^2 + A^3) : (A^2 + A^3) \\
&\quad -f_A(e^1)A^2 : A^2 - f_A(e^1)A^3 : A^3) \\
&= \tfrac{1}{\mu}\left(cos(\phi) sin(\phi)\right) - K(2cos(\phi) sin^3(\phi)), \\
f_A(e^1)(A^1 + A^3) : (A^1 + A^3) &= \tfrac{1}{\mu}\left((cos(\phi) + sin(\phi))^2 + cos^2(\phi)\right) \\
&\quad -K\left(cos(\phi)(cos(\phi) + 2sin(\phi))\right)^2,
\end{aligned}$$

$$
\begin{aligned}
f_A(e^1)A^1 : A^3 &= \tfrac{1}{2}(f_A(e^1)(A^1 + A^3) : (A^1 + A^3) \\
&\quad -f_A(e^1)A^1 : A^1 - f_A(e^1)A^3 : A^3) \\
&= \tfrac{1}{\mu}\left(cos(\phi)sin(\phi)\right) - K\left(2cos^3(\phi)sin(\phi)\right).
\end{aligned}
$$

$$
\begin{aligned}
f_A(e^2)A^1 : A^1 &= \tfrac{1}{\mu}\, sin^2(\phi) - Ksin^4(\phi), \\
f_A(e^2)A^2 : A^2 &= \tfrac{1}{\mu}\, cos^2(\phi) - Kcos^4(\phi), \\
f_A(e^2)A^3 : A^3 &= \tfrac{1}{\mu} - Ksin^2(2\phi), \\
f_A(e^2)(A^1 + A^2) : (A^1 + A^2) &= \tfrac{1}{\mu} - K, \\
f_A(e^2)A^1 : A^2 &= \tfrac{1}{2}(f_A(e^2)(A^1 + A^2) : (A^1 + A^2) \\
&\quad -f_A(e^2)A^1 : A^1 - f_A(e^2)A^2 : A^2 \\
&= -Kcos^2(\phi)sin^2(\phi), \\
f_A(e^2)(A^2 + A^3) : (A^2 + A^3) &= \tfrac{1}{\mu}\left((cos(\phi) - sin(\phi))^2 + cos^2(\phi)\right) \\
&\quad -K\left(cos(\phi)(-2sin(\phi) + cos(\phi))\right)^2, \\
f_A(e^2)A^2 : A^3 &= \tfrac{1}{2}(f_A(e^2)(A^2 + A^3) : (A^2 + A^3) \\
&\quad -f_A(e^2)A^2 : A^2 - f_A(e^2)A^3 : A^3 \\
&= -\tfrac{1}{\mu}\left(cos(\phi)sin(\phi)\right) + K(2cos^3(\phi)sin(\phi)), \\
f_A(e^2)(A^1 + A^3) : (A^1 + A^3) &= \tfrac{1}{\mu}\left((cos(\phi) - sin(\phi))^2 + sin^2(\phi)\right) \\
&\quad -K\left(sin(\phi)(sin(\phi) - 2cos(\phi))\right)^2, \\
f_A(e^2)A^1 : A^3 &= \tfrac{1}{2}(f_A(e^2)(A^1 + A^3) : (A^1 + A^3) \\
&\quad -f_A(e^2)A^1 : A^1 - f_A(e^2)A^3 : A^3) \\
&= -\tfrac{1}{\mu}\left(cos(\phi)sin(\phi)\right) + K\left(2cos(\phi)sin^3(\phi)\right).
\end{aligned}
$$

if $\hat{b} = \Psi(B)$, we have that

$$\hat{b} = \begin{bmatrix} 2\mu_B + \lambda_B & \lambda_B & 0 \\ \lambda_B & 2\mu_B + \lambda_B & 0 \\ 0 & 0 & 2\mu_B \end{bmatrix} \qquad \hat{a} = \begin{bmatrix} 2\mu_A + \lambda_A & \lambda_A & 0 \\ \lambda_A & 2\mu_A + \lambda_A & 0 \\ 0 & 0 & 2\mu_A \end{bmatrix}.$$

and

$$\left(\hat{b} - \hat{a}\right)^{-1} = \begin{bmatrix} \frac{\lambda_B - \lambda_A + 2\mu_B - 2\mu_A}{4(\mu_A - \mu_B)(\lambda_A - \lambda_B + \mu_A - \mu_B)} & \frac{\lambda_A - \lambda_B}{4(\mu_A - \mu_B)(\lambda_A - \lambda_B + \mu_A - \mu_B)} & 0 \\ \frac{\lambda_A - \lambda_B}{4(\mu_A - \mu_B)(\lambda_A - \lambda_B + \mu_A - \mu_B)} & \frac{\lambda_B - \lambda_A + 2\mu_B - 2\mu_A}{4(\mu_A - \mu_B)(\lambda_A - \lambda_B + \mu_A - \mu_B)} & 0 \\ 0 & 0 & \frac{1}{2(\mu_B - \mu_A)} \end{bmatrix}$$

Calling

$$\hat{d^i} = \begin{bmatrix} A_i & D_i & F_i \\ D_i & B_i & E_i \\ F_i & E_i & C_i \end{bmatrix},$$

for $i = 0$

$$\begin{aligned} A_0 &= m_1 f_A(e^1) A^1 : A^1 + m_2 f_A(e^2) A^1 : A^1 \\ B_0 &= m_1 f_A(e^1) A^2 : A^2 + m_2 f_A(e^2) A^2 : A^2 \\ C_0 &= \tfrac{1}{2} \left(m_1 f_A(e^1) A^3 : A^3 + m_2 f_A(e^2) A^3 : A^3 \right) \\ D_0 &= m_1 f_A(e^1) A^1 : A^2 + m_2 f_A(e^2) A^1 : A^2 \\ E_0 &= \tfrac{1}{\sqrt{2}} \left(m_1 f_A(e^1) A^2 : A^3 + m_2 f_A(e^2) A^2 : A^3 \right) \\ F_0 &= \tfrac{1}{\sqrt{2}} \left(m_1 f_A(e^1) A^1 : A^3 + m_2 f_A(e^2) A^1 : A^3 \right). \end{aligned}$$

Therefore

$$\hat{d^1} = \left(\hat{b} - \hat{a}\right)^{-1} + \theta\, \hat{d^0}$$

and, finally

$$\hat{a^*} = \hat{a} + (1 - \theta)(\hat{d^1})^{-1}. \tag{A.1}$$

A.3.4. Direct Method

Another way to obtain formulas for the effective elasticity tensor is by means of successive limits, as in Gutiérrez (1998) and Gutiérrez (2004). With this method we can directly obtain the homogenized or effective elasticity tensor, but it is not easy to iterate with this method to obtain higher rank laminations, because each new lamination requires the inverse of several 2×2 matrices.

First we calculate the rank-1 effective elasticity tensor, then we laminate B in proportion $1 - \theta_1$ with A in proportion θ_1 in direction e_1 as seen in figure A.2.

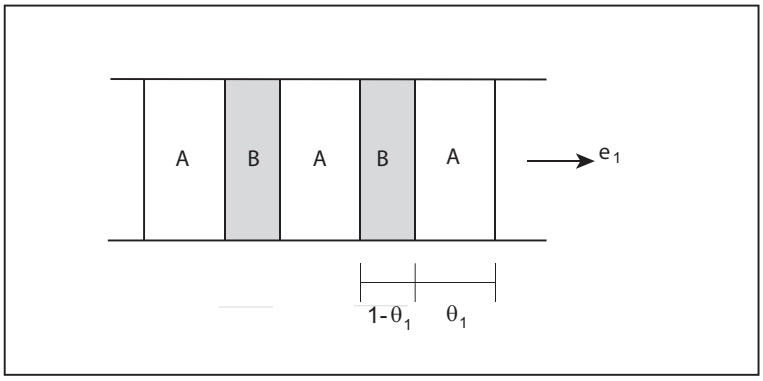

FIGURE A.2. rank-1 laminated material

We form a succession of elasticity tensors C^n that depends on a scale or length factor that goes to zero when n goes to ∞.

We notice that the elasticity tensor C^n depends only in the direction x_1 (parallel with e_1).

$$C^n(x_1) = \chi^n(x_1)A + (1 - \chi^n(x_1))B$$

where χ^n is a sequence of characteristic functions of material A that weakly-$\star$ converges to $\theta_1(x_1)$ in $L^\infty(\Omega;[0,1])$. Although χ^n is always equal to 0 or 1, its limit θ_1 can take any value between 0 and 1.

Assuming A and B are elastic materials the stress-strain relation is

$$\sigma_{ij}^n = C_{ijkl}^n \varepsilon_{kl}^n \qquad i,j,k,l = 1,2\,, \tag{A.2}$$

where $\varepsilon_{kl}^n = \frac{1}{2}\left(\frac{\partial u_k^n}{\partial x_l} + \frac{\partial u_l^n}{\partial x_k}\right)$, $u^n \in \mathbb{R}^2$ is the strain tensor, $\sigma^n \in Sym(2\times 2)$ is the stress tensor and if A and B are isotropic,
$C_{ijkl}^n = \lambda^n(x_1)\delta_{ij}\delta_{kl} + \mu^n(x_1)\left(\delta_{ik}\delta_{jl} + \delta_{il}\delta_{jk}\right)$.

Then,

$$\begin{aligned}
C_{1111}^n &= \lambda^n + 2\mu^n \\
C_{1122}^n &= \lambda^n = C_{2211}^n \\
C_{1112}^n &= 0 = C_{1211}^n \\
C_{2212}^n &= 0 = C_{1222}^n \\
C_{2222}^n &= \lambda^n + 2\mu^n \\
C_{1212}^n &= \mu^n
\end{aligned}$$

Using the standard isometry (see section A.3.2):

$$\hat{c}^n = \begin{bmatrix} \lambda^n + 2\mu^n & \lambda^n & 0 \\ \lambda^n & \lambda^n + 2\mu^n & 0 \\ 0 & 0 & 2\mu^n \end{bmatrix} \quad,\ \hat{\sigma}^n = \hat{c}^n\hat{\varepsilon}^n$$

By means of Tartar (2009), $\sigma_{1j}^n\,,\ j=1,2$ and ε_{22}^n do not oscillate in the x_1 direction. Then for any n, equation A.2 stands, and we can obtain expressions for the oscillating parameters ($\sigma_{22}^n\,,\ \varepsilon_{12}^n\,,\ \varepsilon_{11}^n$) in terms of the non oscillating ones ($\sigma_{12}^n\,,\ \sigma_{11}^n\,,\ \varepsilon_{22}^n$).

$$
\begin{aligned}
\hat{\sigma}^n_{11} &= (\lambda^n + 2\mu^n)\hat{\varepsilon}^n_{11} + \lambda^n \hat{\varepsilon}^n_{22} \\
\rightarrow \quad \hat{\varepsilon}^n_{11} &= \tfrac{1}{\lambda^n + 2\mu^n}\hat{\sigma}^n_{11} - \tfrac{\lambda^n}{\lambda^n + 2\mu^n}\hat{\varepsilon}^n_{22} \qquad (1)
\end{aligned}
$$

$$
\begin{aligned}
\hat{\sigma}^n_{22} &= \lambda^n \hat{\varepsilon}^n_{11} + (\lambda^n + 2\mu^n)\hat{\varepsilon}^n_{22} \\
&= \tfrac{\lambda^n}{\lambda^n + 2\mu^n}\hat{\sigma}^n_{11} + \left(\tfrac{4\mu^n(\lambda^n + \mu^n)}{\lambda^n + 2\mu^n}\right)\hat{\varepsilon}^n_{22} \qquad (2)
\end{aligned}
$$

$$
\begin{aligned}
\hat{\sigma}^n_{12} &= 2\mu^n \hat{\varepsilon}^n_{12} \\
\rightarrow \quad \hat{\varepsilon}^n_{12} &= \tfrac{1}{2\mu^n}\hat{\sigma}^n_{12} \qquad (3)
\end{aligned}
$$

Passing to the limit $n \rightarrow \infty^+$,

$$
\begin{array}{lllllllll}
(1) & \rightarrow & \hat{\varepsilon}^\infty_{11} & = & \alpha\hat{\sigma}^\infty_{11} - \beta\hat{\varepsilon}^\infty_{22} & \rightarrow & \hat{\sigma}^\infty_{11} & = & \tfrac{1}{\alpha}\hat{\varepsilon}^\infty_{11} + \tfrac{\beta}{\alpha}\hat{\varepsilon}^\infty_{22} \\
(2) & \rightarrow & \hat{\sigma}^\infty_{22} & = & \beta\hat{\sigma}^\infty_{11} + \gamma\hat{\varepsilon}^\infty_{22} & \rightarrow & \hat{\sigma}^\infty_{22} & = & \tfrac{\beta}{\alpha}\hat{\varepsilon}^\infty_{11} + \left(\tfrac{\beta^2}{\alpha} + \gamma\right)\hat{\varepsilon}^\infty_{22} \\
(3) & \rightarrow & \hat{\varepsilon}^\infty_{12} & = & \delta\hat{\sigma}^\infty_{12} & \rightarrow & \hat{\sigma}^\infty_{12} & = & \tfrac{1}{\delta}\hat{\varepsilon}^\infty_{12}
\end{array}
$$

with

$$
\begin{aligned}
\alpha &= \theta_1\left(\tfrac{1}{\lambda_A + 2\mu_A}\right) + (1-\theta_1)\left(\tfrac{1}{\lambda_B + 2\mu_B}\right) \\
\beta &= \theta_1\left(\tfrac{\lambda_A}{\lambda_A + 2\mu_A}\right) + (1-\theta_1)\left(\tfrac{\lambda_B}{\lambda_B + 2\mu_B}\right) \\
\gamma &= \theta_1\left(\tfrac{4\mu_A(\lambda_A + \mu_A)}{\lambda_A + 2\mu_A}\right) + (1-\theta_1)\left(\tfrac{4\mu_B(\lambda_B + \mu_B)}{\lambda_B + 2\mu_B}\right) \\
\delta &= \theta_1\left(\tfrac{1}{2\mu_A}\right) + (1-\theta_1)\left(\tfrac{1}{2\mu_B}\right) .
\end{aligned}
$$

Then the rank-1 effective tensor in the standard isometry look is:

$$
\hat{c}^*_1 = \begin{bmatrix} 1/\alpha & \beta/\alpha & 0 \\ \beta/\alpha & \beta^2/\alpha + \gamma & 0 \\ 0 & 0 & 1/\delta \end{bmatrix}
$$

Now to calculate the rank-2 laminate effective tensor, we laminate the rank-1 effective material in proportion $1-\theta_2$ with material A in proportion θ_2 in perpendicular direction e_2 as seen in figure A.3.

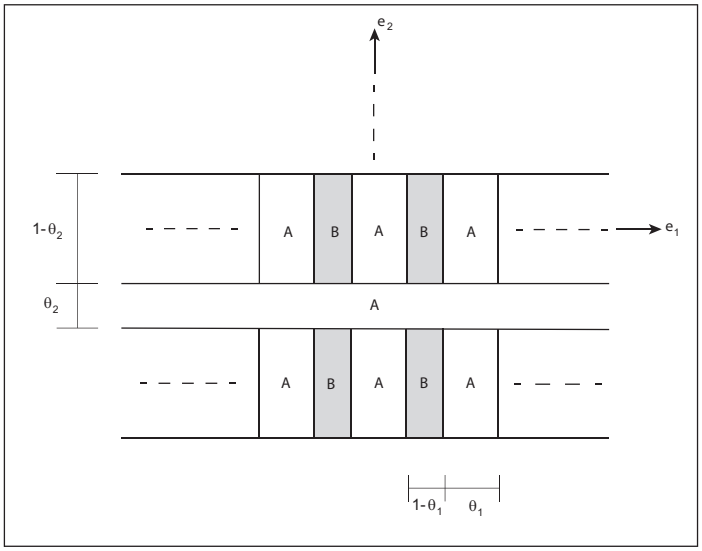

FIGURE A.3. rank-2 laminated material

Now the non oscillating quantities are $\sigma^n_{i2}\,;\ \ i=1,2$ and ε^n_{11}, and looking at the stress-strain relation using the standard isometry, we can write the oscillating quantities $(\sigma^n_{11}\,,\,\varepsilon^n_{12}\,,\,\varepsilon^n_{22})$ in terms of the non oscillating ones $(\sigma^n_{12}\,,\,\sigma^n_{22}\,,\,\varepsilon^n_{11})$.

$$\begin{pmatrix} \hat{\sigma}^n_{11} \\ \hat{\sigma}^n_{22} \\ \hat{\sigma}^n_{12} \end{pmatrix} = \begin{bmatrix} \hat{c}^n_{11} & \hat{c}^n_{12} & \hat{c}^n_{13} \\ \hat{c}^n_{12} & \hat{c}^n_{22} & \hat{c}^n_{23} \\ \hat{c}^n_{13} & \hat{c}^n_{23} & \hat{c}^n_{33} \end{bmatrix} \begin{pmatrix} \hat{\varepsilon}^n_{11} \\ \hat{\varepsilon}^n_{22} \\ \hat{\varepsilon}^n_{12} \end{pmatrix}$$

For each $n \in \mathbb{N}$, $\hat{c}^n_{13} = \hat{c}^n_{23} = 0$, then

$$
\begin{aligned}
\rightarrow \quad \begin{pmatrix} \hat{\sigma}^n_{22} \\ \hat{\sigma}^n_{12} \end{pmatrix} &= \begin{pmatrix} \hat{c}^n_{12} \\ 0 \end{pmatrix} \hat{\varepsilon}^n_{11} + \begin{bmatrix} \hat{c}^n_{22} & 0 \\ 0 & \hat{c}^n_{33} \end{bmatrix} \begin{pmatrix} \hat{\varepsilon}^n_{22} \\ \hat{\varepsilon}^n_{12} \end{pmatrix} \\
\rightarrow \quad \begin{pmatrix} \hat{\varepsilon}^n_{22} \\ \hat{\varepsilon}^n_{12} \end{pmatrix} &= \begin{bmatrix} 1/\hat{c}^n_{22} & 0 \\ 0 & 1/\hat{c}^n_{33} \end{bmatrix} \begin{pmatrix} \hat{\sigma}^n_{22} - \hat{c}^n_{12}\hat{\varepsilon}^n_{11} \\ \hat{\sigma}^n_{12} \end{pmatrix} \\
\rightarrow \quad \hat{\varepsilon}^n_{22} &= \tfrac{1}{\hat{c}^n_{22}}\hat{\sigma}^n_{22} - \tfrac{\hat{c}^n_{12}}{\hat{c}^n_{22}}\hat{\varepsilon}^n_{11} \\
\rightarrow \quad \hat{\varepsilon}^n_{12} &= \tfrac{1}{\hat{c}^n_{33}}\hat{\sigma}^n_{12} \\
\rightarrow \quad \hat{\sigma}^n_{11} &= \hat{c}^n_{11}\hat{\varepsilon}^n_{11} + \hat{c}^n_{12}\left(\tfrac{1}{\hat{c}^n_{22}}\hat{\sigma}^n_{22} - \tfrac{\hat{c}^n_{12}}{\hat{c}^n_{22}}\hat{\varepsilon}^n_{11}\right) \\
&= \left(\hat{c}^n_{11} - \tfrac{(\hat{c}^n_{12})^2}{\hat{c}^n_{22}}\right)\hat{\varepsilon}^n_{11} + \tfrac{\hat{c}^n_{12}}{\hat{c}^n_{22}}\hat{\sigma}^n_{22}
\end{aligned}
$$

Passing to the limit $n \rightarrow \infty$

$$
\begin{aligned}
\hat{\sigma}^\infty_{11} &= A_1\hat{\varepsilon}^\infty_{11} + B_1\hat{\sigma}^\infty_{22} \;\rightarrow\; \hat{\sigma}^\infty_{11} = \left(A_1 + \tfrac{B_1^2}{D_1}\right)\hat{\varepsilon}^\infty_{11} + \tfrac{B_1}{D_1}\hat{\varepsilon}^\infty_{22} \\
\hat{\varepsilon}^\infty_{22} &= -B_1\hat{\varepsilon}^\infty_{11} + D_1\hat{\sigma}^\infty_{22} \;\rightarrow\; \hat{\sigma}^\infty_{22} = \tfrac{B_1}{D_1}\hat{\varepsilon}^\infty_{11} + \tfrac{1}{D_1}\hat{\varepsilon}^\infty_{22} \\
\hat{\varepsilon}^\infty_{12} &= C_1\hat{\sigma}^\infty_{12} \;\rightarrow\; \hat{\sigma}^\infty_{12} = \tfrac{1}{C_1}\hat{\varepsilon}^\infty_{12}\,,
\end{aligned}
$$

where

$$
\begin{aligned}
A_1 &= \theta_2 \tfrac{4\mu_A(\lambda_A+\mu_A)}{\lambda_A+2\mu_A} + (1-\theta_2)\left(\hat{c}_1^*(1,1) - \tfrac{(\hat{c}_1^*(1,2))^2}{\hat{c}_1^*(2,2)}\right) \\
&= \theta_2 \tfrac{4\mu_A(\lambda_A+\mu_A)}{\lambda_A+2\mu_A} + (1-\theta_2)\left(\tfrac{1}{\alpha} - \tfrac{(\beta/\alpha)^2}{\frac{\beta^2}{\alpha}+\gamma}\right) \\
B_1 &= \theta_2 \tfrac{\lambda_A}{\lambda_A+2\mu_A} + (1-\theta_2)\left(\tfrac{\hat{c}_1^*(1,2)}{\hat{c}_1^*(2,2)}\right) \\
&= \theta_2 \tfrac{\lambda_A}{\lambda_A+2\mu_A} + (1-\theta_2)\left(\tfrac{\beta/\alpha}{\frac{\beta^2}{\alpha}+\gamma}\right) \\
C_1 &= \theta_2\left(\tfrac{1}{2\mu_A}\right) + (1-\theta_2)\left(\tfrac{1}{\hat{c}_1^*(3,3)}\right) \\
&= \theta_2\left(\tfrac{1}{2\mu_A}\right) + (1-\theta_2)\delta \\
D_1 &= \theta_2\left(\tfrac{1}{\lambda_A+2\mu_A}\right) + (1-\theta_2)\left(\tfrac{1}{\hat{c}_1^*(2,2)}\right) .
\end{aligned}
$$

Then the rank-2 effective tensor in the standard isometry look is:

$$
\hat{c}_2^* = \begin{bmatrix} A_1 + B_1^2/D_1 & B_1/D_1 & 0 \\ B_1/D_1 & 1/D_1 & 0 \\ 0 & 0 & 1/C_1 \end{bmatrix}
$$

In order to compare the effective tensors $\hat{c}_2^*$ and $\hat{a}^*$ from equation A.1 we need to apply a rotation in angle $-\phi$ to the effective tensor $\hat{c}_2^*$. We define a rotation rotation matrix,

$$
Q(\phi) = \begin{bmatrix} cos(\phi) & sin(\phi) \\ -sin(\phi) & cos(\phi) \end{bmatrix}
$$

Then applying the rotation in the strain-stress relation,

$$\begin{aligned} \sigma &= \mathbb{C}^{\text{eff}}\varepsilon \\ Q\sigma Q^T &= Q\mathbb{C}^{\text{eff}}\varepsilon Q^T \\ &= Q\mathbb{C}^{\text{eff}}Q^T Q\varepsilon Q^T \end{aligned}$$

Calling $\tilde{\sigma} = Q\sigma Q^T$ and $\tilde{\varepsilon} = Q\varepsilon Q^T$ we get,

$$\tilde{\sigma} = Q\mathbb{C}^{\text{eff}}Q^T\tilde{\varepsilon}$$

Therefore the effective elasticity tensor obtained by laminating in perpendicular directions e^1 and e^2 (e_1 and e_2 rotated in angle ϕ) is,

$$\tilde{\mathbb{C}^{\text{eff}}} = Q\mathbb{C}^{\text{eff}}Q^T$$

Using the standard isometry we can find an easy way to obtain the effective elasticity tensor in rotated directions by means of the non-rotated one.

If $\sigma = \begin{bmatrix} \sigma_{11} & \sigma_{12} \\ \sigma_{11} & \sigma_{22} \end{bmatrix}$, then $\hat{\sigma} = \begin{pmatrix} \sigma_{11} \\ \sigma_{22} \\ \sqrt{2}\sigma_{12} \end{pmatrix}$

Now we calculate the rotated tensor $\tilde{\sigma}$,

$$\begin{aligned} \tilde{\sigma} &= Q\sigma Q^T \\ &= \begin{bmatrix} cos(\phi) & sin(\phi) \\ -sin(\phi) & cos(\phi) \end{bmatrix} \begin{bmatrix} \sigma_{11} & \sigma_{12} \\ \sigma_{11} & \sigma_{22} \end{bmatrix} \begin{bmatrix} cos(\phi) & -sin(\phi) \\ sin(\phi) & cos(\phi) \end{bmatrix} \end{aligned}$$

then,

$$\tilde{\sigma}_{11} = \sigma_{11}cos^2(\phi) + \sigma_{22}sin^2(\phi) + \sigma_{12}sin(2\phi)$$
$$\tilde{\sigma}_{22} = \sigma_{11}sin^2(\phi) + \sigma_{22}cos^2(\phi) - \sigma_{12}sin(2\phi)$$
$$\tilde{\sigma}_{12} = -\tfrac{1}{2}\sigma_{11}sin(2\phi) + \tfrac{1}{2}\sigma_{22}sin(2\phi) + \sigma_{12}cos(2\phi)$$

In the standard isometry,

$$\begin{aligned}
\hat{\tilde{\sigma}} &= \begin{pmatrix} \sigma_{11}cos^2(\phi) + \sigma_{22}sin^2(\phi) + \sigma_{12}sin(2\phi) \\ \sigma_{11}sin^2(\phi) + \sigma_{22}cos^2(\phi) - \sigma_{12}sin(2\phi) \\ -\frac{\sqrt{2}}{2}\sigma_{11}sin(2\phi) + \frac{\sqrt{2}}{2}\sigma_{22}sin(2\phi) + \sqrt{2}\sigma_{12}cos(2\phi) \end{pmatrix} \\
&= \begin{bmatrix} cos^2(\phi) & sin^2(\phi) & sin(2\phi)/\sqrt{2} \\ sin^2(\phi) & cos^2(\phi) & -sin(2\phi)/\sqrt{2} \\ -sin(2\phi)/\sqrt{2} & sin(2\phi)/\sqrt{2} & cos(2\phi) \end{bmatrix} \begin{pmatrix} \sigma_{11} \\ \sigma_{22} \\ \sqrt{2}\sigma_{12} \end{pmatrix}
\end{aligned}$$

Calling

$$L = \begin{bmatrix} cos^2(\phi) & sin^2(\phi) & sin(2\phi)/\sqrt{2} \\ sin^2(\phi) & cos^2(\phi) & -sin(2\phi)/\sqrt{2} \\ -sin(2\phi)/\sqrt{2} & sin(2\phi)/\sqrt{2} & cos(2\phi) \end{bmatrix}$$

and using the standard isometry form of the strain-stress relation,

$$\begin{aligned}
\hat{\sigma} &= \hat{c}\hat{\varepsilon} \\
L^{-1}\hat{\tilde{\sigma}} &= \hat{c}L^{-1}\hat{\tilde{\varepsilon}} \\
\hat{\tilde{\sigma}} &= L\hat{c}L^{-1}\hat{\tilde{\varepsilon}}
\end{aligned}$$

Then,

$$\hat{\hat{c}} = L\hat{c}L^{-1}$$

Therefore,

$$\hat{\hat{c}}_2^* = L\hat{c}_2^*L^{-1}$$

Finally by replacing the value of the entries in the matrix $\hat{\hat{c}}_2^*$ we can check that all the entries of this matrix are exactly the same of the ones in matrix $\hat{a}_2^*$ of equation (A.1).